ABSTRACT

Title of dissertation: INERTIAL PARAMETER IDENTIFICATION OF A CAPTURED PAYLOAD ATTACHED TO A ROBOTIC MANIPULATOR ON A FREE-FLYING SPACECRAFT

Nicholas Michael Limparis
Doctor of Philosophy, 2024

Dissertation directed by: Professor Dr. David L. Akin
Department of Aerospace Engineering

The groundwork for the dynamics of a free-flyer with a manipulator has been laid out by Yoshida, Vafa and Dubowsky, and Papadopoulos and Moosovian with the Generalized Jacobian Matrix, Virtual Manipulator, and Barycentric Vector Approach respectively. The identification of parameters for a robot manipulator has also been approached for industrial robots as well as through adaptive control theory. What is proposed is a method for inertial parameter identification and verification for a spacecraft with an attached manipulator that is an extension of the ground-fixed Inverse Direct Dynamic Model to function for a free-flying spacecraft. This method for inertial parameter identification for a spacecraft-manipulator system with an attached client spacecraft, debris, or other grappled payload is developed in this thesis and is experimentally tested using results for a servicer and an "unknown" grappled payload using three separate test beds. The results of the experiments show that the proposed method is capable of identifying the inertial parameters of the servicer and the grappled payload.

INERTIAL PARAMETER IDENTIFICATION OF A CAPTURED PAYLOAD ATTACHED TO A ROBOTIC MANIPULATOR ON A FREE-FLYING SPACECRAFT

by

Nicholas Michael Limparis

Dissertation submitted to the Faculty of the Graduate School of the
University of Maryland, College Park in partial fulfillment
of the requirements for the degree of
Doctor of Philosophy
2024

Advisory Committee:
Professor Dr. David L. Akin, Chair/Advisor
Professor Dr. Craig R. Carignan
Professor Dr. Raymond J. Sedwick
Professor Dr. Norman M. Wereley
Professor Dr. Nikhil Chopra, Dean's Representative

Dedication

To my wife, who has been giving of her time and effort to help me in my journey to meet my goal of completing my doctorate. I know it took *a lot* longer than we had hoped, but I am glad that I have finally completed it. I love you, and thank you for your support.

To my children, you are the loves of my life. I thank you for understanding why dad was always working and making do with the concentrated bursts of my time and attention that you got. I look forward to having many fewer late nights that I instead get to spend with you. I love you both.

To my parents, who have been there for me and supported me in my endeavors. Without your support I could not have accomplished this goal. I know that you are proud of me, and I am proud to be your son. I love you both.

Acknowledgments

I owe my gratitude to all the people who have made this thesis possible and because of whom my graduate experience has been one that I will cherish forever. There are so many who have helped me along the way, my friends, my colleagues, and my mentors. I thank you for your support and guidance. I could not have done this without you. I am grateful for your help and support.

First and foremost, I'd like to thank my advisor, Dave Akin for giving me an incredible opportunity to work on challenging and widely varied array of interesting projects during my extended stay. He has always made himself available for help, advice, and allowed me to take the time I needed to take care of my family when emergencies arose. His "open door" policy has meant that anytime he was in his office and was not actively working with someone else, he would share his time with me. It has been my incredible pleasure to work with and learn from such an extraordinary individual.

I would like to thank the members of my thesis committee, Dr. Raymond Sedwick, Dr. Norman Wereley, Dr. Nikhil Chopra, and Dr. Craig Carignan, for their time and effort in reviewing my thesis and providing feedback. Dr. Carignan's expertise helped me find direction with the theoretical foundation of this thesis when I was struggling. Dr. Nikhil Chopra helped significantly by taking over as my Dean's representative after the untimely passing of Dr. Linda Schmidt. I am grateful for you stepping into the role after much of the work was already done and for your feedback on the final draft and improvements that can be made with my data processing. Dr. Wereley and Dr. Sedwick have always been available to help and have provided encouragement to complete this thesis. Thank you for your time and effort with my thesis.

I would also like to specifically give thanks, in no particular order, to Nicolas Bolatto, Charles Hanner, Daniil Gribok, Joshua Martin, Christopher Carlsen, and Dr. Katherine McBryan. They have all been instrumental in my success, especially with making, running, and processing the experiments that are the core of this thesis. Additionally, I would like to thank Kit Sczudlo for his help with proofreading and the many late nights of bouncing ideas off of him and generally being moral support when I needed it.

I want to show my appreciation to the many students of the Space Systems Lab who have helped me with details of this thesis and the many projects that I have worked on over the years. Furthermore, I would like to thank the many students that I have had the pleasure to mentor over the years. I have learned that I have a passion for teaching from working with you all, and I hope that I have been able to impart some of my collected knowledge to you as well. It has been a pleasure to work with you all and seem some of you grow into the engineers that you are today.

Finally, I want to thank the office staff of the Aerospace Engineering Department. I would not have completed this thesis without the help of Otto Fandino, Laura Thorsen, Leslie Davis, and the rest of the staff in the office. So many last minute purchase orders were filled with your support as well as being instrumental in helping me navigate the bureaucracy of the university and the department. I am grateful for your help and support.

To all those that I may have inadvertently left out, I apologize. I am grateful for your help and support. Thank you all.

Table of Contents

List of Tables

List of Figures

Chapter 1: Introduction and Motivation

This dissertation is focused on the dynamics of a free-floating system of a coupled manipulator and spacecraft system, and the identification of a payload's observable dynamics once grappled. As we continue to launch more and more payloads into space the problem of orbital debris becomes more and more of a concern. The Kessler Syndrome [1] is a scenario in which the density of objects in low Earth orbit is high enough that collisions between objects could cause a cascade of collisions that would make space in low Earth orbit unusable and dangerous to pass through. This is a real concern as the number of objects in low Earth orbit continues to increase. Brook Sullivan characterized satellite failures [2] highlighting the need for servicing, but yet the problem of space debris is a problem of the commons with the largest contributors to space junk largely ignoring the problem. Furthermore, many state space agencies have determined servicing essential to solving many of these problems. [3] A NASA study showed that even if we were to stop launching satellites today, that there is enough debris already in obit to cause a cascading debris field to occur unless 5-10 space objects are removed yearly. [4] With an ever-increasing number of satellites being launched into space, the problem of space debris is only going to get worse. As such we need to develop methods to remove space debris from orbit.

In this dissertation we will be considering the pre- and post-grapple phases of a free-floating spacecraft with a coupled manipulator used to grapple a payload. This system is of interest, as it

is a system that could be used to remove space debris from orbit. Regardless of the configuration of the mission, understanding the dynamics of the system are essential for the ability to control the system and move the payload to a desired location or deorbit the payload without causing further debris.

1.1 Motivation

For the purposes of this dissertation, we will consider the term "payload" to be any object that we would like to interact with. The dynamics of the system are of interest as they will determine the control algorithms that can be used to control the system, will also determine the stability of the system and the ability to control the system, determine the ability to move the payload to a desired location, and most importantly they will determine the ability to deorbit the payload without causing further debris. Unfortunately, the dynamics parameters of the payload objects are very poorly known beforehand. This is due to the fact that the objects are in space and are old, poorly documented, and have been exposed to the harsh environment of space. As such, the dynamics of the system are not well known and are difficult to determine pre-grapple.

With the recognition by space agencies for a need to address the problem of space debris, there has been a push to develop methods to remove space debris from orbit. Methods for active debris capture [5] have been looked at to address the problem of orbital debris. Characterization of tumble [6], proposed detumbling methods [7]–[9], as well as the development of grasping strategies [10]–[12] have been looked at to address the problem of space debris. Many of these methods either assume that you know the dynamics of the object beforehand or instead ignore the dynamics of the object altogether. [9], [13] This is a problem as the dynamics of the object are

important for the initial ability to control the system and move the payload to a desired location or deorbit without causing further debris.

Manipulator control methods are well-developed for ground fixed manipulators, as well as for space manipulators that are attached to a spacecraft. John Craig [14] begins the development of the kinematics for a ground fixed robotic manipulator using the methodology originally developed by Denavit and Hartenberg [15]. He then uses a modified version of the Denavit-Hartenberg (DH) parameters that expresses the robot joints purely from the current joint. These modified DH parameters are used as the basis for the development of the kinematics of the system for a simple serial ground fixed serial manipulator. With the development of the DH parameters, tracking of robot state terms comes down to the simple task of tracking the Jacobian matrix and system state variables. As such both the inverse and forward kinematics of the system can be tracked. Both Peter Corke [16], [17] and John Craig use the kinematic chains to track the dynamics of the manipulator systems modeled.

Denavit-Hartenberg parameters are not the only way to track robot kinematics. There are many other ways to track them including Newton-Euler methods [18], [19], screw theory [20], quaternion kinematics [21], and dual quaternion kinematics [22]. Each method has their own advantages and disadvantages. DH parameters, however are the most widely used method for tracking the kinematics of a robotic manipulator. They are simple to implement and easy to understand, helping to reduce complexity for the user as well as having relatively simple computational complexity [23].

The groundwork for robotic manipulator kinematics and dynamics and eventual advancements in computational capabilities lead to the desire for their use in extreme environments to aid in human exploration. Robotics usefulness as tools has bloomed from initial work in high

energy physics and manipulators for nuclear reactors [23], to deep sea manipulators [24], [25] and eventually to the use of manipulators in space. [3], [26]–[48].

Chapter 2 will review the literature on the dynamics of free-floating systems, manipulator dynamics for space robotics, and some methods for ground based dynamics parameter identification. In Chapter 3 the development of an extended dynamics identification methods for payloads of space robotics will be discussed. Chapter 4 will discuss three test beds for the methods and results from the experimental test beds. Finally, chapter 5 will discuss the conclusions found in this dissertation and future work.

Chapter 2: Literature Review

This literature review will be divided into two main sections. The first section will cover the dynamics of free-floating and free-flying systems and their associated manipulators. The second section will cover methods to identify inertia parameters for grasped payloads. The literature review will be used to provide a foundation for the development of a novel extension to existing inertial parameter identification methodology that will be presented in Chapter 3.

2.1 Coupled Dynamics for Free-Floating and Free-Flying Systems

Some of the first work on the dynamics of a free-floating system to be explored was done by Vafa and Dubowsky [49] and Longman et al. [50]. Vafa and Dubowsky developed the concept of a virtual manipulator and virtual ground to describe the dynamics of a free-floating system. Longman et al. developed the concept of reaction moment compensation to describe the dynamics of a free-floating system. Both of these methods have their own advantages and disadvantages. Reaction moment compensation (RMC) is a method that is simple to implement and has relatively low computational complexity. It does however require the use of reaction wheels or control moment gyros to react the moments of the system. This can lead to a large mass penalty for the system. Although the concept of reaction moment compensation is very a useful stepping stone for the development of dynamics for free-floating systems, methods developed later have been shown to

be more general without introducing the mass penalty for the reaction wheels or control moment gyros needed to react the moments of the system. The underlying methodology that Longman uses for the development of RMC in section 2.1.1, will be used as a portion of the inspiration for the development of a novel inertial parameter identification methodology that will be presented in Chapter 3.

2.1.1 Reaction Moment Compensation

The method of reaction moment compensation was developed by Longman et al. [50] This paper sets up the basis for using a set of reaction wheels or control moment gyros to counteract the forces that are applied to the base spacecraft from the motion of the arm. Reaction moment compensation relies on placing the moment reaction system near the base of the manipulator so that the moments of the robotic arm can be reacted. This reduces the load on the spacecraft attitude control system but does not react translations of the system center of mass. Let us begin by looking at the construction of the kinematic chains for the example system that Longman uses in his paper. This system is shown below in Figure 2.1.

Figure 2.2 shows the vector locations for the system. The vector definitions follow in table 2.1:

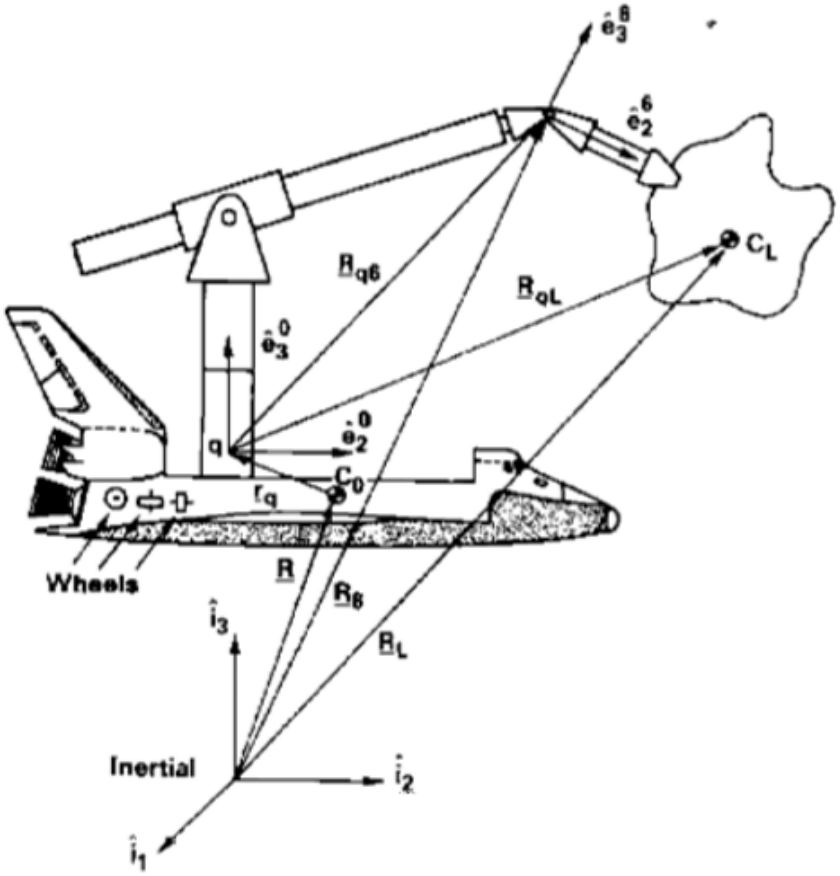

Figure 2.1: Satellite-mounted robot showing reaction wheels and inertial coordinate frames [50]

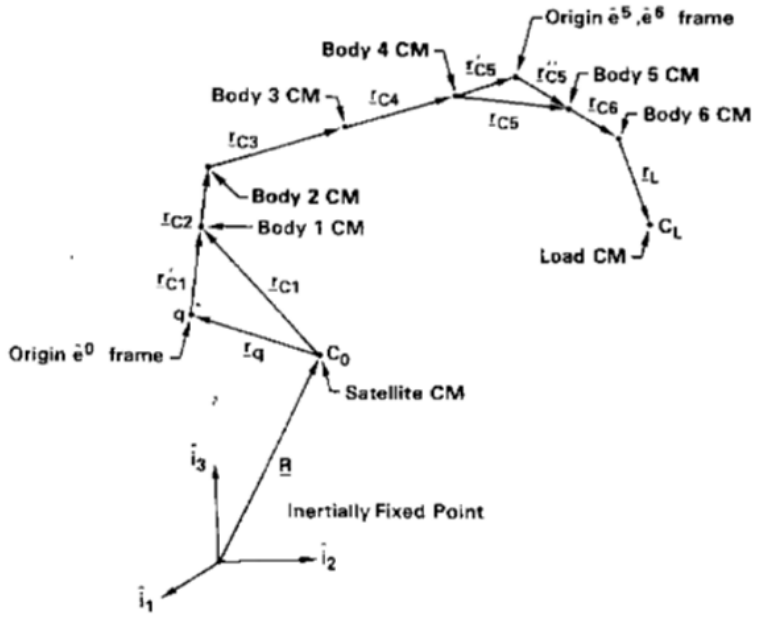

Figure 2.2: Vector Definitions giving locations for the center of mass (CoM) of each body in 2.1 [50]

Variable	Definition
$\mathbf{\Theta}_i$	The ith joint angle or extension
$\mathbf{r}_L$	Vector to the center of mass of the load from body n CoM
$\mathbf{r}_q$	Vector to the center of mass of the load from body n CoM
m_L	Mass of the Load
m_i	Mass of the ith link
$\hat{i}_1, \hat{i}_2, \hat{i}_3$	The 3 unit vectors of the inertially fixed frame
$\hat{e}_1^0, \hat{e}_2^0, \hat{e}_3^0$	The 3 unit vectors of the robot origin frame q
$\hat{e}_1^i, \hat{e}_2^i, \hat{e}_3^i$	The 3 unit vectors of the robot's ith joint frame
$\underline{\mathbf{R}}$	Vector from the inertially fixed frame to the CoM of the satellite
$\underline{\mathbf{R}}_L$	Vector from the inertially fixed frame to the CoM of the Load
$\underline{\mathbf{R}}_i$	Vector from the inertially fixed frame to the CoM of the ith link
$\underline{\mathbf{R}}_{CS}$	Vector from the inertially fixed frame to the CoM of the system
$R_{CS(1,2,3)}$	Vector components of $\underline{\mathbf{R}}_{CS}$
$\mathbf{C}_0$	Point indicating the CoM of the satellite sans manipulator
$\mathbf{C}_L$	Point indicating the CoM of the load
$\mathbf{C}_i$	Point indicating the CoM of the ith link
$\underline{\mathbf{r}}_{ci}$	Vector from the $(i-1)$th CoM to the CoM of the ith link/body
n	Number of links in the manipulator

Table 2.1: RMC Vector Definitions for Figure 2.2

From these vector definitions we can see that the following equations hold true for the system:

$$\mathbf{r}_L = \mathbf{R}_{L1}\hat{i}_1 + \mathbf{r}_{L2}\hat{i}_2 + \mathbf{r}_{L3}\hat{i}_3 \tag{2.1}$$

With the additional choice of Longman to define the inertially fixed frame to be collocated at center of mass of the satellite, C_0, we can see that the following equation holds true for the system:

$$\underline{\mathbf{R}} = \mathbf{R}_1\hat{i}_1 + \mathbf{R}_2\hat{i}_2 + \mathbf{R}_3\hat{i}_3 = \mathbf{R}_1\hat{e}_1^0 + \mathbf{R}_2\hat{e}_2^0 + \mathbf{R}_3\hat{e}_3^0 \tag{2.2}$$

Using the definition for the vector $\underline{\mathbf{R}}_{CS}$ in 2.1 we can see that the following equation is the definition for the center of mass of the system:

$$\left(\sum_{i=0}^{n+1} m_i\right)\underline{\mathbf{R}}_{CS} = \sum_{i=0}^{n+1} m_i \sum_{j=0}^{i} r_{cj} \tag{2.3}$$

where $m_L = m_{n+1}$ and m_0 is the mass of body 0 which is the satellite when $m_{ij} = \sum_{k=i}^{j} m_k$. For the example posited by Longman,the distances between centers of mass in Fig 2.2 are defined as follows:

$$\begin{aligned}
&\mathbf{r}_{c1} = \mathbf{r}_q + \mathbf{r}_0' \\
&\mathbf{r}_q = r_{q1}\hat{e}_1^0 + r_{q2}\hat{e}_2^0 + r_{q3}\hat{e}_3^0 \\
&\mathbf{r}_{c1}' = d_1\hat{e}_3^0, \quad \mathbf{r}_{c2} = d_2\hat{e}_3^0, \quad \mathbf{r}_{c3} = r\hat{e}_2^2 \\
&\mathbf{r}_{c4} = d_4\hat{e}_2^2, \quad \mathbf{r}_{c5} = \mathbf{r}_{c5}' + \mathbf{r}_{c5}'', \quad \mathbf{r}_{c5}' = d_{51}\hat{e}_2^2, \\
&\mathbf{r}_{c5}'' = d_{52}\hat{e}_2^5, \quad \mathbf{r}_{c6} = d_6\hat{e}_2^5, \quad \mathbf{r}_{c7} = \mathbf{r}_L
\end{aligned} \tag{2.4}$$

With

$$\hat{e}_2^2 = -\sin\theta_1 \cos\theta_2 \hat{e}_1^0 + \cos\theta_1 \cos\theta_2 \hat{e}_2^0 + \sin\theta_2 \hat{e}_3^0 \tag{2.5}$$

and for this particular case, $\hat{e}_2^5 = \hat{e}_2^6$. Longman then goes on to show the kinematics and inverse kinematics for the particular example system from [50] skipped here for brevity.

Longman then defines a new example system for the demonstration of the calculation of moments for a ground fixed system and how they would translate to the body of a satellite that the same manipulator would be mounted to. This is shown in Figure 2.3.

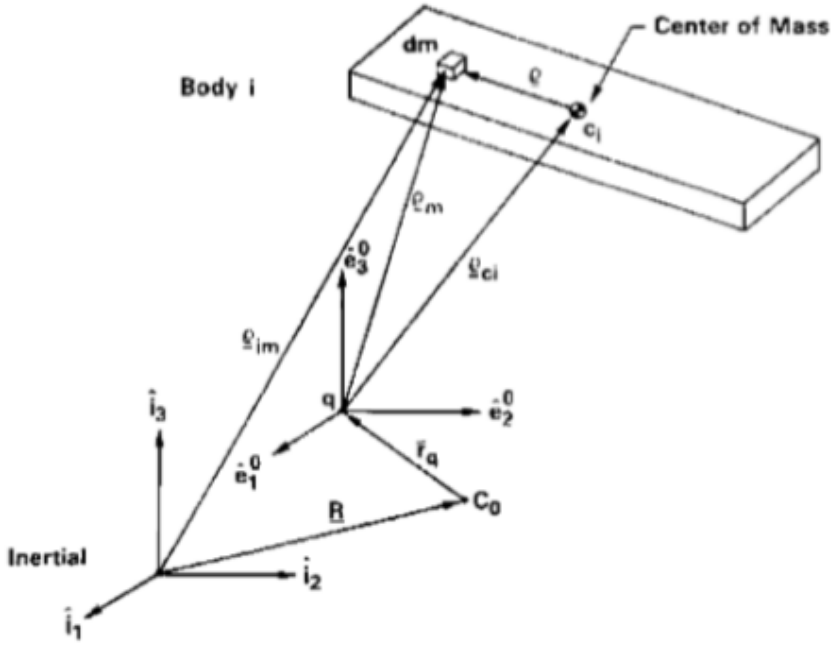

Figure 2.3: Vector Definitions giving locations for the center of mass of each body in 2.1 [50]

From figure 2.3, we can see that vectors are defined to be the values in Table 2.2:

Table 2.2: Longman's Vector Definitions for Figure 2.3

Variable	Definition
m_i	The mass of the ith link relative to the center of mass of the $i-1$ link by the vector r_{ci}
θ_i	The angle between the ith and ith $-$ 1 axes
ρ_{ci}	A vector from point q in the center of bearings for the robot base to the center of mass of the ith link
ρ_m	A vector from point q in the center of bearings for the robot base to the center of mass of the dm
ω^{i0}	Inertial angular velocity of body i
$\mathbf{I}^{ci}$	the inertia dyadic of body i about its center of mass
$\mathbf{M}_f^q$	the sum of moments applied by the base to the robot through the bearings and of the moments applied by the motor mounted in the base, which turns the first link through angle θ_1 assuming that the bearings are frictionless
q	The point chosen to be the inertially fixed frame in the center of the bearings of the base joint
$\mathbf{I}^{ci}$	The inertia dyadic of body i about its center of mass

Longman then considers the total angular moment of the system about the point q in the center of the bearings of the base joint. This is given by the following equation:

$$\mathbf{H}^q = \int_{\text{all bodies}} \rho^m \times \frac{{}^0\partial \rho_m}{\partial t} = \sum_{i=1}^{N} \int_{\text{body } i} \left(\rho^m \times \frac{{}^0\partial \rho_m}{\partial t} \right) dm \tag{2.6}$$

were the pre-superscript on the derivative indicates a vector derivative as seen in the $\hat{e}^0$ coordinates, which are inertial by definition. It is also noted by Longman that $\rho_m = \rho_{ci} + \rho$ and using the fact that the integral over body i of ρdm is zero by definition of the center of mass of the body, it can be seen that the following equation holds true [50]:

$$\begin{aligned}\mathbf{H}^q &= \sum_{i=1}^{N}\left\{m_i\rho_{ci}\times\frac{{}^0\partial\rho_{ci}}{\partial t}+\int_{\text{body } i}\left(\rho\times\frac{{}^0\partial\rho}{\partial t}\right)dm\right\} \\ &= \sum_{i=1}^{N}\left\{m_i\rho_{ci}\times\frac{{}^0\partial\rho_{ci}}{\partial t}+\int_{\text{body } i}\rho\times\left(\frac{{}^i\partial\rho}{\partial t}+\omega^{i0}\times\rho\right)dm\right\}\end{aligned} \tag{2.7}$$

where ω^{i0} is the angular velocity of a coordinate frame fixed in the ith body relative to the $\hat{e}^0$ frame. Longman then simplifies 2.7 by noting that the integral of ρdm over body i is zero and that the $\frac{{}^0\partial\rho}{\partial t}$ term disappears. Using the inertia dyadic I^{ci} eqn 2.7 can be rewritten to the following equation:

$$\mathbf{H}^q = \sum_{i=1}^{N}\left\{m_i\rho_{ci}\times\frac{{}^0\partial\rho_{ci}}{\partial t}+\mathbf{I}^{ci}\cdot\omega^{i0}\right\} \tag{2.8}$$

The derivative of eqn 2.6 is then taken to get the following equation:

$$\begin{aligned}\frac{{}^0\partial\mathbf{H}^q}{\partial t} &= \frac{{}^0\partial}{\partial t}\int_{\text{all bodies}}\left\{\rho_m\times\frac{{}^0\partial\rho_m}{\partial t}dm\right\} \\ &= \int_{\text{all bodies}}\left\{\rho_m\times\frac{{}^0\partial^2\rho_m}{\partial t^2}dm\right\}\end{aligned} \tag{2.9}$$

By definition the second derivative of ρ_m is the inertial acceleration because ρ_m is a position vector from an inertially fixed point q. With this information Longman notes that since the inertial acceleration is multiplied by the mass dm we get a force term $d\mathbf{F}$ that is the total force on the differential mass element. [50] This leads to the following equation:

$$\frac{{}^0\partial\mathbf{H}^q}{\partial t} = \int_{\text{all bodies}}\{\rho_m\times d\mathbf{F}\} = \mathbf{M}_f^q \tag{2.10}$$

where $\mathbf{M}_f^q$ is the sum of all moments about q of the forces applied to all bodies in the system. With the observation that the forces from one link to the next are all internal to the system of bodies and therefore cancel because of Newton's Third Law. Longman concludes that $\mathbf{M}_f^q$ is therefore the sum of all *external* moments on the system of rigid bodies. In the case of this system, the external forces are only the moments exerted on the robot by the fixed base inclusive of all the motor applied torques. The only motor that is considered to be inertially mounted is the motor that turns the first link through angle θ_1 in the robot base. Since Longman is only considering the satellite problem the moments caused by gravitational forces are ignored as they do not apply in this problem. By differentiation of the right side of eqn 2.8 and equating to $\mathbf{M}_q^f$, Longman got the final expression for the bearing moments applied to the robot at its base for an inertially fixed base. This is shown in the following equation:

$$\sum_{i=1}^{N} \left\{ m_i \rho_{ci} \times \frac{{}^0\partial^2 \rho_{ci}}{\partial t^2} + \frac{{}^0\partial}{\partial t} \left(\mathbf{I}^{ci} \cdot \omega^{i0} \right) + \omega^{i0} \times \left(\mathbf{I}^{ci} \cdot \omega^{i0} \right) \right\} = \mathbf{M}_f^q \tag{2.11}$$

using the vector definitions in Table 2.2. Expounding on this equation, Longman notes that $\mathbf{M}_f^q$ being the sum of all moments applied by the base to the robot through the bearings and the moments applied by the motor mounted in the base, which turns the first link through angle θ_1 assuming that the bearings are frictionless. [50] Longman then notes that $\mathbf{M}_f^q$ is therefore the sum of the moments plus the commanded joint 0 motor torque that we would like to react with the reaction wheels.

In order to determine the forces transmitted to the robot through the base joint bearings, Longman then takes the rigid-body sum of the forces on the system from Newton's Law $F = ma$.

This is shown in the following equation:

$$\sum_{j=1}^{N} \mathbf{F}_j = \sum_{j=1}^{N} m_j \frac{{}^0\partial^2 \rho_{ci}}{\partial t^2} \tag{2.12}$$

$$\mathbf{F}_f = \frac{{}^0\partial^2}{\partial t^2} \sum_{j=1}^{N} m_j \rho_{ci} \tag{2.13}$$

$\mathbf{F}_f$ in eqn 2.13 are the desired forces at the base because they are the only external forces, and as such all the internal forces cancel out within the summation.

Equations 2.10 2.11 2.13 are then used to begin an example of application for calculation of the direct base moment and force for a satellite mounted robot. Up to this point Longman has been using the assumption that the base is fixed in an inertial frame. With this example, Longman then goes on to show how the equations change when the base is mounted on a free-floating satellite. The first step is to reexamine the development of eqn 2.11. In this new case we are still interested in the angular momentum of the system $\mathbf{H}^q$ about the point q in the center of the bearings of the base joint. The difference now is that point q is no longer fixed in an inertial frame. This means that equation 2.9 is still valid but that equation 2.10 must be updated as ρ_m is no longer a position vector from an inertially fixed point. This means that the following equation is now valid with reference to figure 2.3:

$$\begin{aligned} \frac{{}^0\partial \mathbf{H}^q}{\partial t} &= \sum_{i=1}^{N} \int_{\text{body } i} \rho_m \times \frac{{}^0\partial^2}{\partial t^2} \left(\rho_{im} - \mathbf{R} - \mathbf{r}_q \right) \partial m \\ &= \sum_{i=1}^{N} \int_{\text{body } i} \rho_m \times \partial \mathbf{F} - \left(\sum_{i=1}^{N} \int_{\text{body } i} \rho_m \partial m \right) \times \frac{{}^0\partial^2 \mathbf{R}}{\partial t^2} \\ &= \mathbf{M}_s^q - \left(\sum_{i=1}^{N} m_i \rho_{ci} \right) \times \frac{{}^0\partial^2 \mathbf{R}}{\partial t^2}, \end{aligned} \tag{2.14}$$

and by using the definition of R_{cs} Longman obtains the following equation:

$$\frac{{}^0\partial \mathbf{H}^q}{\partial t} = \mathbf{M}_s^q - \left[m_{0N}\left(\mathbf{R}_{CS} - \mathbf{R}\right) - m_{1N}\mathbf{r}_q\right] \times \frac{{}^0\partial^2 \mathbf{R}}{\partial t^2} \tag{2.15}$$

where in this case the subscript of s is used to indicate moments in the satellite mounted case for the robot manipulator. Reevaluation of the base constraint forces and summing of Newton's Law for the motion of the center of mass of each rigid body in the system gives the constraint forces for the satellite mounted case. These forces at the base of the robot are the only external forces. This is shown in the following equation:

$$\begin{aligned} \mathbf{F}_s &= \frac{{}^0\partial^2}{\partial t^2}\left[\sum_{i=1}^{N} m_i\left(\mathbf{R} + \mathbf{r}_q + \rho_{ci}\right)\right] \\ &= m_{1N}\frac{{}^0\partial^2 \mathbf{R}}{\partial t^2} + \sum_{i=1}^{N} m_i \frac{{}^0\partial^2 \rho_{ci}}{\partial t^2}, \end{aligned} \tag{2.16}$$

with the understanding that ${}^0\partial^2\mathbf{R}/\partial t^2$, the acceleration of the center of mass of the satellite, is equal to zero we can see that the following equation holds true:

$$\begin{aligned} \frac{{}^0\partial^2}{\partial t^2}\left[m_0\mathbf{R} + m_{1N}\left(\mathbf{R} + \mathbf{r}_q\right) + \sum_{i=1}^{N} m_i\rho_{ci}\right] &= 0, \\ m_{0N}\frac{{}^0\partial^2 \mathbf{R}}{\partial t^2} &= -\sum_{i=1}^{N} m_i \frac{{}^0\partial^2 \rho_{ci}}{\partial t^2}, \end{aligned} \tag{2.17}$$

Longman then substitutes to get the following equation for $\mathbf{F}_s$:

$$\mathbf{F}_s = \left(\frac{-m_{1N}}{m_{0N} + 1}\right)\sum_{i=1}^{N} m_i \frac{{}^0\partial^2 \rho_{ci}}{\partial t^2} \tag{2.18}$$

With this equation and combining the results, Longman proposes a robot as follows in Theorem 1 following the vector definitions in Figures 2.1 and 2.2:

Theorem 1 *Consider a robot consisting of N rigid bodies mounted on a satellite in free space. Let $\mathbf{M}_s^q$ be the moments (about a point q in the center of the bearings of the base joint) exerted by the satellite on the robot including the motor torque applied, and let $\mathbf{F}_s$ be the forces exerted by the satellite on the robot through the bearings. Then $\mathbf{M}_s^q$ and $\mathbf{F}_s$ can be computed for any prescribed robot joint motions from the equations [50]*

From this proposed robot construction we can see that the sum of the moments and forces transmitted to the robot through the base joint bearings are $\mathbf{M}_f^q$ and $\mathbf{F}_\mathrm{f}$ respectively. $\mathbf{M}_s^q$ and $\mathbf{F}_s$, therefore follow as the moment and force for exerted by the spacecraft on the robot through the robot bearings are then given by the following equations:

$$\mathbf{M}_s^q = \sum_{i=1}^{N} \left\{ m_i \rho_{ci} \times \frac{{}^0d^2\rho_{ci}}{dt^2} + \frac{{}^0d}{dt}\left(\mathbf{I}^{ci}\cdot\omega^{i0}\right) + \omega^{i0}\times\left(\mathbf{I}^{ci}\cdot\omega^{i0}\right)\right\} + \left[m_{0N}\left(\mathbf{R}_{CS}-\mathbf{R}\right) - m_{1N}\mathbf{r}_q\right]\times\frac{{}^0d^2\mathbf{R}}{dt^2} \quad (2.19)$$

and

$$\mathbf{F}_s = \frac{m_0}{m_{0N}}\sum_{i=1}^{N} m_i \frac{{}^0\mathrm{d}^2\rho_{ci}}{\mathrm{dt}^2} \quad (2.20)$$

where

Table 2.3: Variable definitions for eqns 2.19 and 2.20

Variable	Definition
m_{ij}	the distances between the center of mass of the ith link and the center of mass of the jth link
$\mathbf{R}$	the vector from the inertially fixed frame to the center of mass of the satellite C_0
$\mathbf{R}_{CS}$	the vector from the inertially fixed frame to the center of mass of the system
$\mathbf{F}_s$	the forces exerted by the satellite on the robot through the bearings
$\mathbf{M}_s^q$	The sum of moments, about a point q in the center of the bearings of the base joint, exerted by the satellite on the robot including the motor torque applied

Corollary 1.1 *Let the moments and forces transmitted to the robot through the base joint bearings be* $\mathbf{M}_f^q$ *and* $\mathbf{F}_\mathrm{f}$ *when the base is inertially fixed and* $\mathbf{M}_s^q$ *and* $\mathbf{F}_s$ *when it is mounted on a free-flying satellite whose attitude is held constant. [50] Then*

$$\mathbf{M}_s^q = \mathbf{M}_f^q + \left[m_{0N}\left(\mathbf{R}_{CS} - \mathbf{R}\right) - m_{1N}\mathbf{r}_q\right] \times \frac{{}^0d^2\mathbf{R}}{dt^2},$$

$$\mathbf{F}_s = \left(\frac{m_0}{m_{0N}}\right)\mathbf{F}_f \tag{2.21}$$

with eqn 2.22 resulting from the conclusion that the reaction moment compensation commands for the three orthogonally mounted reaction wheels are the same as the components of the orthogonal components of moment $\mathbf{M}_r$ that causes the cum of moments about c_0 to be zero.

$$\mathbf{M}^{ci} = 0 = \mathbf{M}_r - \mathbf{M}_s^q - \mathbf{r}_q \times \mathbf{F}_s \tag{2.22}$$

$$\mathbf{M}_r = \mathbf{M}_s^q + \mathbf{r}_q \times \mathbf{F}_s \tag{2.23}$$

where $\mathbf{M}_s^q$ and $\mathbf{F}_s$ are given in Eqns. 2.19 and 2.20. When applying reaction moment compensation, equation 2.23 can be used to calculate the command for the reaction wheels needed to cancel out all attitude disturbances to the satellite that result from motions of the robotic system. Longman's definition of equations is limited in scope in that only moments within the system are accounted for in the dynamics. Reaction moment compensation places strict limits on a real world system that may not strictly follow a commanded path buy may instead use an interpolated path or have errors in path following. The limitation is that not only must the commanded and followed paths be close but the first and second derivatives of the these paths must also be close so that the moments can be reacted. Following a loosely interpolated path may lead to incorrect force being reacted and therefore adding unaccounted for moments to the system. Additionally, this method will not extend to allow translation of the spacecraft to an object in order to grapple. It is assumed that any payload is already grappled and Inertia and mass of payload are known. Furthermore, Makes the assumption that all external forces to the system are known and rigidly attached to, and act upon the manipulator tool tip. A final significant limitation of the reaction moment compensation method is that the spacecraft and manipulator system must be a free-floating system and not free-flying. [50] Translation of the spacecraft system may happen because of motion of the manipulator, however it is not tracked within the dynamics of the system.

2.1.2 Virtual Manipulator

Here we begin with the assumptions that are made by Vafa and Dubowsky [49], [51]–[53] for spacecraft with a rigidly attached serial robotic manipulator in order to construct the equations

for the manipulator and spacecraft system. They make the assumptions that there are no external forces or torques acting on the system and that the parts of the system can be modeled as rigid bodies. A pair of concepts called the virtual manipulator and virtual ground were developed to explain the dynamics of the two systems. A virtual manipulator that is a massless kinematic chain and the virtual ground is an imaginary point in the inertial space of the system that is the point that the virtual manipulator base is attached to. This virtual ground is defined as the center of mass of the complete manipulator and spacecraft system. [49] Under the previously stated assumptions the virtual ground will not move in the inertial space of the system. A significant advantage of this method is that it has the ability to describe motions of the complex system using relatively simple calculations compared to the original system. [53]

As such, the virtual manipulator was developed as a method for planing the dynamics of a spacecraft manipulator system. Such a need arose as at the time there were two methods seen as viable for controlling a free-floating system. The first was to perform the motion with the robotic manipulator and then use a reaction control system to react the moments of the system to maintain desired orientation. The second option was envisioned as a method to plan the motions of the manipulator such that the motion of the spacecraft moments and forces could be minimized. [49] The virtual manipulator is defined as a massless kinematic chain that is attached to the virtual ground. The virtual ground is defined to begin at the center of mass of the complete manipulator and spacecraft system. Under the previously stated assumptions the virtual ground will not move in the inertial space of the system. Nor will the virtual ground move from internal forces such as joint torques, friction, or motions of the manipulator. A significant advantage of this method is that it has the ability to describe motions of the complex system using relatively simple calculations compared to other Newton-Euler methods. [53] Vafa then shows that the

following properties of the virtual manipulator hold true for the system as copied from [49] to maintain clarity.

- Virtual manipulator link lengths remain constant as the manipulator moves.
- The joint between the 1^{st} virtual link and the VG is spherical; the rotations of this joint are equal to the rotations of the spacecraft with respect to inertial space.
- The axis of the i^{th} virtual joint is always parallel to the i^{th} axis of the real system joint.
- The amount of rotation of the i^{th} virtual revolute joint is equal to the rotation of the i^{th} revolute joint of the real system. The displacement of VM prismatic joints are easily calculated from the actual prismatic displacement [53].

We see here in figures 2.4 and 2.5 examples of constructed virtual manipulators for a 2 link planar robot and an N-Link robot system.

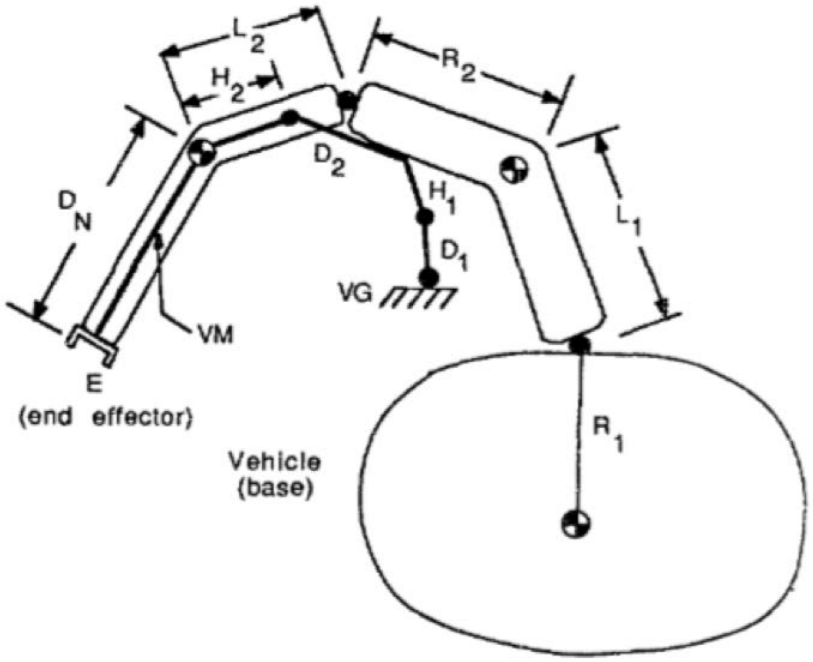

Figure 2.4: A 2 Link Planar Manipulator Arm with Base and End-Effector VM [49]

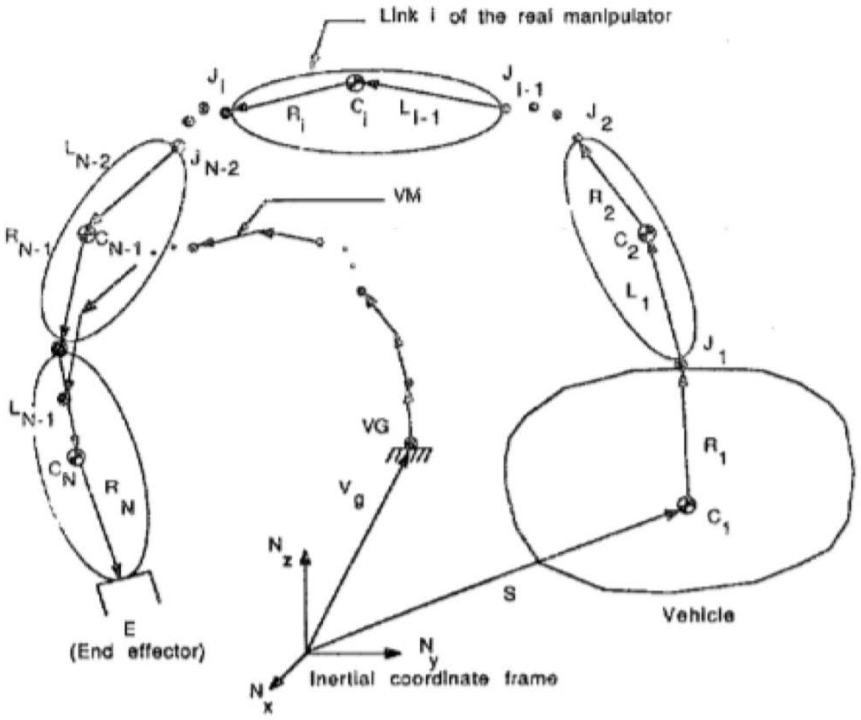

Figure 2.5: A N-Link Manipulator Arm with Base and End-Effector VM [49]

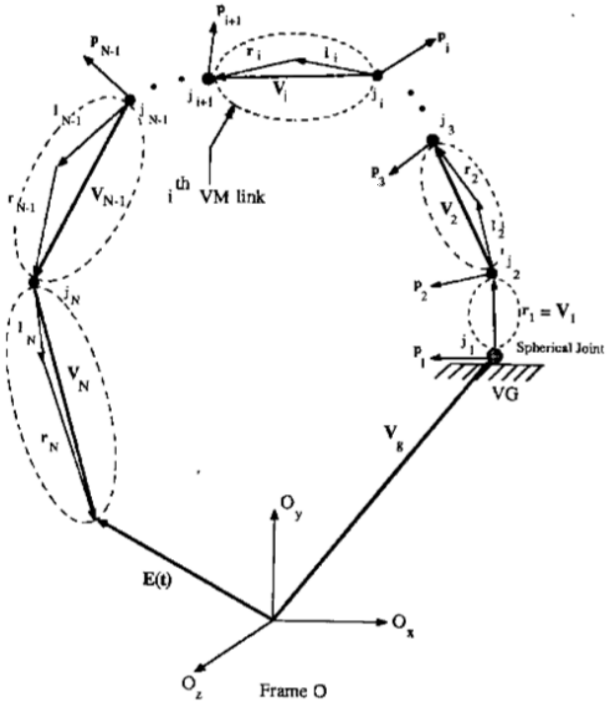

Figure 2.6: A N-Link virtual manipulator for the Real Manipulator in Figure 2.5 [52]

In order to understand these figures and the equations, a table of variable descriptions is presented below.

Table 2.4: Variable definitions for the virtual manipulator [49] [52]

Variable	Definition
$\mathbf{P}_i$	The unit vector representing the axis of rotation (θ_i) or the axis of linear extension (T_i) for the J_ith joint
J_1	A free joint that can rotate about and translate parallel to three orthogonal directions in space. It is located at the spacecraft center of mass [52]
T_i	The linear displacement of joint J_i
θ_i	The rotational angle of joint J_i
$\mathbf{M}_i$	The mass of the i^{th} body
C_i	The center of mass of the i^{th} body
$\mathbf{R}_i$	The vector from C_i to J_{i+1}
$\mathbf{L}_i$	The vector from J_i to C_i
$\mathbf{R}_N$	The vector from C_N to the end effector
$\mathbf{S}(o)$	The vector to the N^{th} body's CoM $\mathbf{S}(t)$ w.r.t. to Frame O at the initial time
$\mathbf{S}(t)$	The vector to the N^{th} body's CoM $\mathbf{S}(t)$ w.r.t. to Frame O at time t
$\mathbf{V}_g$	The vector to the virtual ground at the center of mass of the entire system from the inertial frame O
$\mathbf{E}(t)$	Vector from the inertial frame O to the end effector at time t

Where the vectors $\mathbf{R}_i$, $\mathbf{L}_i$, and $\mathbf{P}_i$ are fixed in the frame of the ith body. [52]

The virtual manipulator is an idealized manipulator with its base at the virtual ground. The manipulator can be constructed such that the end point of the kinematic chain terminates at some arbitrary point on the real manipulator, with this arbitrary point almost always being chosen to terminate at the end-effector of the manipulator.

$$\mathbf{V}_g = \sum_{i=1}^{N} \left[\mathbf{S}(o) - \sum_{q=i}^{N-1} \left(\mathbf{R}_q(o) + \mathbf{L}_{q+1}(o) \right) \right] M_i / M_{tot} \tag{2.24}$$

where $M_{tot} = M_1 + M_2 + ... + M_N$ is the total mass of the system and $\mathbf{S}(o)$ is the vector from the virtual ground to the center of mass of the entire system. [53]

$$\begin{aligned} \mathbf{V}_1 &= \mathbf{r}_1 \\ \mathbf{V}_i &= \mathbf{r}_i + \mathbf{l}_i \quad i = 2, \ldots, N \end{aligned} \tag{2.25}$$

Where

$$\mathbf{r}_i = \mathbf{R}_i \sum_{q=i}^{i} \frac{M_q}{M_{tot}} \tag{2.26}$$

$$\mathbf{l}_i = \mathbf{L}_i \sum_{q=i}^{i} \frac{M_q}{M_{tot}} \tag{2.27}$$

As such it can be seen that the initial end-effector position is given by the following equation:

$$\mathbf{E}(o) = \mathbf{V}_g + \mathbf{V}_1(o) + \mathbf{V}_2(o) + ... + \mathbf{V}_N(o) \tag{2.28}$$

with prismatic joints being represented as virtual prismatic joints with the following equation:

$$\tau_i = \mathbf{T}_i \sum_{q=i}^{i-1} \frac{M_q}{M_{tot}} \tag{2.29}$$

If all the parts of the virtual manipulator are constructed as defined in equations 2.24 through 2.29 then the virtual manipulator will have the same end-effector pose as the real manipulator. [52]. Vafa proves that the following properties will also hold true for the virtual manipulator as seen below:

- The axis of the i^{th} virtual joint, p_i, is always parallel to the i^{th} axis of the real system joint, P_i. [52]

- The virtual manipulator end point will always coincide with the end-effector of the real

manipulator. [52]

- The change in orientation of the real manipulator end-effector is identical to the change in orientation of the virtual manipulator end-effector. [52]

With this Vafa has proven that the kinematic and dynamic motions of the space manipulator system can be calculated from the motions of the virtual manipulator with its base at the stationary virtual ground. [52] As such the significantly simpler fixed base virtual manipulator can be used to calculate the motions of the complex system with a moving base. The use of virtual manipulators for arbitrary points along the real manipulator. Vafa uses the construction of the system equations of motion using virtual manipulators for arbitrary points. The causes the equations to be updated to take into account the position of the point of interest in the manipulator. Finally, Vafa extends the virtual manipulator to, multi-arm systems and closed chain systems, as well as workspace analysis for the manipulator systems. [49], [52], [53]

The virtual manipulator approach has some significant advantages over the previous purely Newton-Euler methods that came before it. First and foremost, the construction of the virtual manipulator is such that the virtual manipulator base remains fixed in the inertial space. This greatly simplifies the manipulator inverse kinematics and allows for a significant decrease in the complexity of calculation for the equations of motion for the system. Additionally, the virtual manipulator is useful for workspace analysis for a free-floating vehicle as well as for some path-planning tasks, such as disturbance minimization to maintain antenna pointing. [49]

Although the virtual manipulator is a valid and kinematically elegant method for the representation of spacecraft manipulator dynamics, it has several limitations for its use for the calculation of inertia parameters for a unknown payload. The first major limitation is that the location of

the virtual ground is defined as the center of mass of the system. If one does not know the mass of the grappled payload, then at best it is a guess where the virtual ground should be and accept error in the motion of the system. This might be able to be corrected for with a controller, but it is not a trivial problem. The second limitation is that the virtual manipulator is defined such that it is assumed the no external forces act on the system, or that duration of the manipulator motion is short enough that external forces like gravity gradients or solar wind pressure among others can be treated as negligible and therefore ignored. [52]

2.1.3 Barycentric Vector Approach

Evangelos Papadopoulos approached the same problem of a coupled dynamical system of spacecraft and serial manipulator by analyzing the barycenter using Lagrangian methods. [54] He made the same assumptions of a free-floating system, with no external forces acting on the system. In his dissertation he demonstrates the existence of dynamic singularities which are functions of the mass and inertia properties of the system. These dynamic singularities cause traditional inverse Jacobian based controllers to fail and transposed Jacobian methods to develop large errors [55] He develops methods of identifying two workspaces of the spacecraft system. *Path Dependent Workspaces* and *Path Independent Workspaces* are explored with the former being all points in the workspace that could lead to a path dependent singularity of the non-holonomic system and the later *Path Independent Workspace* that contains all the points in the workspace that will not lead to a dynamic singularity.

Figure 2.7 shows a free-floating manipulator-spacecraft system. The system is assumed to be free-floating and the only forces acting on the system are the internal forces of the manipulator

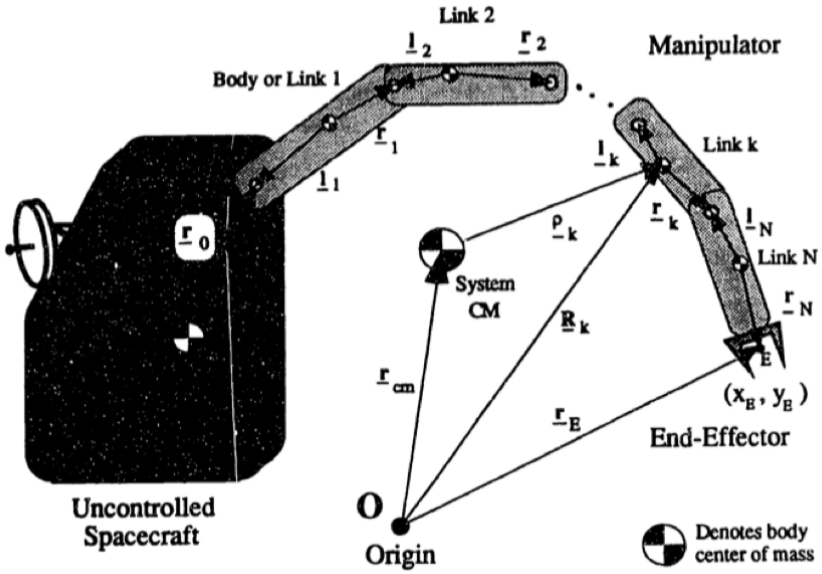

Figure 2.7: Free-Floating spatial robotic manipulator [55]

and the spacecraft.

Papadopoulos uses a Lagrangian approach to develop the equations of motion for the system as it simplifies the structure of the equations of motion.[55] We can see from Figure 2.7 that for a system without external forces for a free-floating manipulator-spacecraft system, the fixed origin **O** can have a vector to an arbitrary point m on body k denoted as $\mathbf{R}_{k,m}$. [56]

$$\mathbf{R}_{k,m} = \mathbf{r}_{cm} + \sum_{i=0}^{N} \mathbf{v}_{ik,m} \tag{2.30}$$

where vector $\mathbf{v}_{ik,m}$ is defined as:

$$\mathbf{v}_{ik,m} \equiv \mathbf{v}_{ik} + \delta_{im}\mathbf{r}_{k,m} \tag{2.31}$$

with δ_{im} being the Kronecker delta function. [56] The vectors $\mathbf{v}_{ik}$ are the barycentric vectors that are defined as:

$$\mathbf{v}_{ik} \equiv \begin{cases} \mathbf{r}_i^* = \mathbf{r}_i - \mathbf{c}_i, & i < k \\ \mathbf{c}_i^* = -\mathbf{c}_i & i = k \\ \mathbf{l}_i^* = \mathbf{l}_i - \mathbf{c}_i & i > k \end{cases} \tag{2.32}$$

where

$$\mathbf{c}_i = \mathbf{l}_i \sum_{j=0}^{i-1} \frac{m_i}{\mathbf{M}} + \mathbf{r}_i \left(1 - \sum_{j=0}^{i} \frac{m_i}{\mathbf{M}}\right) \quad i = 0, \ldots, N \tag{2.33}$$

These vectors are shown in Figure 2.8 [57] and Figure 2.9 [55].

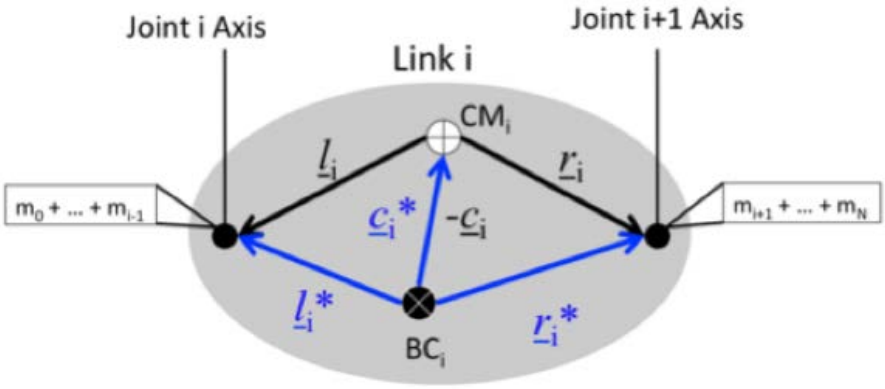

Figure 2.8: Barycenter of link i with related vectors [57]

Using the labels from Figure 2.9 we can define the following terms from Papadopoulos in table 2.5. [55]

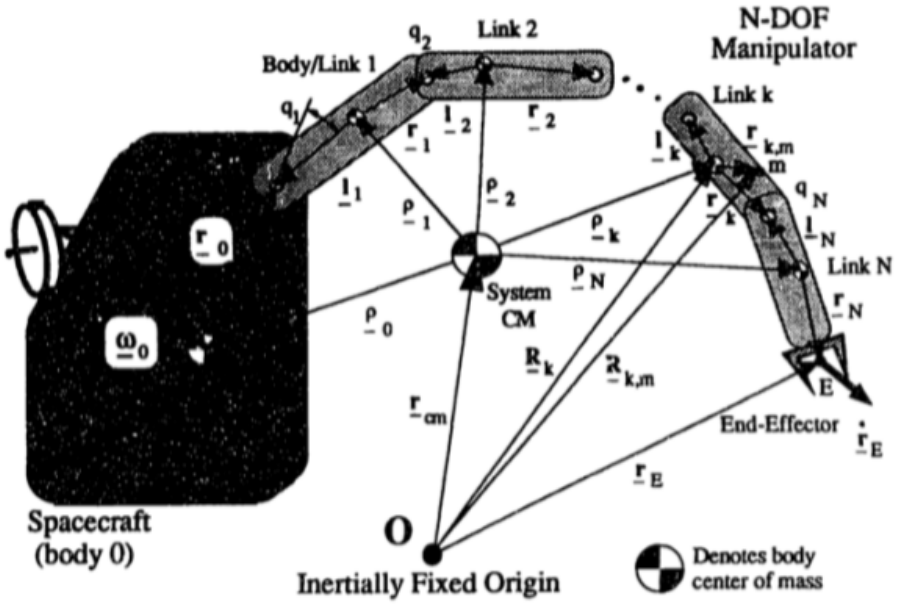

Figure 2.9: Free Floating Spatial robotic manipulator with vectors labeled [55]

Variable	Definition
m_k	The Mass of the k^{th} Link of the robot
I_k	The Rotational inertia of the k^{th} link about it's CoM
O_k	The Origin of the k^{th} joint's coordinate system co-located at the point of rotation for the joint
$\underline{r}_{cm}$	The position of the system CoM in the inertial frame
$\underline{\rho}_k$	The k^{th} link's CoM with respect to the system center of mass
$\underline{l}_k$	The vector from the k^{th} link's CoM to its preceding ("left") joint, toward the base vehicle the base vehicle
$\underline{c}_k$	The vector from the k^{th} link's CoM to its barycenter
$\underline{\mathbf{p}}$	The total linear momentum of the system
$\underline{\mathbf{p}}_0$	The constant total linear momentum for the system with no external forces
$\underline{\dot{r}}_{\text{cm}}$	The velocity of the CoM from the origin
$\mathbf{M}$	Total Mass of the system

Table 2.5: Variable definitions for the barycentric vector approach [55]

The dynamics of the system can be described as a function of potential energy using the aforementioned Lagrangian method. The potential energy of the system is given by the following equation:

$$T = \frac{1}{2}\dot{\boldsymbol{z}}_0^{\top}\mathbf{H}^{+}(\mathbf{q})\dot{\boldsymbol{z}}_0 \tag{2.34}$$

where $\mathbf{H}^{+}(\mathbf{q}) \in \mathbb{R}^{(N+6)\times(N+6)}$ is the positive definite symmetric matrix of the inertia matrix of the system.

$$\mathbf{H}^{+}(\mathbf{q}) = \begin{bmatrix} \mathbf{M1} & \mathbf{0} & \mathbf{0} \\ \mathbf{0} & {}^{0}\mathbf{D}(\mathbf{q}) & {}^{0}\mathbf{D}_{\mathbf{q}}(\mathbf{q}) \\ \mathbf{0} & {}^{0}\mathbf{D}_{\mathbf{q}}(\mathbf{q})^{\mathrm{T}} & {}^{0}\mathbf{D}_{\mathbf{qq}}(\mathbf{q}) \end{bmatrix} \tag{2.35}$$

where $\mathbf{1}$ is the 3×3 unit matrix, ${}^{0}\mathbf{D} \in \mathbb{R}^{3\times3}$ is the system inertia matrix with respect to the system CoM and is a positive definite matrix. ${}^{0}\mathbf{D}_{\mathbf{q}\in\mathbb{R}^{3\times N}}$ and ${}^{0}\mathbf{D}_{\mathbf{qq}} \in \mathbb{R}^{N\times N}$ are defined as: [56]

$$\begin{aligned} {}^{0}\mathbf{D}_{j} &\equiv \sum_{i=0}^{N} {}^{0}\mathbf{D}_{ij} \quad (j = 0, \cdots, N) \\ {}^{0}\mathbf{D} &\equiv \sum_{j=0}^{N} {}^{0}\mathbf{D}_{j} \\ {}^{0}\mathbf{D}_{\mathbf{q}} &\equiv \sum_{j=1}^{N} {}^{0}\mathbf{D}_{j}\,{}^{0}\mathbf{F}_{j} \\ {}^{0}\mathbf{D}_{\mathbf{qq}} &\equiv \sum_{j=1}^{N} {}^{0}\mathbf{F}_{i}^{\top}\,{}^{0}\mathbf{D}_{j}\,{}^{0}\mathbf{F}_{j} \end{aligned} \tag{2.36}$$

with ${}^{0}\mathbf{D}_{ij}$ being functions of the barycentric vectors and the inertia of the system. [55], [56]

$${}^{0}\mathbf{D}_{ij} \equiv \left\{ \begin{array}{ll} -\mathbf{M}\left\{\left({}^{0}\mathbf{l}_{j}^{*\top}\,{}^{0}\mathbf{r}_{i}^{*}\right)\mathbf{1} - {}^{0}\mathbf{l}_{j}^{*}\,{}^{0}\mathbf{r}_{\mathrm{i}}^{*\top}\right\} & \mathrm{i} < \mathrm{j} \\ {}^{0}\mathbf{I}_{i} + \sum_{\mathrm{k}=0}^{N} m_{k}\left\{\left({}^{0}\mathbf{v}_{ik}^{\top}\,{}^{0}\mathbf{v}_{ik}\right)\mathbf{1} - {}^{0}\mathbf{v}_{ik}\,{}^{0}\mathbf{v}_{ik}^{\top}\right\} & \mathrm{i} = \mathrm{j} \\ -\mathbf{M}\left\{\left({}^{0}\mathbf{r}_{j}^{*\top}\,{}^{0}\mathbf{l}_{i}^{*}\right)\mathbf{1} - {}^{0}\mathbf{r}_{j}^{*}\,{}^{0}\mathbf{l}_{i}^{*\top}\right\} & \mathrm{i} > \mathrm{j} \end{array} \right\} \tag{2.37}$$

Finally, Papadopoulos states that it can be shown that if τ is an $N\times1$ vector of joint torques

acting at the joints of the manipulator, that ${}^0\mathbf{f}_{k,m}$ and ${}^0\mathbf{n}_{k,m}$ are the force and torque vectors acting on point m of the k^{th} body, as measured from the spacecraft. [56] $\mathbf{Q}$ is the $(N+6)\times 1$ vector of generalized forces acting on the system.

$$\mathbf{Q} \equiv \begin{bmatrix} 0 \\ 0 \\ \tau \end{bmatrix} + \sum_{k=0}^{N} \sum_{m} \left\{ {}^0\mathbf{J}^{+}_{k,m}(\mathbf{q}) \right\}^{\mathrm{T}} \begin{bmatrix} {}^0\mathbf{f}_{k,m} \\ {}^0\mathbf{n}_{k,m} \end{bmatrix} \tag{2.38}$$

with ${}^0\mathbf{f}_{k,m}$ and ${}^0\mathbf{n}_{k,m}$ being the force and torque vectors acting on point m of the k^{th} body, as measured from the spacecraft. ${}^0\mathbf{J}^{+}_{k,m}(\mathbf{q})$ is the Jacobian matrix of the system given here without proof. [56]

$${}^0\mathbf{J}^{+}_{k,m}(\mathbf{q}) = \begin{bmatrix} \mathbf{1} & -\sum_{i=0}^{N} \left[{}^0\mathbf{T}_i \, {}^i\mathbf{v}_{ik,m} \right]^{\times} & -\sum_{i=0}^{N} \left[{}^0\mathbf{T}_i \, {}^i\mathbf{v}_{ik,m} \right]^{\times} {}^0\mathbf{F}_i \\ \mathbf{0} & \mathbf{1} & {}^0\mathbf{F}_k \end{bmatrix} \tag{2.39}$$

where $[\quad]^{\times}$ denotes the cross product skew-symmetric matrix [58], $\mathbf{0} \in \mathbb{R}^{3\times(N-k)}$ is the zero element matrix, $\mathbf{F}_k$ is defined in eqn 2.40, and ${}^0\mathbf{T}_i$ is the transformation matrix from the i^{th} body to the inertial frame. [56]

$${}^0\mathbf{F_k} \equiv \left[{}^0\mathbf{T}_1 \, {}^1\mathbf{u}_1, \ldots, {}^0\mathbf{T_k} \, {}^{\mathrm{k}}\mathbf{u_k}, \mathbf{0} \right] \quad \mathrm{k} = 1, \ldots, \mathrm{N} \tag{2.40}$$

with ${}^i\mathbf{u}_i$ being the unit column vector in frame i parallel to the i^{th} revolute joint axis. [56] Papadopoulos uses a Quasi-Lagrangian approach to develop the equations of motion for the system. [55], [58]

$$\mathbf{H}^{+}(\mathbf{q})\ddot{\mathbf{z}}_0 + \mathbf{C}^{+}\left(\mathbf{q}, {}^0\omega_0, \dot{\mathbf{q}}\right) = \mathbf{Q} \tag{2.41}$$

where $\mathbf{C}^{+}$ are the non-linear terms of the equations of motion. Equation 2.41 represents the $N+6$ equations of motion for the free-flying system under the effect of external forces and torques as well as internal actuator torques. [56] The generalized forces $\mathbf{Q}$ are given by equation 2.38 and can be decomposed into the unknown disturbance forces, $\mathbf{Q}_d$, and the known control forces, $\mathbf{Q}_c$. [56]

$$\mathbf{Q} = \mathbf{Q}_c + \mathbf{Q}_d \tag{2.42}$$

where the control forces are given by the following equation:

$$\mathbf{Q}_c = \mathbf{J}_q^{\top} \begin{bmatrix} {}^0\mathbf{f}_s \\ {}^0\mathbf{n}_s \\ \tau \end{bmatrix} = \begin{bmatrix} \mathbf{1} & -\sum_{i=0}^{N} \left[{}^0\mathbf{T}_i {}^i\mathbf{v}_{i,S}\right]^{\times} & -\sum_{i=0}^{N} \left[{}^0\mathbf{T}_i {}^i\mathbf{v}_{i,S}\right]^{\times} {}^0\mathbf{F}_i \\ \mathbf{0} & \mathbf{1} & {}^0\mathbf{F} \\ \mathbf{0} & \mathbf{0} & \mathbf{1} \end{bmatrix}^{\top} \begin{bmatrix} {}^0\mathbf{f}_s \\ {}^0\mathbf{n}_s \\ \tau \end{bmatrix} \tag{2.43}$$

with $k = 0$ and $m =$ CoM where the subscript S denotes the spacecraft CoM, ${}^0\mathbf{f}_S$ and ${}^0\mathbf{n}_S$ are the force and torque vectors acting on the spacecraft CoM, τ is the vector of joint torques, and $\mathbf{J}_{\mathbf{q}}^{\top}$ is square and by definition invertible. [56]

With the final equation of motion for the system, Papadopoulos go on to demonstrate that the system can be controlled, motion predicted, as well as coordinated control of the spacecraft and the manipulator. [56] The barycentric vector approach has the advantage of being able to predict the motion of the system and control the system. The barycentric vector approach has the disadvantage of being unable to predict the motion of the system when external forces are acting on the system as seen by the untracked $\mathbf{Q}_d$ term of equation 2.42. [55] Regardless, the barycentric vector approach is a valid method for the prediction of the motion of a free-floating

manipulator-spacecraft system. [56]

2.1.4 Base Parameters of Manipulator Dynamic Models

Mayeda begins by introducing a dynamics model for a robotic manipulator. Each manipulator is considered to be a series of connected rigid links attached as a chain by actuated joints. Mayeda, Yoshida, and Osuka demonstrates that each link of a manipulator consists of 10 link parameters.[18] These parameters consist of the mass, center of mass position, the inertia tensor of the link, and the rotation matrix from the current link to the next link. The system is defined to have a coordinate system defined as (x_i, y_i, z_i) for each link i in the as described in figure 2.10 Link 1 is connected by joint 1 to the base which is considered as link 0. The link origin o_i is the intersection of joint i

$$^{i}L_i = [[L_i]^x \, [0] \, [L_i]^z]^\top \tag{2.44}$$

$$^{i}r_i = [[r_1]^x \, [r_i]^y \, [r_i]^z]^\top \tag{2.45}$$

$$^{i}I_i = \begin{bmatrix} [I_i]^x & [I_i]^{xy} & [I_i]^{xz} \\ [I_i]^{xy} & [I_i]^y & [I_i]^{yz} \\ [I_i]^{xz} & [I_i]^{yz} & [I_i]^z \end{bmatrix} \tag{2.46}$$

Where $^{i}L_i$ is the vector to the next link $^{i}r_i$ is the vector to the link CoM and $^{i}I_i$ is the inertia

tensor for the link i. ${}^{i}A_{j}$ is the rotation matrix from link i to link j

$$ {}^{i}A_{j} = \begin{bmatrix} [{}^{i}A_{j}]_{11} & [{}^{i}A_{j}]_{12} & [{}^{i}A_{j}]_{13} \\ [{}^{i}A_{j}]_{21} & [{}^{i}A_{j}]_{22} & [{}^{i}A_{j}]_{23} \\ [{}^{i}A_{j}]_{31} & [{}^{i}A_{j}]_{32} & [{}^{i}A_{j}]_{33} \end{bmatrix} \tag{2.47} $$

Equation 2.47 shows the rotation from (x_i, y_i, z_i) to (x_j, y_j, z_j); it then follows that

$$ i_v = {}^{i}A_{j} j_v \text{ for any vector } v, \tag{2.48} $$

$$ \left({}^{i}A_{j}\right)^{\top} = {}^{j}A_{i}, \tag{2.49} $$

$$ {}^{i}A_{j} = {}^{i}A_{k}\,{}^{k}A_{j} \tag{2.50} $$

for $0 \leq i, j \leq N$, and

$$ {}^{i-1}A_{i} = \begin{cases} \begin{pmatrix} \cos q_i & -\sin q_i & 0 \\ \sin q_i & \cos q_i & 0 \\ 0 & 0 & 1 \end{pmatrix}, \text{if } z_i \text{ is parallel to } z_{i-1} \\ \begin{pmatrix} \cos q_i & -\sin q_i & 0 \\ 0 & 0 & -1 \\ \sin q_i & \cos q_i & 0 \end{pmatrix}, \text{if } z_i \text{ is perpendicular to } z_{i-1} \end{cases} \tag{2.51} $$

for $2 \leq i \leq N$. [18]

With these equations and conventions, Mayeda now has the transforms needed to be able to look at the equations of motion for a system and see the dynamics model for the manipulator

from Lagrange's equations as

$$\frac{d}{dt}\left(\frac{\partial \kappa}{\partial \dot{q}_i}\right) - \frac{\partial(\kappa - \eta)}{\partial q_i} = n_i, \quad i = 1, 2, \ldots, N \tag{2.52}$$

where κ and η are kinetic and potential energy respectively. n_i is the torque about joint i generated by the actuator for joint i. q_i is the angle of joint i and $\dot{q}_i$ and $\ddot{q}_i$ are the first and second time derivatives of the joint angle. [18]

$$n = \begin{bmatrix} n_1 & n_2 & \cdots & n_N \end{bmatrix}^\top \tag{2.53}$$

$$q = \begin{bmatrix} q_1 & q_2 & \cdots & q_N \end{bmatrix}^\top \tag{2.54}$$

$$\dot{q} = \begin{bmatrix} \dot{q}_1 & \dot{q}_2 & \cdots & \dot{q}_N \end{bmatrix}^\top \tag{2.55}$$

$$\ddot{q} = \begin{bmatrix} \ddot{q}_1 & \ddot{q}_2 & \cdots & \ddot{q}_N \end{bmatrix}^\top \tag{2.56}$$

where

$q_i =$ the joint angle of the i^{th} joint

$\ddot{q}_i =$ the first time derivative of q_i

$\ddot{q}_i =$ the first time derivative of q_i

$\eta_i =$ the actuator torque of the i^{th} joint

$N =$ the number of joints in the manipulator

$$M_i = \sum_{j=i}^{N} m_j, \tag{2.57}$$

$$R_i = M_{i+1} L_i + m_i r_i, \tag{2.58}$$

$$J_i = I_i + M_{i+1} \left((L_i \cdot L_i) E - L_i \otimes L_i \right) \tag{2.59}$$

These are the moments of order 0, 1, 2 of link i at point o_i where E is defined as the identity matrix and $\otimes$ as the tensor product. [18] Mayeda makes note of the change of notation to the constants M_i, J_i and R_i in eqn 2.57, 2.59 and 2.58 respectively. As such, equations 2.60 are shown to be constants and are used to simplify the equations of motion for the system. It can be seen that these equations are composed entirely of m_i, ${}^i r_i$, ${}^i I_i$, ${}^i L_i$, and ${}^i R_i$. [18]

$$\begin{aligned} {}^i R_i &= \left[[R_i]^x [R_i]^y [R_i]^z \right]^t, \\ i_{J_i} &= \begin{bmatrix} [J_i]^x & [J_i]^{xy} & [J_i]^{xz} \\ [J_i]^{xy} & [J_i]^y & [J_i]^{yz} \\ [J_i]^{xz} & [J_i]^{yz} & [J_i]^z \end{bmatrix} \end{aligned} \tag{2.60}$$

Mayeda then uses these base parameters to develop the equations of motion for the system using the Lagrangian dynamics model in eqn 2.52. [18] The equations of motion for the system derived to get the following equations of motion for the system.

$$\begin{aligned} \sum_{j=1}^{N} H(i,j) \ddot{q}_j + \sum_{j=1}^{N} \sum_{k=1}^{N} \left(\frac{\partial H(i,j)}{\partial \dot{q}_k} - \frac{\partial H(k,j)}{2 \partial q_i} \right) \dot{q}_k \dot{q}_j \\ -g \cdot \left(z_i \times \sum_{j=i}^{N} R_j \right) = n_i, \quad i = 1, 2, \ldots, N \end{aligned} \tag{2.61}$$

where

$$
\begin{aligned}
H(i,j) &= z_i \cdot \left(\sum_{k=i}^{N} J_k \right) z_j \\
&+ z_i \cdot \left[\sum_{k=i}^{N-1} \left(2 \left(L_k \cdot \sum_{s=k+1}^{N} R_s \right) E - L_k \otimes \sum_{s=k+1}^{N} R_s - \sum_{s=k+1}^{N} R_s \otimes L_k \right) \right] z_j \\
&+ z_i \cdot \left[\left(\sum_{k=j}^{i-1} L_k \cdot \sum_{s=i}^{N} R_s \right) E - \sum_{k=j}^{i-1} L_k \otimes \sum_{s=i}^{N} R_s \right] z_j
\end{aligned}
\tag{2.62}
$$

Finally, Mayeda notes that for the case where $i \geqq j$ the following holds true

$$
H(i,j) = H(j,i) \tag{2.63}
$$

Equation 2.61 can be seen to be the manipulator model for the system, and can be generated if the joint twist angle of joint i to joint $i-1$ axis, the vector to the next joint ${}^{i}L_i$, the vector to the link CoM ${}^{i}r_i$, the inertia tensor for the link ${}^{i}I_i$, and the mass of the link m_i are known for all links $1 \leq i \leq N$. [18] Mayeda notes that it is important that the dynamics equation is able to be determined if $H(i,j)$ and $g \cdot (z_i \times \sum_{j=i}^{N} R_j)$ are given in the form of functions of q_i. Additionally it is noted that the $10N$ link parameters, m_i, $m_i[r_i]^x$, $m_i[r_i]^y$, $m_i[r_i]^z$, $[I_i]^x$, $[I_i]^y$, $[I_i]^z$, are redundant because in certain circumstances the same dynamic equations can be generated for different values of the link parameters. This makes it potentially impossible to determine the link parameters from the motion of the manipulator. [18]

The final note that Mayeda about eqn 2.61 is that the dynamics equations can be determined if $H(i,j)$ and $g \cdot (z_i \times \sum_{j=i}^{N} R_j)$ are given in terms of q_i. [18] Mayeda goes on to show that two sets of link parameters can be used to generate the same dynamics equations if the same $H(i,j)$ and $g \cdot (z_i \times \sum_{j=i}^{N} R_j)$ for $1 \leqq i,j \leqq N$ are used. This is a significant finding as it shows that

the link parameters are could produce the same and are not necessarily unique and that the same dynamics equations can be generated for different values of the link parameters. This makes it potentially impossible to determine the link parameters from the motion of the manipulator. [18]

Mayeda next shows that the following equations are the base parameters for the system in the case (i) that joint axis 1 is not parallel to the gravity vector g.:

$$\begin{aligned} &[J_i]^z + JY(i) \\ &[R_i]^x, [R_i]^y - RZ(c(i)+1, i+1) \end{aligned} \tag{2.64}$$

for $1 \leqq i \leqq N$

$$\begin{aligned} &[J_i]^x - [J_i]^y + JY(i) \\ &[J_i]^{xy} + [L_i]^x \, RZ(c(i)+1, i+1) \\ &[J_i]^{yz} + [L_i]^z \, RZ(c(i)+1, i+1) \\ &[J_i]^{xz} - [L_i]^x \, RZ(c(i), i+1). \end{aligned} \tag{2.65}$$

for $a(2) \leqq i \leqq N$ where

$$JY(i) = \begin{cases} \sum_{v=a(c(i)+1)}^{b(c(i)+1)} \left[[J_v]^y + 2[L_v]^z \sum_{s=v+1}^{b(c(i)+1)} [R_S]^z \right], & i = b(k) \\ 0, & i \neq b(k) \end{cases} \tag{2.66}$$

for $1 \leqq k \leq K-1$

$$RZ(k,i) = \begin{cases} \sum_{s=i}^{b(k)} [R_S]^z, & a(k) \leqq i \leqq b(k) \\ 0, & i < a(k) \text{ or } i > b(k) \end{cases} \tag{2.67}$$

for $1 \leqq k \leqq K-1$ [18]

In the case (ii) that the first joint axis is parallel to the gravity vector g, the terms $[R_1]^x$ and $[R_1]^y - RZ(2,2)$ should be removed from the parameters in eqn 2.64. The total number of base parameters are then $7N - 4B$ for case (i) and $7N - 4B - 2$ for case (ii) where B is the number of links in the first link cluster. [18]

Additionally, adjacent parallel links are divided from perpendicular links into "link Clusters". $a(1) = 1 < a(2) < a(3) < \cdots < a(K)$ are the joint numbers such that the joint axis $a(i)$ is perpendicular to joint axis $a(i-1)$. $b(i) = a(i+1) - 1$ for $1 \leqq i \leqq K - 1$ and $b(K) = N$ is defined such that links $a(i), a(i+1), \cdots, b(i)$ make up link cluster i with link clusters $i - 1$ and i are connected by joint $a(i)$. The manipulator is said to have K link clusters. Additionally, when a link i is included in link cluster k it is defined $c(i)$ as $c(i) = k$. The final assumption is that $[L_i]^x \neq 0$ for $1 \leqq i \leqq b(1) - 1$ [18]

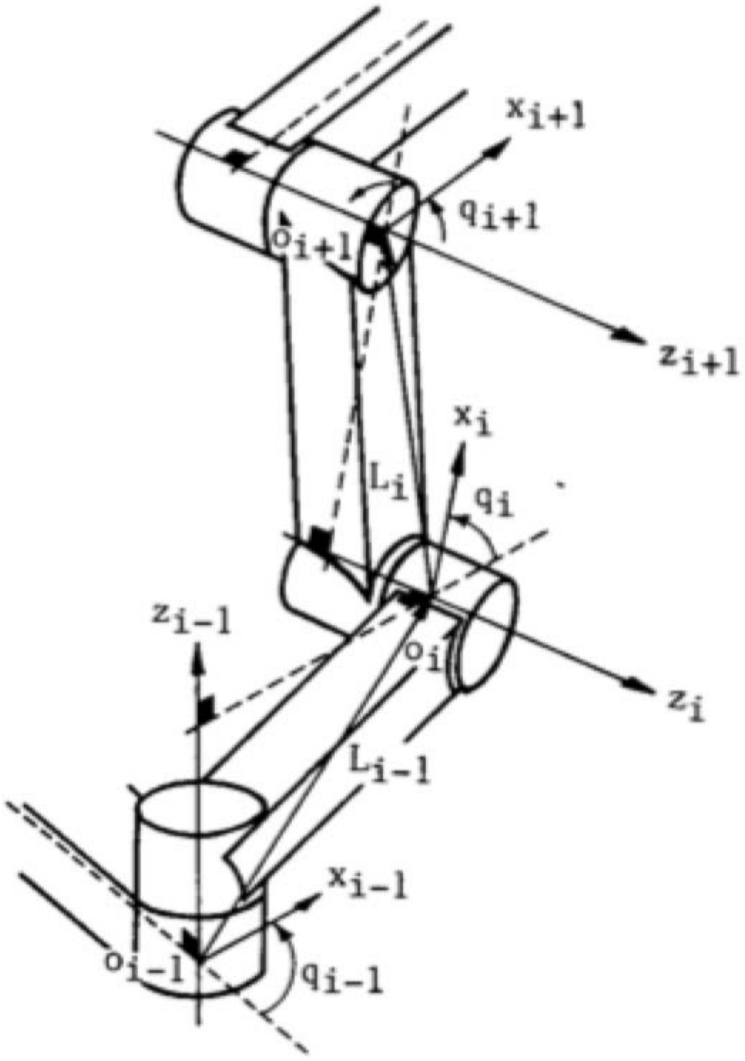

Figure 2.10: Coordinate systems for both parallel and perpendicular manipulator joints[18]

2.1.5 Generalized Jacobian Matrix

Umetani and Yoshida added onto Mayeda's knowledge base with the addition of the Generalized Jacobian Matrix (GJM).[59] The GJM allows for the calculation of inverse kinematics for free-floating system. This method uses an inertial coordinate system Σ_A as the "absolute coordinate system" as seen in figure 2.11. Umetani and Yoshida make 4 main assumptions for their work on the GJM. These assumptions from the paper are as follows.[59]

- The installed manipulator system consists of n links. Each joint has one rotational degree of freedom and is rate-controlled, but the position or attitude of the satellite main body is not controlled at all.
- At an initial state and during the motion, the position and attitude of the robot system are well known from the inertial coordinate system.
- There are no mechanical restrictions nor external forces and torques, so that momentum conservation, and equilibrium of forces and moments, strictly hold true during the operation.
- On the whole, the system is composed of rigid bodies. As for the above assumptions, the systems is regarded [as] a free-flying mechanical chain composed of $n + 1$ rigid bodies

This imposes some significant restrictions to the system. First you have to know the pose and change in pose of the inertial coordinate system if you want to be able to track the motion of the system to some other coordinate system. Second, the system does not track well for servicing applications because of the restriction of no external force or torques since these external forces

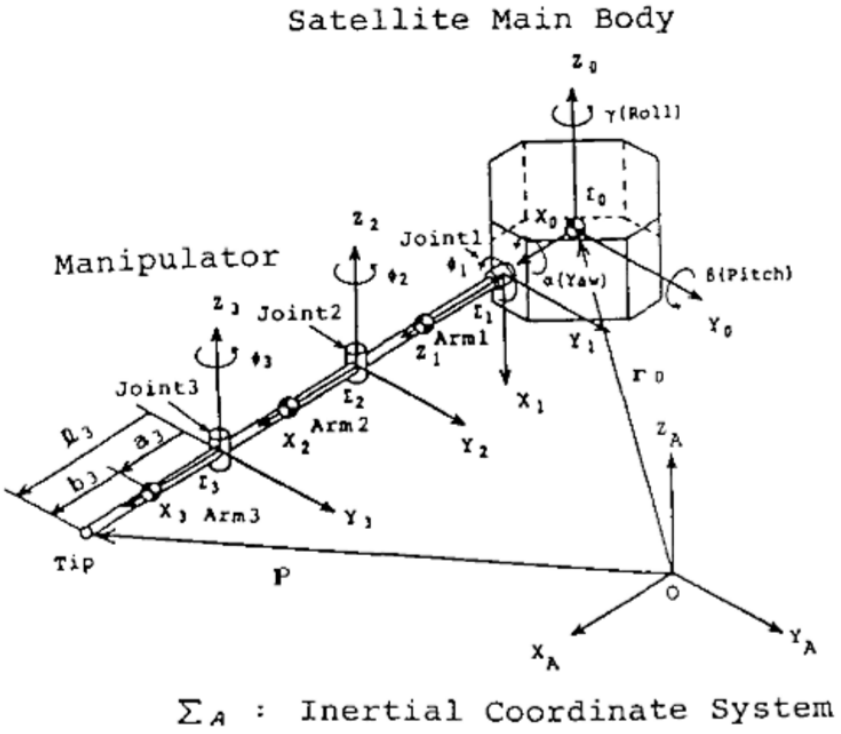

Figure 2.11: Σ_A: Inertial Coordinate System [59]

and torques would most likely be encountered during a satellite servicing operations. What the GJM does will however is solve the problem of tracking the inverse kinematics of the free-flying system. A deficiency seen with both of the methods from Vafa and Dubowsky in subsection 2.1.2, and Longman in subsection 2.1.1.

The development of the Generalized Jacobian Matrix begins with laying out the inertial coordinate system seen in Fig 2.11. The symbols of the figure are defined in [59] as follows

Table 2.6: Variable definitions for the GJM with reference to Fig 2.11

Variable	Definition
$\boldsymbol{r}_i$	Position vector of the mass center of link i
$\boldsymbol{r}_\sigma$	Position vector of the mass center of the entire system
p_n	Position vector of the tip of the manipulator
$\boldsymbol{l}_i$	vector pointing from joint i to joint $i+1$
a_i	Vector pointing from joint i to the mass center of link i
b_i	Vector pointing from the mass center of link i to joint $i+1$
m_i	Mass of link i
w	Total mass of the system
I_i	Inertia matrix of link i with respect to the mass center
ω_i	Angular velocity of link i
α, β, γ	Attitude angles of a satellite main body (yaw, pitch, roll)
ϕ_i	Rotational angle of joint i

where $i = 0 \cdots n$.

All vectors and matrices reference what Yoshida and Umetani call the absolute coordinate system Σ_A. All vectors and matrices have a super- or subscript as defined in appendix I of [59] copied here for clarity of the equations that will follow.

Let link 0 be a satellite main body, link i $(i = 1 \cdots n)$ the i th arm of the manipulator in order, and joint i a joint which connects link $i-1$ and link i. The i th coordinate system $\Sigma_i : (x_i, y_i, z_i)$ for $i = 1 \cdots n$ is assigned to be an orthogonal coordinate system fixed on link i which originates in joint i and the axis z_i corresponds to its rotational axis. Exceptionally, the 0th coordinate system Σ_0 is fixed on a satellite main body which originates in its gravity center, and the absolute (inertial) coordinate system Σ_A is fixed in the space.

To clarify the reference coordinate system of vectors and matrices, vectors are affixed with a superscript on the left side of the symbol such that ${}^i\boldsymbol{r}_j$ indicates a vector $\boldsymbol{r}_j$ with reference to the i th coordinate system, and matrices are affixed with super- and

subscripts such that ${}^{i}[\boldsymbol{I}_j]_i$ indicates a matrix $\boldsymbol{I}_j$ with reference to the i th coordinate system.

Using the system defined above Umetani and Yoshida define the "*Fundamental Equations*" of the system beginning with the geometrical definition of the center of mass of the system:

$$\sum_{i=0}^{n} m_i r_i = r_G \sum_{i=0}^{n} m_i \tag{2.68}$$

with the first derivative of r_i in eqn 2.68 giving the translational momentum conservation as well as the rotational momentum conservation, in eqns 2.69 and 2.70 respectively:

$$\sum_{i=0}^{n} m_i \dot{r}_i = \text{ const.} \tag{2.69}$$

$$\sum_{i=0}^{n} (\boldsymbol{I}_i \omega_i + m_i r_i \times \dot{r}_i) = \text{ const.} \tag{2.70}$$

From figure 2.11 we can see the relation between links as:

$$r_i - r_{i-1} = a_i + b_{i-1} \tag{2.71}$$

This relation allows for the characteristic equation of the manipulator to be written as:

$$p_n = r_0 + b_0 + \sum_{i=1}^{n} \boldsymbol{l}_i \tag{2.72}$$

Umetani and Yoshida show that equations 2.68 and 2.71 are simultaneous equations for r_i and can be solved for r_i as:

$$ {}^{A}r_i = \sum_{j=1}^{n} K_{ij} \left({}^{A}A_i {}^{i}a_i + {}^{A}A_{i-1} {}^{i-1}b_{i-1} \right) + {}^{A}r_G \tag{2.73} $$

were the coefficients K_{ij} are defined as:

$$ K_{ij} = \begin{cases} \left(\sum_{l=0}^{j-1} m_i \right) / w & (i \geqq j) \\ - \left(\sum_{l=j}^{n} m_i \right) / w & (i < j) \end{cases} \tag{2.74} $$

with K_{ij} being a function of the mass ratio of each link. Umetani and Yoshida then differentiate with respect to time to get eqn 2.73 which is the velocity of the center of mass of each link.

$$ {}^{A}\dot{r}_i = \sum_{j=1}^{n} K_{ij} \left({}^{A}\dot{A}_i {}^{i}a_i + {}^{A}\dot{A}_{i-1} {}^{i-1}b_{i-1} \right) + {}^{A}\dot{r}_G \tag{2.75} $$

Umetani and Yoshida then show the differentiation of the transformation matrix A as:

$$ {}^{A}\dot{A}_i = \sum_{k=0}^{i} \dot{\phi}_k \frac{\partial^A A_i}{\partial \phi_k} \tag{2.76} $$

where ϕ_k is the rotational angle of joint k. Umetani and Yoshida then show that the $\dot{r}_i$ written using eqn 2.76 as:

$$ {}^{A}\dot{r}_i = \sum_{j=0}^{n} v_{ij} \dot{\phi}_j + {}^{A}\dot{v}_G \tag{2.77} $$

where v_{ij} is defined as:

$$ v_{ij} = \sum_{k=0}^{i} K_{ik} \left(\frac{\partial^A A_i}{\partial \phi_j} {}^{i}a_i + \frac{\partial^A A_{i-1}}{\partial \phi_j} {}^{i-1}b_{i-1} \right) \tag{2.78} $$

and v_G is the initial velocity of the center of mass of the entire system and is consistent with eqn 2.68. Umetani and Yoshida then show that equation 2.77 means that $\dot{r}_i$ is a linear combination of vector v_{ij} and angular velocity $\dot{\phi}_j$. Additionally it is noted that the angular velocity of each link with respect to its mass center ω_i can also be written in a similar form:

$$ {}^{A}\omega_i = \sum_{j=0}^{i} {}^{A}A_j{}^{j}\omega_j = \sum_{j=0}^{i} \left({}^{A}A_j{}^{j}u_j\right)\dot{\phi}_j + \omega_G \tag{2.79} $$

where u_j is a unit vector along the rotational axis of joint j and ω_G is the initial angular velocity of the entire system and is shown to be consistent with eqn 2.70.

With all of this defined, Umetani and Yoshida then define the characteristic equation of the manipulator as:

$$ \boldsymbol{P} = f(\boldsymbol{\phi}) \tag{2.80} $$

where

$$ \boldsymbol{P} = (p_1, p_2, \cdots, p_m)^\top \qquad \text{The task space} $$

$$ \boldsymbol{\phi} = (\phi_1, \phi_2, \cdots, \phi_m)^\top \qquad \text{The joint space} $$

Yoshida [59] then shows that the Jacobian matrix can be obtained via the first time derivative of the characteristic equation 2.80

$$ \dot{\boldsymbol{P}} = \boldsymbol{J}(\boldsymbol{\phi})\dot{\boldsymbol{\phi}} \tag{2.81} $$

$$\boldsymbol{J}(\boldsymbol{\phi}) = \frac{\partial \boldsymbol{f}}{\partial \boldsymbol{\phi}} \tag{2.82}$$

where $\boldsymbol{J}(\boldsymbol{\phi})$ is the Jacobian matrix. Yoshida then shows the expanded characteristic equation for a satellite fixed manipulator to be:

$$^{A}\dot{\boldsymbol{p}}_n = {}^{A}\dot{\boldsymbol{r}}_0 + {}^{A}\dot{A}_0{}^{0}\boldsymbol{b}_0 + \sum_{i=1}^{n} {}^{A}\dot{A}_i{}^{i}\boldsymbol{l}_i. \tag{2.83}$$

where $^{A}\dot{\boldsymbol{r}}_0 + {}^{A}\dot{A}_0{}^{0}\boldsymbol{b}_0$ is the rotation and translation of the base satellite and $\dot{\boldsymbol{P}}_0 = (\boldsymbol{v}_G^{\top}, \boldsymbol{\omega}_G^{\top})^{\top}$ is the initial translational and rotational movement of the base satellite. [59]

$$\dot{\boldsymbol{P}} = \begin{bmatrix} \dot{p}_n \\ \\ \omega_n \end{bmatrix} = \bar{\boldsymbol{J}}(\boldsymbol{\phi})\dot{\boldsymbol{\phi}} + \dot{\boldsymbol{P}}_0 \tag{2.84}$$

$$\bar{\boldsymbol{J}}(\boldsymbol{\phi})\dot{\boldsymbol{\phi}} = \begin{bmatrix} \overline{\boldsymbol{J}}_{\alpha} & \overline{\boldsymbol{J}}_{\beta} & \overline{\boldsymbol{J}}_{\gamma} & \overline{\boldsymbol{J}}_{\phi_1} & \dots & \overline{\boldsymbol{J}}_{\phi_n} \\ {}^{A}\boldsymbol{A}_{\alpha} i & {}^{A}\boldsymbol{A}_{\beta} j & {}^{A}\boldsymbol{A}_{\gamma} k & {}^{A}\boldsymbol{A}_0 k & \dots & {}^{A}\boldsymbol{A}_n k \end{bmatrix} \cdot \begin{bmatrix} \dot{\alpha} \\ \dot{\beta} \\ \dot{\gamma} \\ \dot{\phi}_1 \\ \vdots \\ \dot{\phi}_n \end{bmatrix}$$

The expanded characteristic equation components for a satellite fixed manipulator are then shown

to be:

$$\dot{\boldsymbol{P}} = \begin{bmatrix} \dot{p}_n \\ \omega_n \end{bmatrix} = \bar{\boldsymbol{J}}(\boldsymbol{\phi})\dot{\boldsymbol{\phi}} + \dot{\boldsymbol{P}}_0 \tag{2.85}$$

$$= \begin{bmatrix} \overline{\boldsymbol{J}}_\alpha & \overline{\boldsymbol{J}}_\beta & \overline{\boldsymbol{J}}_\gamma & \overline{\boldsymbol{J}}_{\phi_1} & \cdots & \overline{\boldsymbol{J}}_{\phi_n} \\ {}^A\boldsymbol{A}_\alpha i & {}^A\boldsymbol{A}_\beta j & {}^A\boldsymbol{A}_\gamma k & {}^A\boldsymbol{A}_0 k & \cdots & {}^A\boldsymbol{A}_n k \end{bmatrix} \cdot \begin{bmatrix} \dot{\alpha} \\ \dot{\beta} \\ \dot{\gamma} \\ \dot{\phi}_1 \\ \vdots \\ \dot{\phi}_n \end{bmatrix} + \dot{\boldsymbol{P}}_0$$

where

$$\bar{\boldsymbol{J}}(\boldsymbol{\phi}) = \begin{cases} v_{0i} + {}^A\dot{\boldsymbol{r}}_0 + {}^A\dot{A}_0{}^0\boldsymbol{b}_0 & + \sum_{j=i}^{n} \frac{\partial {}^A A_j}{\partial \phi_i} j l_j \quad (\phi = \alpha, \beta, \gamma) \\ v_{0i} & + \sum_{j=i}^{n} \frac{\partial {}^A A_j}{\partial \phi_i} j l_j \quad (i = 1 \cdots n) \end{cases} \tag{2.86}$$

with i, j, k being unit vectors, and $\dot{P}_0 = (v_G^\top, \omega_G^\top)^\top$ the initial translational and rotational movement of the base satellite. [59] It is also noted that the vector v_{ij} defined in equation 2.78 is a function of the mass ratio k_{ij}. As such the equation can be divided into a satellite part and a manipulator part as follows:

$$\dot{\boldsymbol{P}} = \bar{\boldsymbol{J}}_S\dot{\boldsymbol{\phi}}_S + \bar{\boldsymbol{J}}_M\dot{\boldsymbol{\phi}}_M + \dot{\boldsymbol{P}}_0 \tag{2.87}$$

where

$$\boldsymbol{\phi}_S = (\alpha, \beta, \gamma)^\top \qquad \text{attitude angles of the satellite main body}$$

$$\boldsymbol{\phi}_M = (\phi_1, \phi_2, \cdots, \phi_n)^\top \qquad \text{joint angles of the manipulator}$$

with $\bar{\boldsymbol{J}}_S$ and $\bar{\boldsymbol{J}}_M$ being the Jacobian matrices of the satellite and manipulator respectively. $\bar{\boldsymbol{J}}_S$ is a $m \times 3$ matrix and $\bar{\boldsymbol{J}}_M$ is a $m \times n$ matrix with $\bar{\boldsymbol{J}} = [\bar{\boldsymbol{J}}_S, \bar{\boldsymbol{J}}_M]$ being a $m \times (3+n)$ matrix. [59]

2.1.5.1 Inverse Kinematics With the GJM

Equation 2.87 is seen to be the kinematic equation for the manipulator spacecraft system. It shows a relationship between the joint angles $\boldsymbol{\phi}_m$ (n variables), the spacecraft attitude angles $\boldsymbol{\phi}_m$ (3 variables), and the end-effector velocity $\dot{\boldsymbol{P}}$. The issue arises for the inverse kinematics of the system in that the system is underdetermined. This is because the number of variables is greater than the number of equations. This is shown by the system having m linear relations to $3+n$ unknown variables. As such, Umetani and Yoshida introduce a conservation of momentum law on the system to allow the unknown attitude angular velocities $\dot{\boldsymbol{\phi}}_S$ to be solved for. Umetani and Yoshida propose that by substituting eqn 2.77 and eqn 2.79 into eqn 2.70 and then the momentum conservation law can be written as and linear combination with attitude and joint angular velocities as:

$$\left[\bar{\boldsymbol{I}}_{\alpha}, \bar{\boldsymbol{I}}_{\beta}, \bar{\boldsymbol{I}}_{\gamma}, \bar{\boldsymbol{I}}_{\phi_1} \cdots \bar{\boldsymbol{I}}_{\phi_n}\right] \begin{bmatrix} \dot{\alpha} \\ \dot{\beta} \\ \dot{\gamma} \\ \dot{\phi}_1 \\ \vdots \\ \dot{\phi}_n \end{bmatrix} = \boldsymbol{L}_0 \tag{2.88}$$

where

$$\bar{\boldsymbol{I}}_{\phi_i} = \left(\sum_{j=i}^{n} {}^{A}\boldsymbol{A}_j{}^{j} \left[\boldsymbol{I}_j\right]_j {}^{j}\mathcal{A}_A \right) {}^{A}\boldsymbol{A}_i{}^{i}\boldsymbol{u}_i + \sum_{j=0}^{n} m_j {}^{A}\boldsymbol{r}_j \times \boldsymbol{v}_{ij}$$

As with equation 2.87 the equation 2.88 can be divided into a satellite part and a manipulator part as follows:

$$\bar{\boldsymbol{I}}_s \dot{\boldsymbol{\phi}} + \bar{\boldsymbol{I}}_m \dot{\boldsymbol{\phi}}_m = \boldsymbol{L}_0 \tag{2.89}$$

It can be seen that $\bar{\boldsymbol{I}}_s$ and $\bar{\boldsymbol{I}}_m$ are 3×3 and $3 \times n$ matrices respectively. $\bar{\boldsymbol{I}}_s$ is the inertia matrix of the satellite main body and $\bar{\boldsymbol{I}}_m$ is the inertia matrix of the manipulator with $\boldsymbol{L}_0$ being the initial momentum of the system. Umetani and Yoshida note that both $\bar{\boldsymbol{I}}_s$ and $\bar{\boldsymbol{I}}_m$ are neither symmetrical matrices nor are they tensors. [59]

Rewriting eqn 2.89 in terms of the attitude angular velocity $\dot{\boldsymbol{\phi}}_S$ gives:

$$\dot{\boldsymbol{\phi}}_S = -\bar{\boldsymbol{I}}_S^{-1} \bar{\boldsymbol{I}}_M \dot{\boldsymbol{\phi}}_M + \bar{\boldsymbol{I}}_S^{-1} \boldsymbol{L}_0 \tag{2.90}$$

therefore eqn 2.87 can be rewritten as:

$$\dot{\boldsymbol{P}} = \left(\bar{\boldsymbol{J}}_M - \bar{\boldsymbol{J}}_S \bar{\boldsymbol{I}}_S^{-1} \bar{\boldsymbol{I}}_M\right) \dot{\boldsymbol{\phi}}_M + \dot{\boldsymbol{P}}_0 \tag{2.91}$$

when the constant term $\dot{\boldsymbol{P}}_0 + \bar{\boldsymbol{J}}_S \bar{\boldsymbol{I}}_S^{-1} \boldsymbol{L}_0$ is rewritten as $\dot{\boldsymbol{P}}_0$

Umetani and Yoshida look at the form of equation 2.91 and note that the manipulator portion of the extended Jacobian $\bar{\boldsymbol{J}}_M$ is 'compensated for a disturbance of reactive movement of the base body' [59]. They note the magnitude of the reactive disturbance is a proportional function of the ratio of inertias of manipulator and satellite main body; $\bar{\boldsymbol{I}}_S^{-1} \bar{\boldsymbol{I}}_M$. From this proportionality, it can be seen that the larger the the inertia of the satellite main body is compared to the manipulator, the smaller the reactive disturbance will be. As such, they also note that as the ratio of the satellite main body to the manipulator inertia approaches infinity, the reactive disturbance approaches zero, as would be expected for a ground fixed manipulator. [59] Furthermore, eqn 2.91 contains the conventional Jacobian matrix and therefore can be used as a general expression for the Jacobian matrix of manipulators with a free-flying base body. Umetani and Yoshida dub this the Generalized Jacobian Matrix, $\boldsymbol{J}^*$, and can be substituted into eqn 2.91 to get the new characteristic equation defined as:

$$\dot{\boldsymbol{P}} = \bar{\boldsymbol{J}}^* \dot{\boldsymbol{\phi}}_M + \dot{\boldsymbol{P}}_0 \tag{2.92}$$

with $\boldsymbol{J}^*$, the Generalized Jacobian Matrix, defined as:

$$\bar{\boldsymbol{J}}^* = \bar{\boldsymbol{J}}_M - \bar{\boldsymbol{J}}_S \bar{\boldsymbol{I}}_S^{-1} \bar{\boldsymbol{I}}_M \tag{2.93}$$

It can be seen that equation 2.92 is a linear combination of the joint angular velocities $\dot{\boldsymbol{\phi}}_M$

and the base joint rotational and translational initial conditions $\dot{\boldsymbol{P}}_0$ and is expressed as a set of closed-form linear equations. [59] Furthermore, the inverse transformation can be solved if $\bar{\boldsymbol{J}}^*$ is non-singular.

$$\dot{\boldsymbol{\phi}}_M = \left[\bar{\boldsymbol{J}}^*\right]^{-1}\left(\dot{\boldsymbol{P}} - \dot{\boldsymbol{P}}_0\right) \tag{2.94}$$

With all of these components in place, Umetani and Yoshida then show an example of solving direct kinematics, the inverse kinematics, and the attitude control problem. For the direct kinematics problem, it is shown that although the motion of the system is tracked there is a significant effect on the satellite attitude. The note that this the same effect that was proposed by Vafa and Dubowsky in their virtual manipulator paper [49], pertaining to cyclic manipulator motion demonstrating the non-holonomic nature of the system. For the inverse kinematics problem, it is shown that the manipulator can be controlled to track a desired motion of the end-effector. For the attitude control problem, it is shown that the attitude of the satellite can be controlled to track a desired attitude. [59] Umetani and Yoshida look at the attitude control problem through the lens of Yamada's work [27] and Peter C Hughes' work [58], [60] to solve for the attitude of the base spacecraft.

For this problem, $\boldsymbol{L}_C$ is defined as the counter momentum of the spacecraft main body reaction wheels or thrusters. By reorganizing equation 2.89, the momentum conservation law, and substituting in $\boldsymbol{L}_C$, the equation can be rewritten as:

$$\bar{\boldsymbol{I}}_s\dot{\boldsymbol{\phi}}_s + \bar{\boldsymbol{I}}_m\dot{\boldsymbol{\phi}}_m + \boldsymbol{L}_c = 0 \tag{2.95}$$

with this equation we can see that the change of the satellite main body momentum is controlled

to zero, e.g $\dot{\boldsymbol{\phi}}_s = 0$. In this case equations 2.87 and 2.95 can be rewritten to get:

$$\dot{\boldsymbol{P}} = \bar{\boldsymbol{J}}_M \dot{\boldsymbol{\phi}}_M + \dot{\boldsymbol{P}}_0 \tag{2.96}$$

$$\bar{\boldsymbol{I}}_m \dot{\boldsymbol{\phi}}_m + \boldsymbol{L}_C = 0 \tag{2.97}$$

This case where $\dot{\boldsymbol{\phi}}_s = 0$ is the same core idea contained in previous work. Longman et al. [50] pointed out this same manipulator kinematics and dynamics of the base spacecraft in equations 2.96 and 2.97 respectively. Equation 2.97 represents the same concept as reaction moment compensation. As such, the required counter moment, $\boldsymbol{L}_C$ can be calculated as:

$$^A\boldsymbol{L}_C = -\bar{\boldsymbol{I}}_m \bar{\boldsymbol{J}}_m^{-1} (\dot{\boldsymbol{P}} - \dot{\boldsymbol{P}}_0) \tag{2.98}$$

Umetani and Yoshida's Generalized Jacobian Matrix is of significant importance. Development of the Generalized Jacobian Matrix is incredibly important for the development of free-floating manipulator systems. The GJM allows for the development of a manipulator system that can be used for satellite servicing operations by encapsulating the overall dynamics of the spacecraft base and robotic manipulator system while still tracking the expected result of if the inertia of the base spacecraft goes towards infinity. Under the infinite inertia case the GJM decomposes into the classical ground fixed jacobian matrix. Verification of this work in a further paper [61] and validation of the concepts of Longman et al. and Vafa and Dubowsky only add to the importance of the Generalized Jacobian Matrix. This work is, however, limited in that it still is only valid for a free-floating system. The GJM is the basis for the further work of Yoshida and the guaranteed workspace (GWS) which is discussed briefly in the next section.

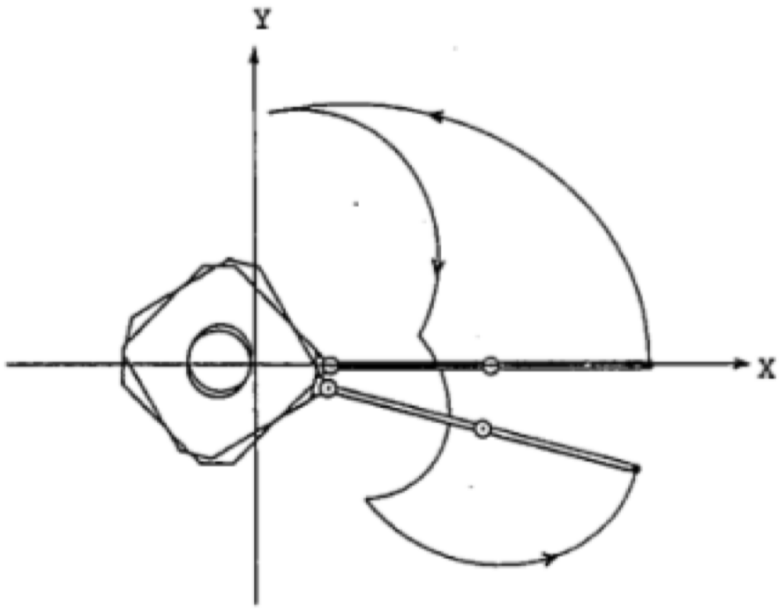

Figure 2.12: Non-holonomic behavior of a cyclic-manipulator motion [62]

2.1.6 Guaranteed Workspace

Yoshida continued the work developed with his mentor and added the concept of the guaranteed workspace (GWS)[62]. Yoshida developed the GWS to address one of the issues of free-flyer manipulator motion in that the system is inherently non-holonomic. Figure 2.12 depicts this non-holonomic behavior showing that you can traverse a series of motions with the manipulator system that in a fixed base manipulator would result in the same end-effector position but imparts a rotation in the pose of the free-flyer.

What stands to be reasoned next is the tracking of the translation of the spacecraft. Using the coordinate system see in figure 2.13 we can see that the kinetic energy, $\boldsymbol{T}$, of the spacecraft for the joint velocities $\dot{\boldsymbol{q}} = \left(\boldsymbol{v}_0^\top, \boldsymbol{\omega}_0^\top, \dot{\boldsymbol{\phi}}^\top\right)^\top$ is defined by Yoshida to be:

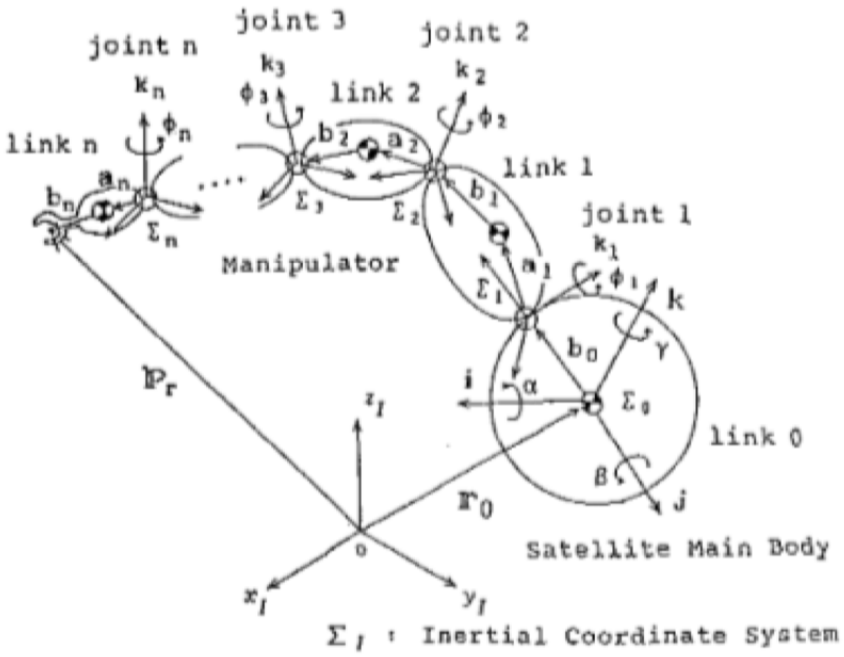

Figure 2.13: Σ_A: Inertial coordinate system [62]

$$\boldsymbol{T} = \frac{1}{2}\left[\boldsymbol{v}_0^\top \boldsymbol{\omega}_0^\top \dot{\boldsymbol{\phi}}^\top\right] \boldsymbol{H} \begin{bmatrix} \boldsymbol{v}_0 \\ \boldsymbol{\omega}_0 \\ \dot{\boldsymbol{\phi}} \end{bmatrix} \tag{2.99}$$

where $\dot{\boldsymbol{r}}_0 \equiv \boldsymbol{v}_0$ and $\boldsymbol{H}(\phi)$ is the inertia matrix of the system.

For the case of a free-flyer manipulator system with no external forces or moments acting on the system, the momentum of the system is conserved. Additionally, the variables $\boldsymbol{v}_0$, $\boldsymbol{\omega}_0$ and $\dot{\boldsymbol{\phi}}$ are not independent as the manipulator motion will cause the base spacecraft to translate and rotate in a "non-holonomic" fashion. As such, Yoshida shows that the translational and rotational momentum, $\boldsymbol{P}$ and $\boldsymbol{L}$ of the spacecraft can be expressed as:

$$\begin{bmatrix} \boldsymbol{P} \\ \boldsymbol{L} \end{bmatrix} = \boldsymbol{I}_s \begin{bmatrix} \boldsymbol{v}_0 \\ \boldsymbol{\omega}_0 \end{bmatrix} + \boldsymbol{I}_m \dot{\boldsymbol{\phi}} = 0 \tag{2.100}$$

with the assumption that the total momentum of the system is zero. Equations of motion for the system can then be derived via the Lagrange method with the kinetic energy equation 2.99 and the constraints of equation 2.100. The development of these equations can be found in Yoshida's paper [62] and are not replicated here as it will not be helpful to the development of this thesis. This work eventually culminates with using the techniques to operate the NASDA Engineering Test Satellite VII (ETS-VII). ETS-VII is documented in the papers by Inaba and Oda [35]–[38] and shows the successful operation of the ETS-VII manipulator system and spacecraft. Overall the GJM is useful for motion control and the GWS is useful for path planning. The combination of the GJM and GWS allows for the development of a free-flyer manipulator system that can be used for satellite servicing operations by encapsulating the overall dynamics and workspace of the free-flyer manipulator system.

2.1.7 Passive Spherical Joint Approximation of Manipulator Joints

Stoneking[19] started from the problem definition in that he needed to identify the complex non-linear dynamics of a formation of spinning spacecraft with flexible appendages and bang-bang based thruster control for the spacecraft. Stoneking took the approach of modeling the system as a series of rigid bodies connected by passive spherical joints. Each spacecraft is modeled as a tree of rigid bodies connected by passive spherical joints or gimbaled joint. This is a very interesting approach to pull out system dynamics by inspection through the use of having each of the building blocks defined using Newton's and Euler's equations to each individual "ele-

ment" of the spacecraft. We see in Figure 2.14 an example of a diagram of two bodies connected by a passive spherical joint.

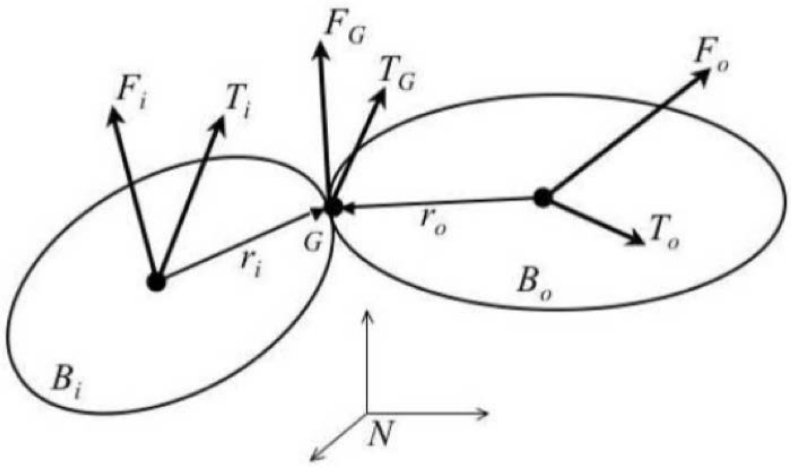

Figure 2.14: Two Bodies Connected by a Spherical Joint[19]

Stoneking defines the translational motion as $m\dot{v} = F$ which is Newton's second law and the rotational motion as a Euler's equation for a rigid body as $I\dot{\omega} = T - \omega \times H$. Importantly Stoneking notes that the overdot operator $\dot{(\ )}$ represents a time derivative in the local frame and that time derivatives of frame A in the inertial Frame N by the following equation

$$ {}^{N}\frac{\partial}{\partial t}(v) = {}^{A}\frac{\partial}{\partial t}(v) + {}^{N}\omega^{A} \times v = \dot{v} + {}^{N}\omega^{A} \times v \tag{2.101} $$

Using the information from figure 2.14 and equation 2.101 Stoneking defines the equations of motion by inspection for the two bodies B_i and B_o connected by the passive spherical joint G in the inertial frame N.

$$I_i\dot{\omega}_i = T_i - \omega_i \times H_i + T_G + r_i \times F_G \tag{2.102}$$

$$I_o\dot{\omega}_o = T_o - \omega_o \times H_o - T_G - r_o \times F_G \tag{2.103}$$

$$m_i\dot{v}_i = F_i + F_G \tag{2.104}$$

$$m_o\dot{v}_o = F_o - F_G \tag{2.105}$$

where F_G and T_G are the constraint force and torque of the passive joint.

Symbol	Description
ω_i, ω_o	Angular velocity
v_i, v_o	Velocity of mass center
I_i, I_o	Central moments of inertia
m_i, m_o	Mass
r_i, r_o	Vector from mass center to joint
H_i, H_o	Central angular momentum
F_i, F_o	Resultant external force
T_i, T_o	Resultant external torque

Table 2.7: Symbols for the Newton-Euler equations in equation 2.102-2.105

The frames for differentiation of ω_i and ω_o are the frames associated with B_i and B_o respectively. This differs for v_i and v_o as the frames of differentiation is N as the local frame. Stoneking states that the each spherical joint the constraint torque represents the material elasticity and the damping as well as and additional control torques at the joints. The goal is to eliminate the constraint forces F_G and T_G is assumed to be calculable by the user. The signs of F_G and T_G are defined arbitrarily to act in a positive sense on B_i and in a negative sense for B_o. This is all done in the absence of any momentum storage devices. [19] Stoneking then introduces a term called the "Joint Constraint" by equating the equations for velocity of G in N:

$$v_G = v_i + \omega_i \times r_i = v_o + \omega_o \times r_o \tag{2.106}$$

which differentiating with respect to time, in N, gives the constraint equation:

$$\dot{v}_i + \dot{\omega}_i \times r_i + \omega_i \times (\omega_i \times r_i) = \dot{v}_o + \dot{\omega}_o \times r_o + \omega_o \times (\omega_o \times r_o) \tag{2.107}$$

Equations 2.102 - 2.107 are the 5 vector equations that will be used to solve for the five vector unknowns $\dot{\omega}_i$, $\dot{\omega}_o$, $\dot{v}_i$, $\dot{v}_o$, and F_G. Stoneking then introduces two new notational operators, the over-tilde operator ($\tilde{}$) for a 3 x 3 skew-symmetric matrix such that $\tilde{x}y = x \times y$ and the over-bar operator ($\bar{}$) for a symmetric matrix such that $\bar{x}y = x \times (x \times y)$. These are defined further in the equations below:

$$\tilde{x} = \begin{bmatrix} 0 & -x_3 & x_2 \\ x_3 & 0 & -x_1 \\ -x_2 & x_1 & 0 \end{bmatrix}, \quad \bar{x} = \begin{bmatrix} -x_2^2 - x_3^2 & x_1 x_2 & x_1 x_3 \\ x_2 x_1 & -x_3^2 - x_1^2 & x_2 x_3 \\ x_3 x_1 & x_3 x_2 & -x_1^2 - x_2^2 \end{bmatrix}$$

noting that $-\tilde{x} = x^\top$. Now rewriting equations 2.102 - 2.107 in terms of the new operators we get in matrix form:

Items Expressed in B_i	Items Expressed in B_o	Items Expressed in N
I_i	I_o	$v_i, \dot{v}_i$
$r_i, \tilde{r}_i$	$r_o, \tilde{r}_o$	$v_o, \dot{v}_o$
$\omega_i, \dot{\omega}_i, \tilde{\omega}_i, \bar{\omega}_i$	$\omega_o, \dot{\omega}_o, \tilde{\omega}_o, \bar{\omega}_o$	F_i
T_i	T_o	F_o
H_i	H_o	F_G
T_G		

Table 2.8: Dynamic elements expressed in reference frames B_i, B_o, and N [19]

$$\begin{bmatrix} I_i & 0 & 0 & 0 & -\tilde{r}_i \\ 0 & I_o & 0 & 0 & \tilde{r}_o \\ 0 & 0 & m_i\mathbf{1} & 0 & -\mathbf{1} \\ 0 & 0 & 0 & m_o\mathbf{1} & \mathbf{1} \\ -\tilde{r}_i^\top & \tilde{r}_o^\top & -\mathbf{1} & \mathbf{1} & 0 \end{bmatrix} \begin{Bmatrix} \dot{\omega}_i \\ \dot{\omega}_o \\ \dot{v}_i \\ \dot{v}_o \\ F_G \end{Bmatrix} = \begin{Bmatrix} T_i - \tilde{\omega}_i H_i + T_G \\ T_o - \tilde{\omega}_o H_o - T_G \\ F_i \\ F_o \\ \bar{\omega}_i r_i - \bar{\omega}_o r_o \end{Bmatrix} \tag{2.108}$$

where $\mathbf{1}$ is the 3×3 identity matrix.

In order to solve this system of all of the components need to be in the same basis frame. Stoneking defines the following transformation matrices to transform the components of the system into the same frame. The transformation matrix between reference frames X and Y is the direction cosine matrix ${}^{X}C^{Y}$. For example, a vector v is expressed in the Y frame as ${}^{Y}v$ and in the X frame as [19]:

$${}^{X}v = {}^{X}C^{YY}v$$

noting that ${}^{Y}C^{X} = \left({}^{X}C^{Y}\right)^{\top} = \left({}^{X}C^{Y}\right)^{-1}$. Equation 2.108 can be rewritten with the introduction

of bases as:

$$\begin{bmatrix} I_i & 0 & 0 & 0 & -\tilde{r}_i{}^i C^N \\ 0 & I_o & 0 & 0 & \tilde{r}_o{}^o C^N \\ 0 & 0 & m_i\mathbf{1} & 0 & -\mathbf{1} \\ 0 & 0 & 0 & m_o\mathbf{1} & \mathbf{1} \\ -{}^N C^i \tilde{r}_i^\top & {}^N C^o \tilde{r}_o^\top & -\mathbf{1} & \mathbf{1} & 0 \end{bmatrix} \begin{Bmatrix} \dot{\omega}_i \\ \dot{\omega}_o \\ \dot{v}_i \\ \dot{v}_o \\ F_G \end{Bmatrix} = \begin{Bmatrix} T_i - \tilde{\omega}_i H_i + T_G \\ T_o - \tilde{\omega}_o H_o - {}^o C^i T_G \\ F_i \\ F_o \\ {}^N C^i \bar{\omega}_i r_i - {}^N C^o \bar{\omega}_o r_o \end{Bmatrix} \tag{2.109}$$

Equation 2.109 is the initial building block for the N-Dimensional multibody case. When assembled into a N-Dimensional multibody system, the system will be of order $6N + 3(N-1)$ for the three rotational degrees of freedom, three translational degrees of freedom, and the three constraint equations for each body. [19] This is the end result that is needed to generate the equations of motion for the system and Stoneking further fleshes out the equations for momentum storage devices and reduction of the number of equations in the system.

This paper is an interesting approach to the the application of Newton-Euler motion for a multibody system. The approach is very interesting in that it is a very simple approach for the development of the equations of motion for a multibody system and the explicitness of the resultant equations. With this method we can see how the traditional jacobian for a system could be applied to separate the system of equations and put it into a more traditional format for robot kinematics.

Regardless, none of the methods in section 2.1 are direct methods for the identification of the inertial parameters of a free-floating manipulator system. The next section will look at the methods that are used for the identification of the inertial parameters of a robotic manipulator

system.

2.2 Robot Modeling of Dynamics and Control with the Goal of Inertial Parameter Identification

Up to this point we have looked at the modeling of the dynamics of a spacecraft with and attached manipulator. The next step is to look at the modeling of the dynamics of a robotic manipulator with the goal of inertial parameter identification in mind. We begin with another survey of the literature to see what methods are available for inertial parameter identification of a robotic manipulator system.

2.2.1 Estimators and Observers

The area of study that is control theory is a prime area of potential knowledge for the estimation of inertial parameters. State Observers or State Estimators are used to provide an estimate of one of the internal states of a real system. State Estimators are used in cases where one wishes to solve a control problem for a system that has a physical state that is not fully known. This goal seems well-matched with the problem of inertial parameter identification, and in need of further exploration.

For example, say there is a simple rigid pendulum that we know the length of the pendulum and know the mass of the swinging weight that is actuated by a motor. If an insect was to land on the mass of the system, and we needed to have the controller for the system keep the same oscillation frequency as existed before the insect landed on the mass, an estimator could observe the output data from the system sensor, motor current, pendulum angle and angular velocity, and

use those quantities to solve for an updated pendulum mass. Although this is a significant simplification, the underlying concept that an estimator can solve for changes in system parameters is significant and worth further investigation for the purposes of inertial parameter identification for a payload of unknown mass for a free-flying robotic manipulator.

We can begin our investigation with a survey of work done on estimators for robotic systems. Jean-Jacques Slotine[63]–[71], Arimoto[72], Nanos [73], Z. Chen [21], and Xiao-yan Yu [74] have all contributed work in the area of estimators and observer, with some more focused on the application for robotic manipulators. Among the many applications contained within these papers, the estimation of the inertial parameters of a robotic manipulator is of primary interest for this thesis.

Arimoto *et al.* [72] worked with PD-Type and PI-Type "learning" controllers. They describe these "learning" controllers as differing from classical and modern control techniques in that the control laws for the system are designed and implemented in advance based upon an educated guess of the system which then corrects itself based upon the feedback from the system. The "learning" controller is then able to adapt to the system and learn the system parameters. This is a very interesting concept and is a very interesting approach to the problem of inertial parameter identification. [72] Arimoto et. al. used the work of Heinzinger et. al. [75] and Bondi et. al. [76] to develop the learning controller. A diagrammatic representation of the types learning controllers are shown in figures 2.15, 2.16, and 2.17 below. The learning controller concept may applicable and a viable approach to the problem of inertial parameter identification, however with significant modifications for the problem of inertial parameter identification for a free-floating manipulator system.

A more modern version of this work is the work of Xiao-yan Yu [74]. Yu *et al.* developed

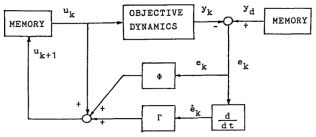

Figure 2.15: PD Type Learning Controller [72]

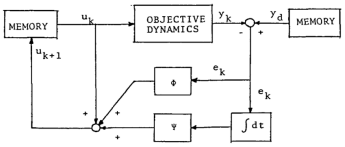

Figure 2.16: PI Type Learning Controller [72]

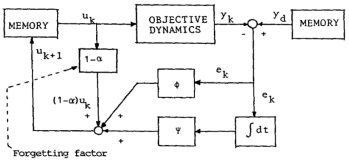

Figure 2.17: PI Type Learning Controller with Forgetting Factor [72]

a method for adaptive control of a flexible joint free-floating space manipulator. The method is based on the work of Slotine and Li [65], [66], [77], Siciliano [78], as well as many others within the area of adaptive controllers making it a potential approach to the problem of inertial parameter identification. The work of Yu *et al.* is interesting as skips the need to identify inertial parameter identification for flexible serial manipulators. [74] Although the work is not directly related to the problem of inertial parameter identification for a spacecraft with a manipulator, the work is a very interesting approach to non-linear flexible joint dynamics and control and demonstrates the potential for the use of adaptive control for the problem of inertial parameter identification.

Wei *et al.* [13], [79] looked at the use of prescribed performance controllers to stabilize the motion of a spacecraft with a manipulator captured unknown payload post-capture. The controllers were able to stabilize the systems with this unknown payload, however the work does not address the problem of inertial parameter identification for the unknown payload. In fact, Wei goes so far as to state that they have explicitly avoided including the inertial parameters in the control law because it "dramatically decreases the complexity of the controller design design of the combined spacecraft with large uncertainty owing to the fact that the tedious identification of inertial parameters is avoided." [79] The work of Wei *et al.* is still interesting, although not applicable to this problem, as it demonstrates the potential for the use of prescribed performance

controllers for the stabilization post-capture allowing for other potential methods to solve the problem of inertial parameter identification.

From the survey of the methods within estimators and observers we can see that there is potential for the use of adaptive control and learning controllers for the problem of inertial parameter identification, however with significant caveats. The need for a good beginning estimate, or as in the case of Wei *et al.* avoidance of the problem altogether, shows that estimators, observers, and other control theory based approaches may not be best suited to identifying the unknown inertial parameters of a payload.

2.2.2 Inverse and Direct Dynamic Models

From consideration of where robotics may have a need for internal parameter identification of unknown payloads, manufacturing and the world of industrial robotics seems to be a good starting point for investigation. A first method of interest in the realm of inertial parameter Identification is that of the Inverse and Direct Dynamic Models (IDDM) methods. Here, the system is defined as a rigid robotic serial manipulator that has n degrees of freedom (DOF). The model associates the quantities, $q, \dot{q}, \ddot{q} \in \mathbb{R}^n$, to the forces that are applied to the system written as: $\boldsymbol{\tau}_{idm} \in \mathbb{R}^n$. [80]–[83]

$$\boldsymbol{M}(\boldsymbol{\chi}, q)\ddot{q} + \boldsymbol{C}(\boldsymbol{\chi}, q, \dot{q})\dot{q} + \boldsymbol{g}(\boldsymbol{\chi}, q) + \boldsymbol{\zeta}(\boldsymbol{\chi}, \dot{q}) = \boldsymbol{\tau}_{idm} \tag{2.110}$$

The terms of equation 2.110 are $\boldsymbol{M}(\boldsymbol{\chi}, q)\ddot{q} \in \mathbb{R}^{n\times n}$ is the generalized inertia matrix and $\boldsymbol{C}(\boldsymbol{\chi}, q, \dot{q}) \in \mathbb{R}^{n\times n}$ is the Coriolis and centripetal effects matrix, $\boldsymbol{g}(\boldsymbol{\chi}, q) \in \mathbb{R}^n$ is the gravitational torque vector, and $\boldsymbol{\zeta}(\boldsymbol{\chi}, \dot{q}) \in \mathbb{R}^n$ is the friction vector. The vector $\boldsymbol{\chi} \in \mathbb{R}^p$ is the vector

of dynamic parameters of the system. [80] The vector $\boldsymbol{\chi}$ is defined as the concatenation of the dynamic parameters of each link of the system as shown in equation 2.111.

$$\boldsymbol{\chi} = \left[\boldsymbol{\chi}_1^\top \; \boldsymbol{\chi}_2^\top \cdots \boldsymbol{\chi}_n^\top\right]^\top \in \mathbb{R}^p \tag{2.111}$$

Here we see the set of all dynamics parameters for the full system. Eqn 2.112 show the breakdown of $\boldsymbol{\chi}_j$ for the link j.

$$\boldsymbol{\chi}_j = [XX_j, XY_j, XZ_j, YY_j, YZ_j, ZZ_j, MX_j, MY_j, MZ_j, M_j, Ia_j, Fv_j, Fc_j]^\top \tag{2.112}$$

The elements of the inertia tensor $\boldsymbol{L}_j$ of link j is XX_j, XY_j, XZ_j, YY_j, YZ_j, ZZ_j. MX_j, MY_j, MZ_j are the first moments of the link center of mass. The link center of mass (CoM) is defined from the link origin, $\boldsymbol{\mathcal{L}}_j$, as point X_j, Y_j, Z_j. The scalar M_j is the mass of link j. $\mathbf{I}a_j$ is the inertia of actuator and transmission system of link j. [82] The elements of the vector $\boldsymbol{\zeta}_j$ are Fv_j which is the viscous friction coefficient and Fc_j which is the Coulomb friction coefficient.

Now it is defined that $\boldsymbol{h}(\boldsymbol{\chi}, q, \dot{q}) \in \mathbb{R}^n$ combines the coriolis, centripetal, gravitational, and friction effects of the system into a single term.[80]

$$\boldsymbol{h}(\boldsymbol{\chi}, q, \dot{q}) = \boldsymbol{C}(\boldsymbol{\chi}, q, \dot{q})\dot{q} + \boldsymbol{g}(\boldsymbol{\chi}, q) + \boldsymbol{\zeta}(\boldsymbol{\chi}, \dot{q}) \tag{2.113}$$

This allows for the equation 2.110 to be rewritten as the Direct Dynamic Model (DDM) [80], [82] as shown in equation 2.114. The DDM is a second order differential equation that can be solved for the joint accelerations $\ddot{q}$ given the joint positions q, joint velocities $\dot{q}$, and the applied generalized forces $\boldsymbol{\tau}_{idm}$ and the vector of dynamic properties $\boldsymbol{\chi}$.

$$\ddot{\boldsymbol{q}} = \boldsymbol{M}^{-1}(\boldsymbol{\chi}, q)\left(\boldsymbol{\tau}_{idm} - \boldsymbol{h}(\boldsymbol{\chi}, q, \dot{q})\right) \tag{2.114}$$

It can be seen that the DDM is a non-linear function of the dynamic parameters $\boldsymbol{\chi}$ and the joint positions q, joint velocities $\dot{q}$, and robot state vector $\boldsymbol{x} = \left[q^\top, \dot{q}^\top\right]^\top \in \mathbb{R}^{2n}$.

The IDM however is linear in $\boldsymbol{\chi}$ and therefore the applied generalized forces $\boldsymbol{\tau}_{idm}$ can be written as eqn 2.115.

$$\boldsymbol{\tau}_{idm} = \boldsymbol{Y}_{\boldsymbol{\chi}}(\ddot{q}, \dot{q}, q)\boldsymbol{\chi} \tag{2.115}$$

Taking the derivative of eqn 2.115 with respect to $\boldsymbol{\chi}$ we get eqn 2.116.

$$\frac{\partial \boldsymbol{\tau}_{idm}}{\partial \boldsymbol{\chi}} = \boldsymbol{Y}_{\boldsymbol{\chi}}(\ddot{q}, \dot{q}, q) \tag{2.116}$$

$\boldsymbol{Y}_{\boldsymbol{\chi}}(\ddot{q}, \dot{q}, q) \in \mathbb{R}^{n \times p}$ is seen to be the Jacobian matrix in closed form of $\boldsymbol{\tau}_{idm}$ with respect to $\boldsymbol{\chi}$. The Jacobian matrix is a function of the joint accelerations $\ddot{q}$, joint velocities $\dot{q}$, and joint positions q. Additionally, $\boldsymbol{Y}_{\boldsymbol{\chi}}$ is a regressor that is a function of the joint accelerations $\ddot{q}$, joint velocities $\dot{q}$, and joint positions q. [80] It is important to note Eqn 2.115 is only linear if the friction $\boldsymbol{\zeta}(\boldsymbol{\chi}, \dot{\boldsymbol{q}})$ is linear with respect to $\boldsymbol{\chi}$. Moreover, it is assumed that the vectors $\boldsymbol{q}, \dot{\boldsymbol{q}}, \ddot{\boldsymbol{q}}$ and $\boldsymbol{\tau}_{idm}$ are free from noise. Linearity of the system is assumed for the first order approximation of this system, but may not hold true for a more complex system. [80], [83]

2.2.2.1 Computation of the base parameters of the manipulator dynamic model

It is noted that the kinetic and potential energy are linear in the inertial parameters of the system, and therefore the dynamics model is also linear in the inertial parameters [81]. The dynamic model of the system is as follows:

$$\boldsymbol{\tau}_{idm} = \sum_{j=1}^{N_p} \mathbf{D}^{\mathrm{j}} \mathbf{K}_{\mathrm{j}} = \mathbf{D}\mathbf{K} \tag{2.117}$$

where:

Table 2.9: Terms for the dynamic model of the 1 DOF manipulator

Variable	**Dimension**	**Definition**
$\mathbf{D}$	$n \times N_p$	matrix that is a function of $q, \dot{q}, \ddot{q}$
$\mathbf{K}$	$N_p \times 1$	The vector of the standard inertial parameters of a link representing for each link a mass, three elements for the first moments, six elements for the inertia tensor, and
N_p	$11n$	The number of parameters in the system
$\mathbf{D}^{\mathrm{j}}$		The j^{th} column of the matrix $\mathbf{D}$
$\mathbf{K}_{\mathrm{j}}$		The j^{th} element of the vector $\mathbf{K}$

Following the methods developed by Khalil in [81] and Mayada in [18], we can show that there are several different circumstances that can effect and determine the base parameters of the system.

Case 1: $\mathbf{K}_j$ has no effect on the system dynamics if:

$$\mathbf{D}^j = 0 \tag{2.118}$$

Therefore $\mathbf{K}_j$ can be set to zero in equation 2.117 while having no effect on the value of $\boldsymbol{\tau}_{idm}$ and consequently $\mathbf{K}_j$ can be eliminated.

Case 2: $\mathbf{K}_j$ can be grouped with some other parameters $\mathbf{K}_{j1}, \cdots, \mathbf{K}_{jr}$ if the $\mathbf{D}^j$ column is linearly dependent of $\mathbf{D}^{j1}, \cdots, \mathbf{D}^{jr}$ such that:

$$\mathbf{D}^j = t_{j1}\mathbf{D}^{j1} + \cdots + t_{jr}\mathbf{D}^{jr} \tag{2.119}$$

where all t_{jk} are constants.

In this case, the column $\mathbf{D}^j$ and the parameter $\mathbf{K}_j$ can be eliminated while the parameters $\mathbf{K}_{j1}, \cdots, \mathbf{K}_{jr}$ will be replaced by parameters $\mathbf{KR}_{j1}, \cdots, \mathbf{KR}_{jr}$ where $\mathbf{KR}_{jp} = \mathbf{K}_{jp} + t_{jp}\mathbf{K}_j$ for $p = 1, \cdots, r$. This operation will be repeated until the elimination of all the parameters with dependent columns at which point the minimal inertial parameter vector $\mathbf{K_B}$ will be obtained.

The selection of parameters eliminated begins with the eliminations of parameters with the highest subscript in the inertial parameter vector $\mathbf{K}$ and continues until the elimination of all parameters with dependent columns. Just as with the elimination of the parameters of $\mathbf{K}$, the elimination of the columns of $\mathbf{D}$ is done in the same manner starting with the columns with the highest subscript and continuing towards the first column. The parameters of link j of vector $\mathbf{K}_j$ are defined as follows:

$$\mathbf{K}_j = \left[XX_j, XY_j, XZ_j, YY_j, YZ_j, ZZ_j, MX_j, MY_j, MZ_j, M_j, I_{a_j}\right]^\top \tag{2.120}$$

It can be seen that $\mathbf{K}_b$ is directly related to the linear dependence of the columns of $\mathbf{D}$. Making the assumption that b is the rank of the matrix $\mathbf{D}$, the columns of $\mathbf{D}$ can be written as a linear combination of the first b columns of $\mathbf{D}$ as follows:

$$\boldsymbol{\tau}_{idm} = [\mathbf{D1}\ \mathbf{D2}] \begin{bmatrix} \mathbf{K1} \\ \\ \mathbf{K2} \end{bmatrix} \tag{2.121}$$

where:

- $\mathbf{D1}$ is a matrix of the first b independent columns of $\mathbf{D}$
- $\mathbf{D2}$ is the dependent columns of $\mathbf{D}$ with $\mathbf{D2} = \mathbf{D1}\boldsymbol{\beta}$, where $\boldsymbol{\beta}$ is a constant matrix.

As such, the equation 2.121 can be rewritten as:

$$\boldsymbol{\tau}_{idm} = \mathbf{D1}\,[\mathbf{K1} + \boldsymbol{\beta}\mathbf{K2}] = \mathbf{D1}\ \mathbf{K_B} \tag{2.122}$$

A formalized general numerical method for the computation of the base parameters of the system is presented in [82, Appendix 5], [84] using QR decomposition. An additional method for the computation of the base parameters of the system is presented in [82, Section 9.3.4] using energy methods. Part of the QR decomposition method is clarified in [80] and presented here.

$$\boldsymbol{W}_{\chi}\boldsymbol{P} = \boldsymbol{Q} \begin{bmatrix} \boldsymbol{R} \\ \\ \mathbf{0}_{(r-b)\times p} \end{bmatrix} \tag{2.123}$$

where for $r = nN, \boldsymbol{Q} \in \mathbf{O}(r)$, with the upper triangular matrix of rank $b < p, \boldsymbol{R} \in \mathbb{R}^{b\times p}$, and $\boldsymbol{P} \in \mathbf{O}(p)$ is a permutation matrix. The permutation matrix $\boldsymbol{P}$ is by default chosen to be such that the diagonal values of $\boldsymbol{R}$ are in decreasing order[80]. $\overline{\boldsymbol{P}} \in \mathbb{R}^{b\times p}$ is the matrix of the first b columns of $\boldsymbol{P}$ and $\underline{\boldsymbol{P}} \in \mathbb{R}^{p\times(p-b)}$ is the matrix of the last $p-b$ columns of $\boldsymbol{P}$, equation 2.123 can be written as:

$$\underbrace{\begin{bmatrix} \boldsymbol{W}_\chi \overline{\boldsymbol{P}} & \boldsymbol{W}_\chi \underline{\boldsymbol{P}} \end{bmatrix}}_{\boldsymbol{W}_\chi \boldsymbol{P}} = \underbrace{\begin{bmatrix} \overline{\boldsymbol{Q}} & \underline{\boldsymbol{Q}} \end{bmatrix}}_{Q} \begin{bmatrix} \overline{\boldsymbol{R}} & \underline{\boldsymbol{R}} \\ \mathbf{0}_{(r-b)\times p} & \end{bmatrix}$$

$$= \begin{bmatrix} \overline{\boldsymbol{Q}}\,\overline{\boldsymbol{R}} & \overline{\boldsymbol{Q}}\underline{\boldsymbol{R}} \end{bmatrix} \tag{2.124}$$

$$= \overline{\boldsymbol{Q}}\,\overline{\boldsymbol{R}} \begin{bmatrix} \mathbf{1}_{b\times b} & \overline{\boldsymbol{R}}^{-1}\underline{\boldsymbol{R}} \end{bmatrix}$$

$$= \boldsymbol{W}_\chi \overline{\boldsymbol{P}} \begin{bmatrix} \mathbf{1}_{b\times b} & \overline{\boldsymbol{R}}^{-1}\underline{\boldsymbol{R}} \end{bmatrix}$$

with $\overline{\boldsymbol{R}} \in \mathbb{R}^{b\times b}$ and $\underline{\boldsymbol{R}} \in \mathbb{R}^{b\times(p-b)}$ are the first b and the last $p-b$ columns of $\boldsymbol{R}$, respectively. $\boldsymbol{P}$ is orthogonal and therefore it can be shown that:

$$\boldsymbol{W}_\chi \boldsymbol{\chi} = \begin{bmatrix} \boldsymbol{W}_\chi \overline{\boldsymbol{P}} & \boldsymbol{W}_\chi \underline{\boldsymbol{P}} \end{bmatrix} \begin{bmatrix} \overline{\boldsymbol{\chi}} \\ \underline{\boldsymbol{\chi}} \end{bmatrix} \tag{2.125}$$

with $\overline{\boldsymbol{\chi}} = \overline{\boldsymbol{P}}^\top$ allowing for the substitution in equation 2.125 to be written as:

$$\boldsymbol{W}_\chi \boldsymbol{\chi} = \boldsymbol{W}_\chi \overline{\boldsymbol{P}} \begin{bmatrix} \mathbf{1}_{b\times b} & \overline{\boldsymbol{R}}^{-1}\underline{\boldsymbol{R}} \end{bmatrix} \begin{bmatrix} \overline{\boldsymbol{\chi}} \\ \underline{\boldsymbol{\chi}} \end{bmatrix} \tag{2.126}$$

$$= \boldsymbol{W}_\chi \overline{\boldsymbol{P}} \boldsymbol{\beta} \tag{2.127}$$

The *non-bijective* mapping between the base parameter vector $\boldsymbol{\beta}$ and the standard parameter vector $\boldsymbol{\chi}_s$ is defined as follows:

$$\boldsymbol{\beta} = \begin{bmatrix} \overline{\boldsymbol{P}}^\top & \overline{\boldsymbol{R}}^{-1}\underline{\boldsymbol{R}}\,\underline{\boldsymbol{P}}^\top \end{bmatrix} \boldsymbol{\chi} \tag{2.128}$$

With this the problem of robot identification can be solved by estimating the value of $\boldsymbol{\beta}$ such that the dynamic behavior of the model matches that of the actual robot while tracking the planned excitation trajectory. Leboutet continues to note that some of the base parameters may only have a very minor influence on the dynamic behavior of the robot and therefore can be eliminated in usage of the method. [80] A further reduced set of parameters is called the *"essential parameters"* [85], but this further elimination is beyond the scope for this thesis.

2.2.2.2 Calculation of the Inertial Parameters of a Manipulator System via the Inverse Dynamic Identification Model

The identification model in general form is as follows:

$$\boldsymbol{\tau}_{idm} = \mathbf{ID}(\boldsymbol{\chi}_s, \ddot{q}, \dot{q}, q) \tag{2.129}$$

where

- $\boldsymbol{\tau}_{idm}$ is the $(n \times 1)$ vector of the input torques
- $\boldsymbol{\chi}_s$ is the $(N_s \times 1)$ vector of the standard inertial parameters of the system
- $\ddot{q}, \dot{q}, q$ are the $(n \times 1)$ vectors of the acceleration, velocity, and position of the system
- $\mathbf{ID}$ is the identification model
- $\boldsymbol{\chi}_s$ is the vector of the standard (base) inertial parameters of the system
- N_s is the number of independent links and $s \leq n$ where n is the number of links

A model can be chosen such that the link inertial parameters obtain the linear dynamic model in relation to the inertial parameters, such that the torques can be written as:

$$\boldsymbol{\tau}_{idm} = \boldsymbol{Y}_{\boldsymbol{\chi}}(q, \dot{q}, \ddot{q})\boldsymbol{\chi}_s = \sum_{i=1,N_s} \boldsymbol{Y}_{\boldsymbol{\chi}}^{i}\, \boldsymbol{\chi}_{si} \tag{2.130}$$

where:

- $\boldsymbol{Y}_{\boldsymbol{\chi}}$ is the $(n \times N_s)$ matrix of the regressor
- $\boldsymbol{Y}_{\boldsymbol{\chi}}^{i}$ is the vector of the regressor for the ith column of $\boldsymbol{Y}_{\boldsymbol{\chi}}$
- $\boldsymbol{\chi}_{si}$ is the i^{th} element of $\boldsymbol{\chi}_s$
- $\boldsymbol{\chi}_s$ is the vector of manipulator standard inertial parameters such that - $\boldsymbol{\chi}_s = \left[\boldsymbol{\chi}_s^{1\top}, \boldsymbol{\chi}_s^{2\top}, \cdots, \boldsymbol{\chi}_s^{n\top}\right]^{\top}$
- $\boldsymbol{\chi}_s^j$ is the vector of the dynamics parameters of the j^{th} joint and link

and the vector $\boldsymbol{\chi}_s^j$ is defined as:

$$\boldsymbol{\chi}_s^j = \left[XX_j, XY_j, XZ_j, YY_j, YZ_j, ZZ_j, MX_j, MY_j, MZ_j, M_j, I_{a_j}, F_{sj}, F_{vj}\right]^{\top} \tag{2.131}$$

The columns of the matrix $\boldsymbol{Y}_{\boldsymbol{\chi}}(q, \dot{q}, \ddot{q})$ are obtained by the recursive Newton-Euler algorithm for the dynamic model of the system. It calculates the input torques $\boldsymbol{\tau}_{idm}$ in terms of the inertial parameters of the system $\boldsymbol{\chi}_s$, such that the i^{th} column of $\boldsymbol{Y}_{\boldsymbol{\chi}}$ is given by:

$$\boldsymbol{Y}_{\boldsymbol{\chi}}^{i} = \mathbf{ID}(\ddot{q}, \dot{q}, q, \text{ where } \boldsymbol{\chi}_s^i = 1, \boldsymbol{\chi}_s^j = 0 \text{ for } j \neq i) \tag{2.132}$$

From here the next step is to determine the base parameters of the system. The base parameters of the system are the inertial parameters of the manipulator that are excited by the motion of the manipulator, and are therefore identifiable. Once they have been identified, a sufficient number of samples t_i, for $i = 1, \cdots, N_c$ are taken such that $(n \times N_c) \gg N_b$ where N_b is the number of base parameters of the system, to obtain an over-determined system of $n \times N_c$ equations in N_b unknowns.

$$\boldsymbol{Y} = \boldsymbol{W}\boldsymbol{\chi} + \boldsymbol{\rho} \tag{2.133}$$

where:

- $\boldsymbol{Y}$ is the $(n \times N_c)$ matrix of the measured or estimated input torques
- $\boldsymbol{W}\boldsymbol{\chi}$ is the collected data for the system, predicted by the model
- $\boldsymbol{\rho}$ is the $((n \times N_c) \times 1)$ vector of errors between the data in $\boldsymbol{Y}$ and the predicted data in $\boldsymbol{W}\boldsymbol{\chi}$
- $\boldsymbol{W}(q, \dot{q}, \ddot{q})$ is the $((n \times N_c) \times N_b)$ observation matrix

$\boldsymbol{Y}$ and $\boldsymbol{W}$ are obtained by the equations of each joint on all the trajectory such that:

$$\boldsymbol{Y} = \begin{bmatrix} \boldsymbol{Y}_1 \\ \boldsymbol{Y}_2 \\ \vdots \\ \boldsymbol{Y}_n \end{bmatrix}, \boldsymbol{W} = \begin{bmatrix} \boldsymbol{W}_1 \\ \boldsymbol{W}_2 \\ \vdots \\ \boldsymbol{W}_n \end{bmatrix} \tag{2.134}$$

where $\boldsymbol{Y}_i$ and $\boldsymbol{W}_i$ are a representation of all equations of joint i.

In order to solve the over-determined system of equations in 2.133, the ordinary (OLS) or weighted (WLS) least squares method is used. Khalil notes that Although OLS and other methods can be used, the WLS method is preferred as it has performed the best to the authors knowledge [83].

The estimation of $\boldsymbol{\chi}$ is obtained as the OLS solution of the system of equations in 2.133 as follows:

$$\hat{\boldsymbol{\chi}} = \underset{\chi}{\text{Arg}\cdot\min}\|\rho\|^2 = \boldsymbol{W}^+\boldsymbol{Y} \tag{2.135}$$

where $\boldsymbol{W}^+ = (\boldsymbol{W}^\top\boldsymbol{W})^{-1}\boldsymbol{W}^\top$ is the pseudo-inverse of $\boldsymbol{W}$.

When $\boldsymbol{W}$ is full rank, the LS solution, $\hat{\boldsymbol{\chi}}$ is unique. However, when $\boldsymbol{W}$ is not full rank, the solution is not unique, and the solution is not guaranteed to be the true value of $\boldsymbol{\chi}$. Khalil notes that rank deficiency can come from two sources:

- Structural rank deficiency: The model has dependencies between the parameters and can be solved by calculating the base parameters of the system

- Data rank deficiency: The data is noisy in the experimental values of $q, \dot{q}, \ddot{q}$ samples in the $\boldsymbol{W}$ matrix. This can be solved by better planning of trajectories to excite the parameters of the system.

In the experimental world, it is difficult to impossible to obtain measurements or estimates of $\boldsymbol{\Gamma}(t_i), \boldsymbol{q}(t_i), \dot{\boldsymbol{q}}(t_i), \ddot{\boldsymbol{q}}(t_i)$ that provide clean data. For the case of noisy data, the matrices $\boldsymbol{Y}$ and $\boldsymbol{W}$ are perturbed by the noise in the data, and therefore the LS solution may lead to a bias estimation if the two random matrices are not independent. With the coefficients of the observation matrix $\boldsymbol{\Phi}(q, \dot{q}, \ddot{q})$ being non-linear functions of $q, \dot{q}, \ddot{q}$, it is not possible to get the bias and

variance of the LS solution. As such, a twofold strategy is used to reduce the bias and variance of the LS solution:

- Data filtering: The data is filtered to reduce the noise in the data (usually a low pass filter)

- Closed loop identification: The data is generated in such a way that the system tracks the motion and ensures that the excitation is as planned

To cancel high frequency torque ripple in $\boldsymbol{\tau}_{idm}$, a low pass filter is used to filter the data of both the $\boldsymbol{Y}$ vector and the columns of the observation matrix $\boldsymbol{W}$. Additionally, the data can be decimated, such as the Matlab *decimate* function to reduce the number of samples and the computational time of the identification process.

Continuing with the calculation we consider the standard deviations and estimate them while assuming $\boldsymbol{W}$ to be deterministic, and ρ to be a mean additive independent Gaussian noise, with a standard deviation of σ_p [82, Chapter 4] such that:

$$\mathbf{C}_\rho = \mathrm{E}\left(\rho\rho^\top\right) = \sigma_p^2 \mathbf{I}_r \tag{2.136}$$

where $\mathrm{E}()$ is the expectation operator and $\mathbf{I}_r$ is the identity matrix of size $r \times r$. An unbiased estimation of σ_p is given by:

$$\sigma_p^2 = \frac{\|\boldsymbol{Y} - \boldsymbol{W}\hat{\boldsymbol{\chi}}\|^2}{r - c} \tag{2.137}$$

Using this estimate we get the following covariance matrix for estimation error:

$$\mathbf{C}_{\hat{\chi}} = \mathrm{E}\left[(\chi - \hat{\chi})(\chi - \hat{\chi})^{\mathrm{T}}\right] = \sigma_\rho^2 \left(\mathbf{W}^{\mathrm{T}}\mathbf{W}\right)^{-1} \tag{2.138}$$

The standard deviation $\sigma_{\hat{\chi}_j}$ and its relative value $\sigma_{\hat{\chi}\,jr}\%$ are given by:

$$\sigma_{\hat{\chi}j} = \sqrt{\mathbf{C}_{\hat{\chi}}(j,j)} \tag{2.139}$$

$$\sigma_{\hat{\chi}_{jr}\%} = 100\frac{\sigma_{\hat{\chi}j}}{|\hat{\chi}_j|} \tag{2.140}$$

The equations for joint i will be weighted by the inverse of the standard deviation of the error calculated using the equations of joint i.

Chapter 3: Methodology for Dynamics Parameter Identification of Dexterous Free-Flyers

Based upon all the work that has been done by others, it can be noticed that there is a gap in the knowledge base for the identification of inertial parameters for the payload of a free-flying spacecraft with an attached dexterous manipulator. Although the contributions of Longman *et al.'s* Reaction Moment Compensation [50], Vafa *et al.'s* virtual manipulator [49], [52], [53], Papadopoulos *et al.'s* Barycentric Vector Approach [54]–[57], and Moosavian *et al.'s* Direct Path Method [86]–[88] all are important contributions to dynamics for free flying spacecraft. However, Yoshida *et al.'s* Generalized Jacobian Matrix (GJM) [44], [45], [62], [89]–[92] will integrate better with the methodology of both inverse and direct dynamic models for inertial parameter identification of an unknown payload, and therefore will be used for the following derivations. Nevertheless, the ideas and methods from the other contributions will be used as a lens by which to draw inspiration from for the development of the extended-inverse direct dynamic model (ExIDDM) for inertial parameter identification of a free-flying spacecraft with an attached dexterous manipulator.

3.1 Insights From Existing Literature

Prior work has shown that there are methods for extending work from a ground fixed manipulator to that of a free flying spacecraft. The work of Yoshida extended the work of Mayada for ground fixed manipulators. The work of Longman extended the work of many others to look at the reaction forces that the manipulator applies to the spacecraft and then use momentum storage devices to react those forces. Each of the methods in literature have limitations, as do all methods of modeling systems, and they will be explored as a lens by which to gather further insights into how existing inertial parameter identification methods can be extended into the realm of free-flying spacecraft with attached robotic manipulators. A quick summary of the limitations of existing methods will highlight the need for this work.

3.1.1 Limitations of Existing Methods

From the existing work, we can see that the major limitations of existing methods are as follows.

- Many of the methods for the dynamics of spacecraft mounted dexterous manipulators, are for free-floating systems
- All the spacecraft dynamics methods make the assumption that the mass and inertia of a payload to be grappled is already known for both the capture phase and the post-capture phase within a reasonable percentage of error
- Existing Inertial parameter identification methods for robotic manipulators assume that the robot is rigidly attached to the ground and therefore react their forces into their mount

- Observers and estimators from control theory require direct observability of the state of the system to be estimated before they can be used
- Prescribed performance control methods ignore the problem of parameter identification and assume that the system is controllable and attempts to adapt without knowing the true parameters of the system

Although these limitations are not insurmountable, they do highlight the need for a new method for payload inertial parameter identification for free-flying spacecraft with attached dexterous manipulators.

3.1.2 Insights from Existing Methods Used to Extend Ground Fixed Manipulators to Free-Flying Spacecraft

The existing methods from literature for extending ground fixed manipulators to that of a free-floating or free-flying spacecraft were highlighted through section 2.1 and the subsections within. The methods of Longman et al. [50], Vafa et al. [49], [52], [53], Papadopoulos et al. [54]–[57], and Moosavian et al. [86]–[88] all have their merits and their limitations. The work of Yoshida et al. [44], [45], [62], [89]–[92] has shown that the GJM method can be used to extend the work of Mayada [18] for ground fixed manipulators to free-flying spacecraft. The GJM is a generalized method for deriving the equations of motion for a free-flying spacecraft with an attached manipulator and demonstrates how to generate a Jacobian for a combined spacecraft and manipulator system.

Longman et al. [50] showed that the reaction forces from a manipulator can be reacted into momentum storage devices to reduce the reaction forces that the spacecraft must react. This

method is limited in that it requires the reaction forces to be reacted into momentum storage devices and that the payload characteristics are already known. It did however show that the methods for ground fixed manipulators can be extended to free-floating spacecraft.

The work of Yoshida et al. [44], [45], [62], [89]–[92] has shown that the Generalized Jacobian Matrix (GJM) can be used to extend the work of Mayada [18] for ground fixed manipulators to free-flying spacecraft. The GJM can be used in the same way as a ground fixed manipulator Jacobian, but for deriving the equations of motion for a free-flying spacecraft with an attached manipulator. The process that Yoshida et al. used to derive the equations of motion for a free-flying spacecraft with an attached manipulator provided much of the inspiration for the following ExIDDM method.

For inertial parameter identification, the initial work for the IDDM method was done by Khalil *et al.* [81] Further work was done to extend the IDDM method to work with non-linear methods and with improved performance in certain cases [80] Nevertheless, the linear IDDM method will be used for the following derivations to show that extension of the method is possible to the ExIDDM method for free-flying spacecraft with attached dexterous manipulators.

Figure 3.1 shows a visual summary of the methods from literature that will be used as inspiration for the development of the ExIDDM for inertial parameter identification of a free-flying spacecraft with an attached dexterous manipulator.

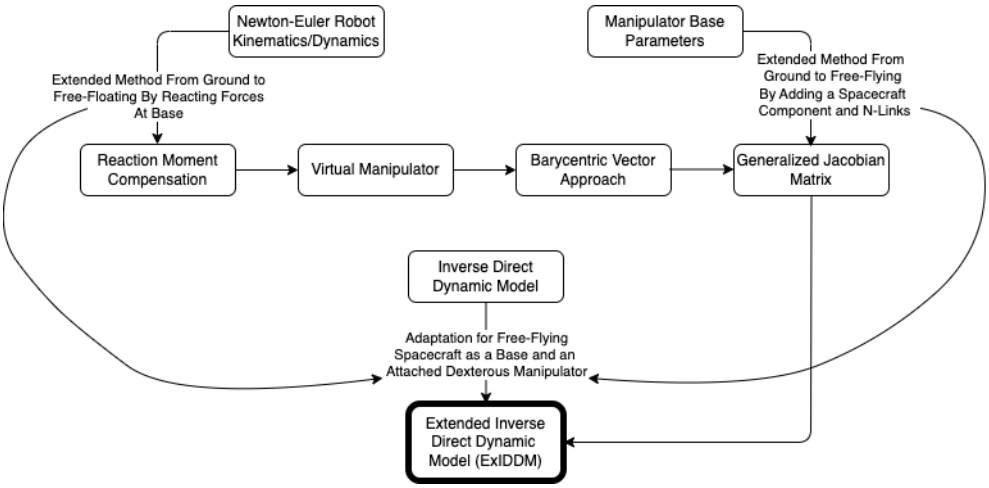

Figure 3.1: Inspiration Diagram

3.2 The Extended-Inverse Direct Dynamic Model (ExIDDM) for Inertial Parameter Identification

3.2.1 Inverse Direct Dynamic Model - Review from Literature

Let us bring in equation 2.110 as a starting point for this derivation, repeated here for clarity.

$$\boldsymbol{M}(\boldsymbol{\chi}, q)\ddot{q} + \boldsymbol{C}(\boldsymbol{\chi}, q, \dot{q})\dot{q} + \boldsymbol{g}(\boldsymbol{\chi}, q) + \boldsymbol{\zeta}(\boldsymbol{\chi}, \dot{q}) = \boldsymbol{\tau}_{idm}$$

where the terms for this equation are defined as follows:

Table 3.1: IDDM Terms for repeated equation 2.110

Variable	**Definition**
$\boldsymbol{M}(\boldsymbol{\chi}, q)\ddot{q} \in \mathbb{R}^{n\times n}$	Generalized inertia matrix for the system containing inertial parameters for all components
$\boldsymbol{C}(\boldsymbol{\chi}, q, \dot{q})\dot{q} \in \mathbb{R}^{n\times n}$	Coriolis and centripetal effect matrix for the system
$\boldsymbol{g}(\boldsymbol{\chi}, q) \in \mathbb{R}^{n}$	Gravitational torque vector for the system
$\boldsymbol{\zeta}(\boldsymbol{\chi}, \dot{q}) \in \mathbb{R}^{n}$	Friction vector for the system
$\boldsymbol{\tau}_{idm} \in \mathbb{R}^{n}$	Input torque vector for the system
$\boldsymbol{\chi} \in \mathbb{R}^{n}$	Inertial parameters matrix for the system

$\boldsymbol{\chi}$ is the inertial parameters matrix for the system and is defined in equation 2.111 repeated as follows:

$$\boldsymbol{\chi} = \left[\boldsymbol{\chi}_1^\top \; \boldsymbol{\chi}_2^\top \cdots \boldsymbol{\chi}_n^\top\right]^\top \in \mathbb{R}^p$$

with a single link inertial parameter vector from equation 2.112 repeated here:

$$\boldsymbol{\chi}_j = [XX_j, XY_j, XZ_j, YY_j, YZ_j, ZZ_j, MX_j, MY_j, MZ_j, M_j, Ia_j, Fv_j, Fc_j]^\top$$

and the single link inertia tensor broken out here:

$$\boldsymbol{L}_j = [XX_j, XY_j, XZ_j, YY_j, YZ_j, ZZ_j]^\top \tag{3.1}$$

The terms for equations are repeated in table 3.2 for clarity.

Table 3.2: Terms for repeated equations 2.111 and 2.112

Variable	**Definition**
$\boldsymbol{\chi}$	The inertial parameters matrix for the system
$\boldsymbol{\chi}_j$	The inertial parameters matrix for the j^{th} link
n	The number of DOF in the system
$\boldsymbol{L}_j$	The Inertia tensor for the j^{th} link
$XX_j, XY_j, XZ_j, YY_j, YZ_j, ZZ_j$	The elements of the Inertia tensor for the j^{th} link
MX_j, MY_j, MZ_j	The first moments of the j^{th} link CoM
M_j	Mass of the j^{th} link
$\boldsymbol{I}a_j$	Inertia of actuator and gear train the j^{th} link
$\boldsymbol{\zeta}_j$	Viscous and Coulomb friction $[\boldsymbol{F}v_j \boldsymbol{F}c_j]^\top$ of the j^{th} link
$\boldsymbol{F}v_j$	Viscous friction of the j^{th} link
$\boldsymbol{F}c_j$	Coulomb friction of the j^{th} link

$$\boldsymbol{\mathcal{L}}_j = [X_j, Y_j, Z_j]^\top \tag{3.2}$$

$$\boldsymbol{\zeta}_j = [Fv_j, Fc_j]^\top \tag{3.3}$$

Following along with the substitutions, assumptions, and derivations from section 2.2.2, we can see that the finalized equations for the IDDM method are as follows with equations 2.113, 2.114, 2.115, 2.116 repeated here for clarity.

$$\begin{aligned}
\boldsymbol{h}(\boldsymbol{\chi}, q, \dot{q}) =& \boldsymbol{C}(\boldsymbol{\chi}, q, \dot{q})\dot{q} + \boldsymbol{g}(\boldsymbol{\chi}, q) + \boldsymbol{\zeta}(\boldsymbol{\chi}, \dot{q} \\
\ddot{\boldsymbol{q}} =& \boldsymbol{M}^{-1}(\boldsymbol{\chi}, q)\left(\boldsymbol{\tau}_{idm} - \boldsymbol{h}(\boldsymbol{\chi}, q, \dot{q})\right) \\
\boldsymbol{\tau}_{idm} =& \boldsymbol{Y}_{\boldsymbol{\chi}}(\ddot{q}, \dot{q}, q)\boldsymbol{\chi} \\
\frac{\partial \boldsymbol{\tau}_{idm}}{\partial \boldsymbol{\chi}} =& \boldsymbol{Y}_{\boldsymbol{\chi}}(\ddot{q}, \dot{q}, q)
\end{aligned}$$

Where $\boldsymbol{Y}_{\boldsymbol{\chi}}(\ddot{q}, \dot{q}, q) \in \mathbb{R}^{n \times p}$ is seen to be the Jacobian matrix in closed form of $\boldsymbol{\tau}_{idm}$ with respect to $\boldsymbol{\chi}$. With all the terms for the IDDM refreshed from the literature, we can now begin to look at the extension of the IDDM to include the inertial parameters of a payload to be grappled by a free-flying spacecraft with an attached dexterous manipulator.

3.3 Derivation of the Extended-Inverse Direct Dynamic Model for Inertial Parameter Identification

We begin the derivation for the extended inverse direct dynamic model (ExIDDM) by looking at the nature of the equations for the IDDM to understand how the transition to a free-flying spacecraft effects the original IDDM equations. We will then look at the equations for the GJM to

understand how the integration into the IDDM equations will happen. Finally, we will look at the derived equations for the ExIDDM to understand how the ExIDDM equations for the free-flying spacecraft with an attached dexterous manipulator behaves. Looking at eqn 2.110 we can see that the IDDM equations have a gravity term, $\boldsymbol{g}(\boldsymbol{\chi}, q)$, that will not be present in microgravity and therefore will be equal to zero as seen in eqn 3.4.

$$\boldsymbol{M}(\boldsymbol{\chi}, q)\ddot{q} + \boldsymbol{C}(\boldsymbol{\chi}, q, \dot{q})\dot{q} + \cancel{\boldsymbol{g}(\boldsymbol{\chi}, q)} + \boldsymbol{\zeta}(\boldsymbol{\chi}, \dot{q}) = \boldsymbol{\tau}_{idm} \tag{3.4}$$

$\boldsymbol{M}(\boldsymbol{\chi}, q)\ddot{q}$ remains invertible by definition. Additionally, drawing inspiration from the derivation of the GJM we add two terms to the $\boldsymbol{\chi}$ matrix. The first added term is the $\boldsymbol{\chi}_0^\top$ term which represents the spacecraft not present in the original IDDM. The second added term to $\boldsymbol{\chi}$ is the inertial parameter matrix for the payload "link", $\boldsymbol{\chi}_{n+1}^\top$. These terms are added to the $\boldsymbol{\chi}$ matrix as seen in eqn 3.5 at the beginning and end similar to what Umetani and Yoshida did with the GJM [2.1.5].

$$\boldsymbol{\chi}_{Ex} = \left[\boldsymbol{\chi}_0^\top \ \boldsymbol{\chi}_1^\top \ \boldsymbol{\chi}_2^\top \cdots \boldsymbol{\chi}_n^\top \ \boldsymbol{\chi}_{n+1}^\top\right]^\top \tag{3.5}$$

With this extension we now have a mechanism to discuss the inertially fixed motion of the spacecraft-manipulator-payload system for the calculation of the ExIDDM.

$$\dot{P} = \begin{bmatrix} \dot{p}_n \\ \omega_n \end{bmatrix} = \bar{\boldsymbol{J}}(\boldsymbol{\phi})\dot{\boldsymbol{\phi}} + \dot{\boldsymbol{P}}_0 \text{ (From GJM)}$$

$$\frac{\partial \boldsymbol{\tau}_{idm}}{\partial \boldsymbol{\chi}} = \boldsymbol{Y}_{\boldsymbol{\chi}}(\ddot{q}, \dot{q}, q) \text{ (From IDDM)}$$

with the individual variables of the ExIDDM defined in table 3.3.

Variable	Definition
$\boldsymbol{M}(\boldsymbol{\chi}, q)\ddot{q} \in \mathbb{R}^{(n+2)\times(n+2)}$	Generalized inertia matrix for the system containing inertial parameters for all components
$\boldsymbol{Y}_{\boldsymbol{\chi}}(\ddot{q}, \dot{q}, q) \in \mathbb{R}^{(n+2)\times p}$	Jacobian matrix with respect to $\boldsymbol{\chi}$
$\boldsymbol{\tau}_{idm} \in \mathbb{R}^{n+2}$	Input torque vector for the system
$\boldsymbol{\chi} \in \mathbb{R}^{n+2}$	Inertial parameters matrix for the system
$\dot{\boldsymbol{P}}_0 = (\boldsymbol{v}_G^\top, \boldsymbol{\omega}_G^\top)^\top$	Initial translational and rotational movement of the base satellite
${}^A\dot{\boldsymbol{r}}_0 + {}^A\dot{A}_0{}^0\boldsymbol{b}_0$	Rotation and translation of the base satellite in the GJM

Table 3.3: ExIDDM variables modified by extension

Here we can see that the GJM, $\bar{\boldsymbol{J}}^*(\boldsymbol{\phi})$, is used in the repeated equation for the equations of motion for the system $\dot{\boldsymbol{P}}$ from equation 2.91 and 2.92 repeated here for clarity.

$$\dot{\boldsymbol{P}} = \left(\bar{\boldsymbol{J}}_M - \bar{\boldsymbol{J}}_S \bar{\boldsymbol{I}}_S^{-1} \bar{\boldsymbol{I}}_M\right) \dot{\boldsymbol{\phi}}_M + \dot{\boldsymbol{P}}_0 \qquad \text{(2.91 revisited)}$$

$$\dot{\boldsymbol{P}} = \bar{\boldsymbol{J}}^* \dot{\boldsymbol{\phi}}_M + \dot{\boldsymbol{P}}_0 \qquad \text{(2.92 revisited)}$$

and the Generalized Jacobian Matrix $\bar{\boldsymbol{J}}^*(\boldsymbol{\phi})$ is defined in equation 2.93 repeated here for clarity.

$$\bar{\boldsymbol{J}}^* = \bar{\boldsymbol{J}}_M - \bar{\boldsymbol{J}}_S \bar{\boldsymbol{I}}_S^{-1} \bar{\boldsymbol{I}}_M \qquad \text{(2.93 revisited)}$$

Substituting in the Jacobian from equation 2.85 we get the following equation for the GJM.

$$\dot{\boldsymbol{P}} = \begin{bmatrix} \dot{p}_n \\ \omega_n \end{bmatrix} = \bar{\boldsymbol{J}}(\boldsymbol{\phi})\dot{\boldsymbol{\phi}} + \dot{\boldsymbol{P}}_0 \tag{3.6}$$

$$= \begin{bmatrix} \overline{\boldsymbol{J}}_\alpha & \overline{\boldsymbol{J}}_\beta & \overline{\boldsymbol{J}}_\gamma & \overline{\boldsymbol{J}}_{\phi_1} & \cdots & \overline{\boldsymbol{J}}_{\phi_n} \\ {}^A A_\alpha \boldsymbol{i} & {}^A \boldsymbol{A}_\beta \boldsymbol{j} & A {}^A A_\gamma \boldsymbol{k} & {}^A A_0 \boldsymbol{k} & \cdots & A_n \boldsymbol{A} \end{bmatrix} \cdot \begin{bmatrix} \dot{\alpha} \\ \dot{\beta} \\ \dot{\gamma} \\ \dot{\phi}_1 \\ \vdots \\ \dot{\phi}_n \end{bmatrix} + \dot{\boldsymbol{P}}_0$$

where

$$\bar{\boldsymbol{J}}(\boldsymbol{\phi}_i) = \begin{cases} v_{0i} + {}^A \dot{\boldsymbol{r}}_0 + {}^A \dot{A}_0{}^0 \boldsymbol{b}_0 & + \sum_{j=i}^{n} \frac{\partial^A A_j{}^j}{\partial \phi_i} l_j \quad (\phi = \alpha, \beta, \gamma) \\ v_{0i} & + \sum_{j=i}^{n} \frac{\partial^A A_j{}^j}{\partial \phi_i} l_j \quad (i = 1 \cdots n) \end{cases} \tag{3.7}$$

$$\frac{\partial \boldsymbol{\tau}_{idm}}{\partial \boldsymbol{\chi}} = \boldsymbol{Y}_{\boldsymbol{\chi}}(\ddot{q}, \dot{q}, q) + \dot{\boldsymbol{P}}_0 \tag{3.8}$$

with the individual variables:

$$\boldsymbol{Y}_{\boldsymbol{\chi}}(\ddot{q}, \dot{q}, q) \in \mathbb{R}^{(n+2)\times p} = \text{Jacobian matrix with respect to } \boldsymbol{\chi}$$

$$\boldsymbol{\tau}_{idm} \in \mathbb{R}^{n+2} = \text{Input torque vector for the system}$$

$$\boldsymbol{\chi} \in \mathbb{R}^{n+2} = \text{Inertial parameters matrix for the system}$$

$$\dot{\boldsymbol{P}}_0 = (\boldsymbol{v}_G^\top, \boldsymbol{\omega}_G^\top)^\top = \text{Initial translational and rotational movement of the base satellite}$$

$${}^A\dot{\boldsymbol{r}}_0 + {}^A\dot{A}_0{}^0\boldsymbol{b}_0 = \text{Rotation and translation of the base satellite in the GJM}$$

The addition of the $\dot{\boldsymbol{P}}_0$ allows for the tracking of the initial conditions of the system that was not tracked with the IDDM method as it was defined to be rigidly fixed to the ground. This addition allows for the tracking of the initial conditions of the system and the inertial parameters of the spacecraft and payload grappled by the free-flying spacecraft with an attached dexterous manipulator. The ExIDDM method is now fully defined and ready for use in the inertial parameter identification of a free-flying spacecraft with an attached dexterous manipulator.

There however do exist some limitations for the ExIDDM method, just as there are with the IDDM method. The limitations of the ExIDDM method are as follows:

- $\boldsymbol{\tau_{idm}}$ is only linear if $\boldsymbol{\zeta}(\boldsymbol{\chi}, \ddot{q})$ is linear w.r.t. $\boldsymbol{\chi}$
- The vectors $\boldsymbol{q}, \dot{\boldsymbol{q}}, \ddot{\boldsymbol{q}}$ and $\boldsymbol{\tau}_{idm}$ are assumed to be free from noise
- Linearity is assumed in the system, which may not hold true for particularly complex systems or systems with long flexible links
- Only observable states can be found with the ExIDDM method. These base dynamics

parameters are sometimes grouped with other parameters in the system and may not be directly observable

With this construction of the variables and the equations for the ExIDDM method, it is possible to use the various Inverse Dynamics Identification Methods (IDIM) to identify the observable inertial parameters of a free-flying spacecraft with an attached dexterous manipulator.

Chapter 4: Experimental Validation of the Extended Inverse Direct Dynamic Model for Inertial Parameter Identification

4.1 Introduction

The extended inverse direct dynamic model (ExIDDM) for inertial parameter identification of a captured payload attached to a robotic manipulator on a free-flying spacecraft was validated experimentally using several simulation environments.

The first simulation environment used was an air bearing table. The air bearing table is a flat surface that uses a thin layer of air to support the payload. This allows the payload to move with very little friction. The air bearing table was used to simulate the microgravity environment of space. However, it is not a perfect simulation as all objects on the table are still subject to the forces of gravity as well has having two rotational axes and one translational axis limited by the reaction forces of the table. The air bearing table was used to validate the ExIDDM in a controlled environment before moving on to more complex simulation environments. Additionally, as this method was being developed it was originally targeted for identification of the spacecraft's inertial parameters. The air bearing table was used to validate the ExIDDM for this purpose as well.

The second simulation environment used was parabolic flights. Parabolic flights are a

method of simulating microgravity by flying an aircraft in a parabolic trajectory. This allows the aircraft to experience brief periods of microgravity. Parabolic flights were used to validate the ExIDDM in a more realistic microgravity environment. The parabolic flights were also used to validate the ExIDDM for the identification of the spacecraft's inertial parameters.

The third simulation environment used was a suborbital flight. Suborbital flights are a method of reaching the edge of space without entering orbit. Suborbital flights were used to validate the ExIDDM in a more realistic space environment. The suborbital flights Was the first of the simulation environments to be used to validate the ExIDDM for the identification of the payload's inertial parameters.

First, before the experiments are described, it is important to cover how the mass moment of inertia can be empirically determined for the objects of the system being tested. Each of the sections and subsections following will describe each of the three simulation environments, experiments, and the results of each experiment.

4.2 Empirical Determination of the Mass Moment of Inertia

The mass moment of inertia is a tensor, and is defined as the sum of the products of the mass of each particle in the object and the square of the distance from the axis of rotation. Mass moment of inertia is a measure of an object's resistance to changes in its rotation. The bifilar vertical-axis torsional pendulum method is a simple method of determining the mass moment of inertia of an object by measuring the period of oscillation of the object suspended by two strings. The mass moment of inertia of the object can be calculated using the period of oscillation and the geometry of the object. An example of the Bifilar Vertical-Axis Torsional Pendulum is shown in

Figure 4.1 and follows the method presented by Jardin [93].

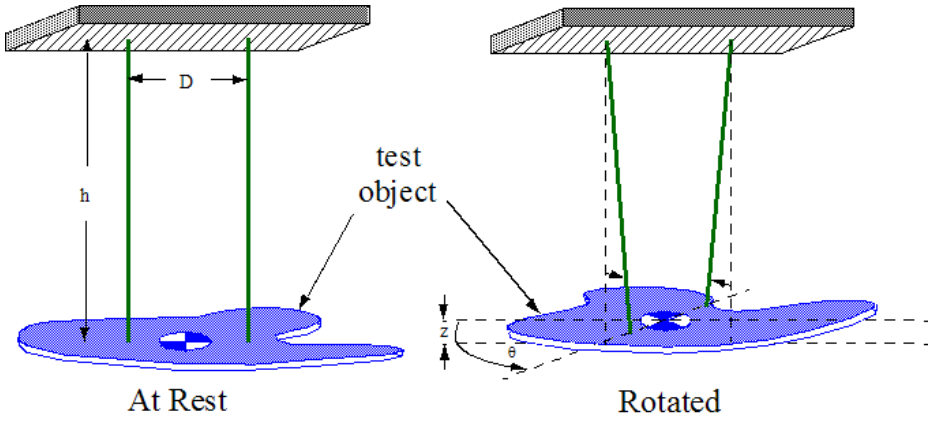

Figure 4.1: Bifilar Vertical-Axis Torsional Pendulum [93]

Using a Lagrangian approach the mass moment of inertia can be calculated using the following linearized equation that ignores the insignificant energy of the raising and lowering of the test object and suspension wires.

$$T = \frac{1}{2} I \dot{\Theta}^2 \tag{4.1}$$

In this equation, T is the total kinetic energy of the system, I is the mass moment of inertia about the vertical axis (Z), and $\dot{\Theta}$ is the angular velocity of the system. The gravitational potential energy of the system is given by:

$$V = mgz \tag{4.2}$$

where V is the gravitational potential energy, m is the mass of the object, g is the acceleration due to gravity, and z is the height displacement of the object center of gravity. The total energy of the system is the sum of the kinetic and potential energy:

The damping force of the system's rotational motion is the via aerodynamic drag and vis-

cous damping of the suspension wires. The damping force is given by the model:

$$Q = -K_D\dot{\Theta}|\dot{\Theta}| - C\dot{\Theta} \tag{4.3}$$

where Q is the damping force, K_D is the drag coefficient, and C is the viscous damping coefficient. The total energy of the system is the sum of the kinetic and potential energy and the Lagrangian dynamics of the system are given by the following equation of motion:

$$\ddot{\Theta} + \left(\frac{K_D}{I}\dot{\Theta}|\dot{\Theta}| + \frac{C}{I}\dot{\Theta}\right) + \left(\frac{mgD^2}{4Ih}\right)\frac{\sin\Theta}{\sqrt{1 - 0.5\left(\frac{D}{h}\right)^2(1-\cos\Theta)}} = 0 \tag{4.4}$$

A simplified version of this non-linear equation of motion can be used to determine the mass moment of inertia of the object, and can be linearized by making the assumptions of a small angle of oscillation and ignoring the damping coefficient. The linearized equation of motion is given by:

$$I = \left(\frac{mgD^2}{4h\omega_n^2}\right) \tag{4.5}$$

An advantage of the linearized model is that the measurements of the system are greatly simplified to measuring the frequency of oscillations, ω_n, and the geometry of the object, but does come at the expense of accuracy of the measured values [93].

4.3 Air Bearing Table

The air bearing experiment was conducted in the University of Maryland's Advanced Robotics Development Laboratory. The air bearing table is a flat surface consisting of a quar-

ter inch thick sheet of plate glass on top of a metal optical bench. The air bearing carriage rides on a cushion of air that is supplied by two liquid CO_2 bottles that flow through a regulator and into the air bearing carriage distribution manifold. From there it is distributed to the 3 air bearing pucks. This can be seen in Figures 4.2 and 4.3.

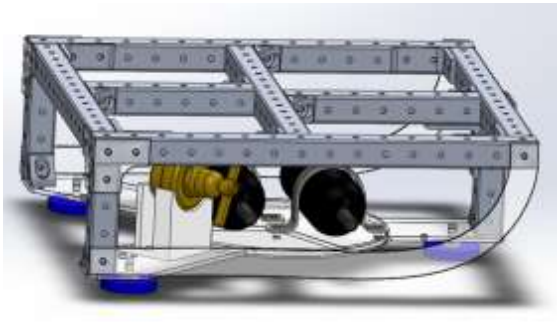

Figure 4.2: Air Bearing Carriage CAD

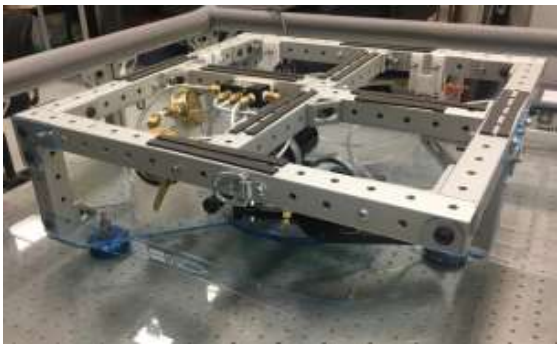

Figure 4.3: Air Bearing Carriage

An air bearing table is the simplest platform used to simulate the microgravity environment of space. It also has significant limitations as it is not a perfect simulation of microgravity. The air bearing carriage is limited to one rotational axes and two translational axes. As such, any cross coupling forces and torques are reacted into the table and therefore some information is lost in the system.

4.3.1 Air Bearing Table Experiment: Configuration

On top of the carriage was placed the ExoSPHERES [94] vehicle that was used as the base spacecraft for these experiments. It was developed as part of a joint NASA-DARPA program for astronaut assistance in space outside the International Space Station. The ExoSPHERES vehicle was attached to the air bearing carriage using straps and markers for placement on the carriage. Specifications of the ExoSPHERES vehicle can be found in Table 4.1.

Parameter	Value
Mass	23.1 Kg
Length	0.45 m
Width	0.45 m
Height	0.41 m

Table 4.1: ExoSPHERES Vehicle Specifications Without Propulsion System

Figure 4.4 shows the ExoSPHERES vehicle attached to the air bearing carriage. The cold gas propulsion system for the ExoSPHERES vehicle was removed for these experiments as the focus was on the inertial parameters of the spacecraft and not the translation of the spacecraft.

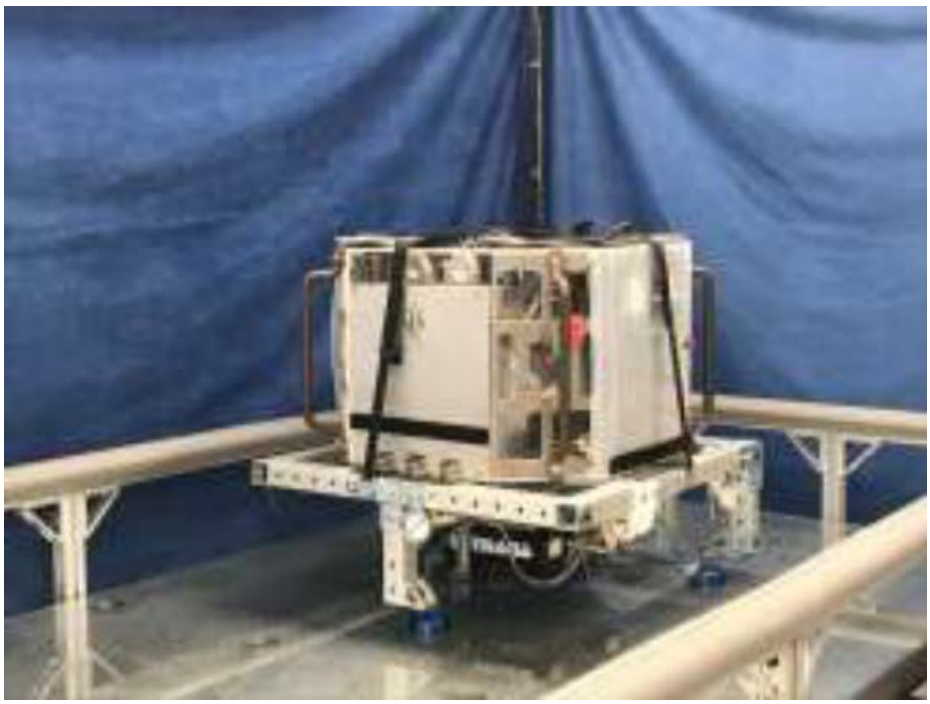

Figure 4.4: ExoSPHERES Vehicle on Air Bearing Carriage without Manipulator Arm

The DYMAFLEX (Dynamic Manipulator Flight Experiment) manipulator arm was then attached to the top plate of the base spacecraft to complete the spacecraft and manipulator system. The DYMAFLEX manipulator arm was developed by the University of Maryland Space Systems Laboratory and was used as the robotic manipulator arm of a free-flying spacecraft. The DYMAFLEX manipulator arm was attached to the ExoSPHERES vehicle using a custom mount-

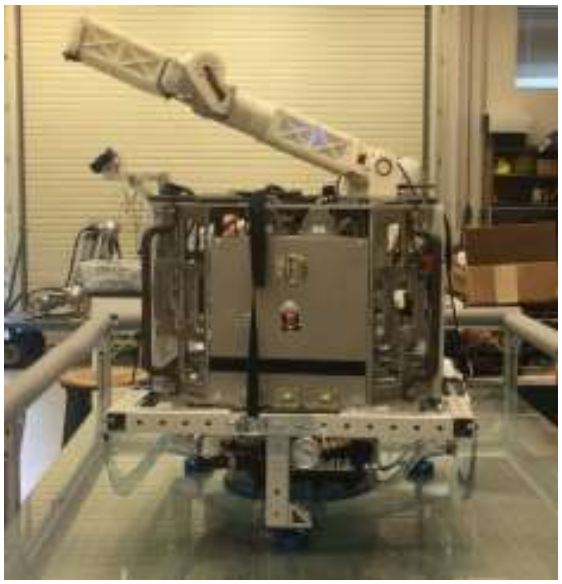

Figure 4.5: ExoSPHERES and DYMAFLEX on Air Bearing Table: Front

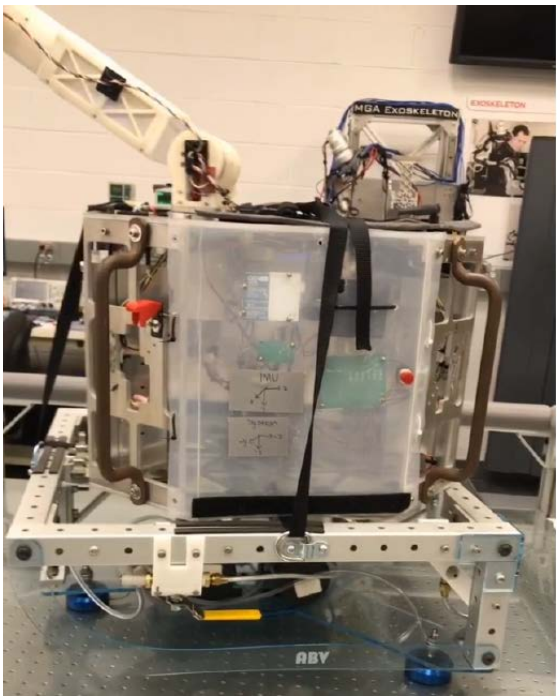

Figure 4.6: ExoSPHERES and DYMAFLEX on Air Bearing Table: Side

ing plate that replaced the original top plate of ExoSPHERES. A rendering from the CAD model used to manufacture the DYMAFLEX manipulator arm is shown in Figure 4.7. The combined spacecraft and manipulator system on the air bearing table is shown in Figures 4.5 and 4.6.

As one of the simplest methods to simulate the microgravity environment of space, an air bearing table is a good place to start. The air bearing table was used to generate data in a controlled environment before moving on to more complex simulation environments. Additionally, as this method was being developed it was originally targeted for identification of the spacecraft's inertial parameters, and as such there is no payload for the system and the identification of the spacecraft's inertial parameters was the focus of the experiment.

For the purposes of simplicity in description, the combination of the air-bearing carriage, ExoSPHERES, and DYMAFLEX manipulator will be referred to as the Air Bearing Vehicle

(ABV). The ABV system has multiple sensors on the system to collect data for both control and logging for post-processing. The sensors used for the ABV system are as follows:

Sensor	Type	Location
ExoSPHERES vehicle IMU	Memsense nIMU	ExoSPHERES C&DH Box
Robot Joint 2 IMU	InvaSense MPU-6050	DYMAFLEX Joint 2
Robot Joint 5 IMU	InvaSense MPU-6050	DYMAFLEX Joint 5
Robot Joint Incremental Encoders	US Digital EM1 1250CPR	DYMAFLEX Joints 1-5

Table 4.2: ABV Sensor Suite

The ExoSPHERES vehicle IMU is used to collect data on the spacecraft's motion and orientation. The DYMAFLEX manipulator arm has two IMUs, one at the base of the arm and one at the tip of the arm. The IMUs are used to collect data on the manipulator arm's motion and orientation. The DYMAFLEX manipulator arm also has incremental encoders in each joint to record the manipulator's kinematic motion. The data from the sensors is collected by two separate data acquisition system that records the data for post-processing. ExoSPHERES' main C&DH system records the data from the ExoSPHERES IMU and the DYMAFLEX manipulator encoders. Data from the DYMAFLEX IMUs are recorded by a separate data acquisition system that is run by an Arduino UNO R3 and logged to a SD card. The data from the two systems is synchronized by a sharp impulse that is recorded by both systems to be used as a time synchronization reference. Figure 4.12 shows the general locations of the IMUs on the ABV system and Figure 4.13 shows the coordinate system of the ABV system.

The DYMAFLEX robotic manipulator is a serial robotic manipulator that has five Degrees-of-Freedom (DOF). All five of the DOF are revolute joints. Kinematically the robot is a pure revolute YPRPR manipulator. The first joint is a yaw joint that rotates the manipulator arm about the vertical axis. The second joint is a pitch joint that rotates the manipulator arm about the

horizontal axis. The third joint is a revolute joint that rotates the elbow of the manipulator arm. Joint 4 is a revolute joint that pitches the second link of the manipulator arm. The fifth joint is a revolute joint at the end of the arm that rotates the end effector tool drive. The manipulator arm is shown in Figure 4.7 with the joints numbered. The encoders are attached to the motor on the input side of the 100:1 Harmonic Drive gearbox giving a 125,000 Counts Per Revolution (CPR) resolution or 500,000 Pulses Per Revolution (PPR) resolution. Using the logged data the encoders are used to measure the position of the manipulator arm and are used to calculate the velocity and acceleration of the manipulator arm.

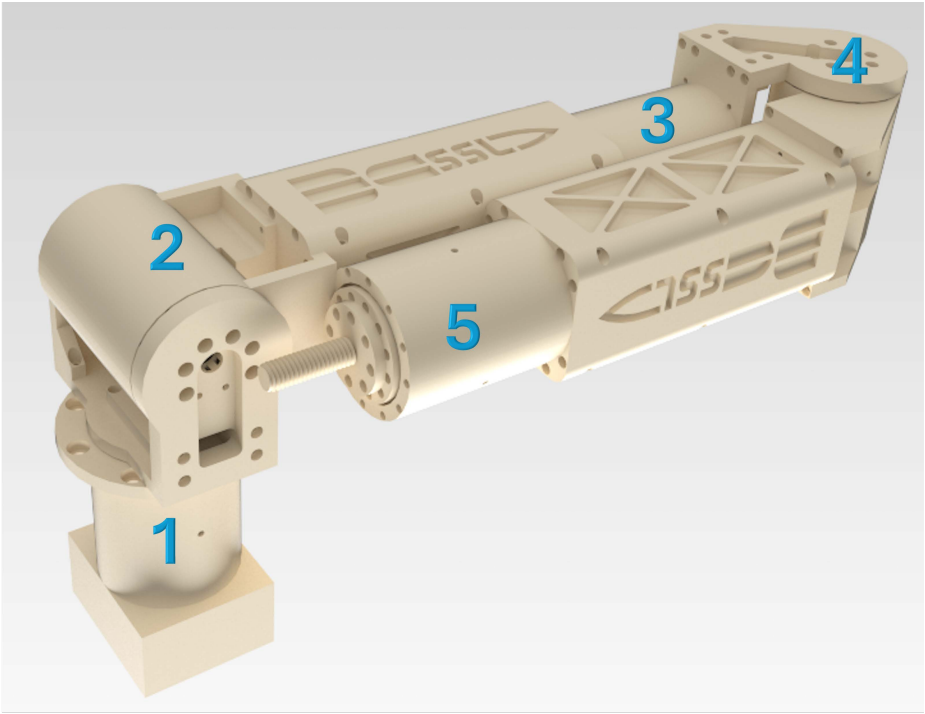

Figure 4.7: DYMAFLEX Manipulator Arm with Joint Numbers

As a point of reference for robot motion, pitch and yaw for the manipulator arm are defined as follows. Yaw is motion of the first joint and pitch is limited to motion of the second joint for the purposes of these experiments. Figures 4.8 and 4.9 show the pitch and yaw of the DYMAFLEX manipulator arm respectively.

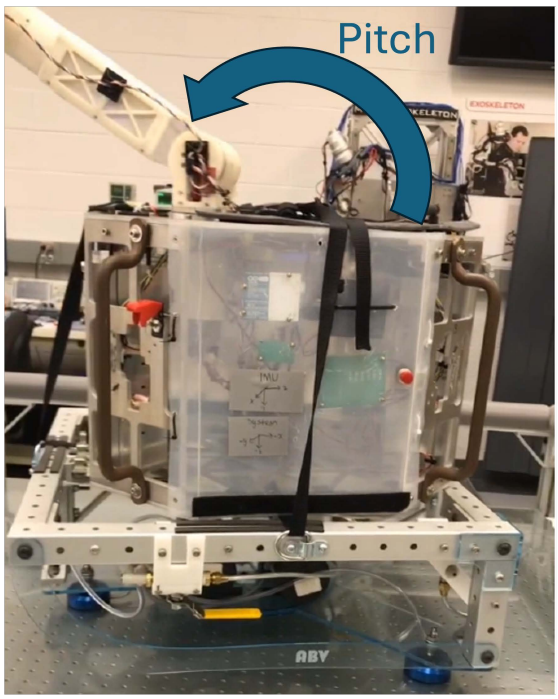

Figure 4.8: Manipulator Arm Pitch

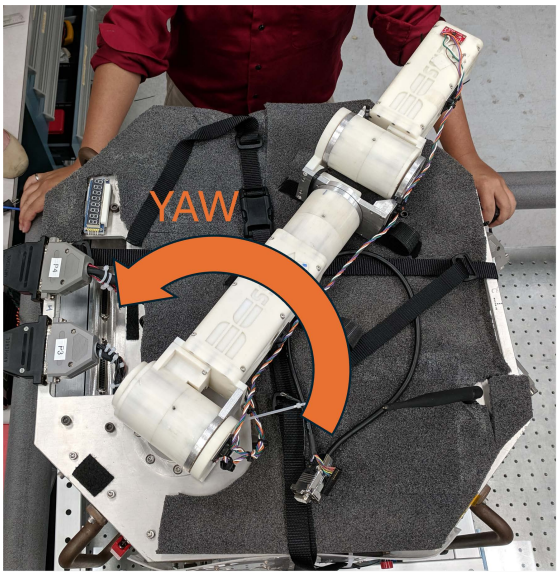

Figure 4.9: Manipulator Arm Yaw

The motions for the system can be subdivided into three types of motions, at three different speeds. The motions are pure pitch motions, pure yaw motions, and combined pitch and yaw motions. Speeds are categorized as slow, medium, and fast. The slow speed is defined as a motion that has a manipulator tip velocity of 5 cm/s, the medium speed is defined as a motion that has a manipulator tip velocity of 10 cm/s, and the fast speed is defined as a motion that has a manipulator tip velocity of 25 cm/s. The motions are performed in a series of 10-15 second motions that are repeated for each speed and type of motion. The data from the IMUs and encoders are recorded for each motion and used for post-processing.

4.3.2 Air Bearing Table Experiment: Procedure

The first step before any testing of the system was to prepare the air bearing table for use. Cleaning the air bearing surface of dust and debris that may have settled on the surface was the

first step. This was to ensure that the air bearing pucks would not catch on the debris and cause additional drag to the system. The next step was to level the table to the gravity vector. This was done by adjusting the height of the table legs with a precision machinist level placed on the table surface and the bubble was centered. The level used for this procedure was a Starret 98Z-12 that has an accuracy of 0.42 mm per meter, though any similarly accurate level would also be sufficient when likewise calibrated before use. This procedure was performed in 7 locations across the table in the two adjustable orientations of the table and repeated until the level bubble was centered in all the 14 positions. These positions can be seen in Figure 4.10.

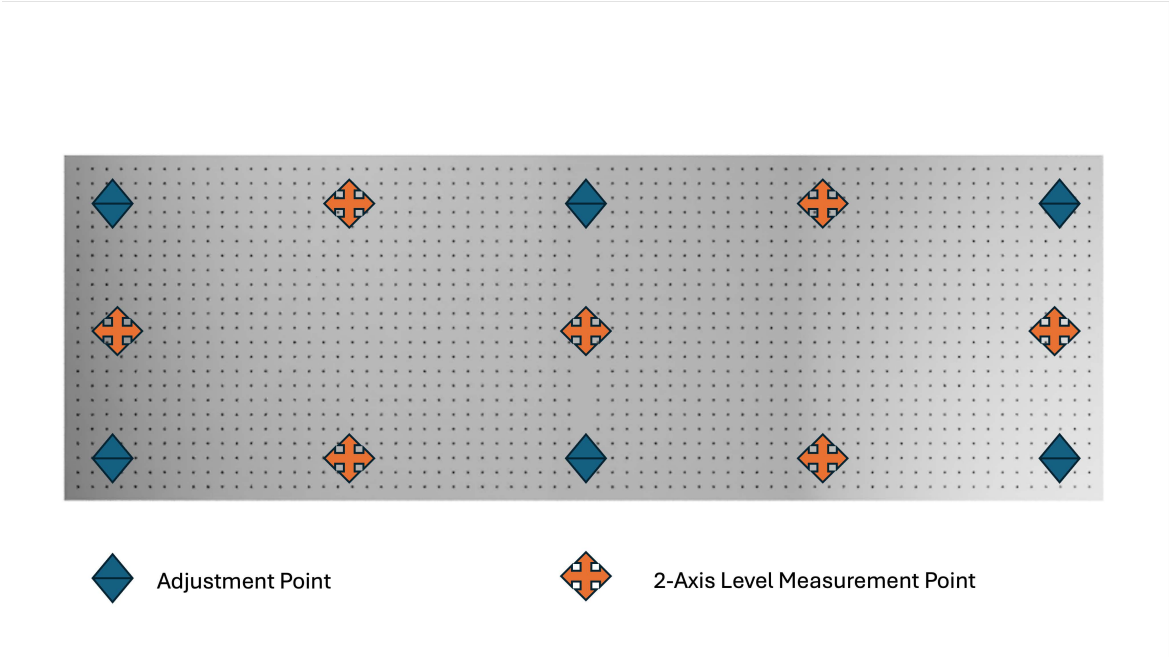

Figure 4.10: Air Bearing Table Leveling

Once the table was prepared the Air bearing carriage was charged with CO_2 and the spacecraft system was energized and initialized for operation. The Inertial measurement system for the manipulator arm was initialized and the data recording system turned on. There is no direct linkage between the ExoSPHERES vehicle and the DYMAFLEX manipulator arm, inertial mea-

surement systems and so synchronization was performed by tapping the air bearing carriage with a rubber mallet to create a sharp impulse that was recorded by both systems to be used as a time synchronization reference.

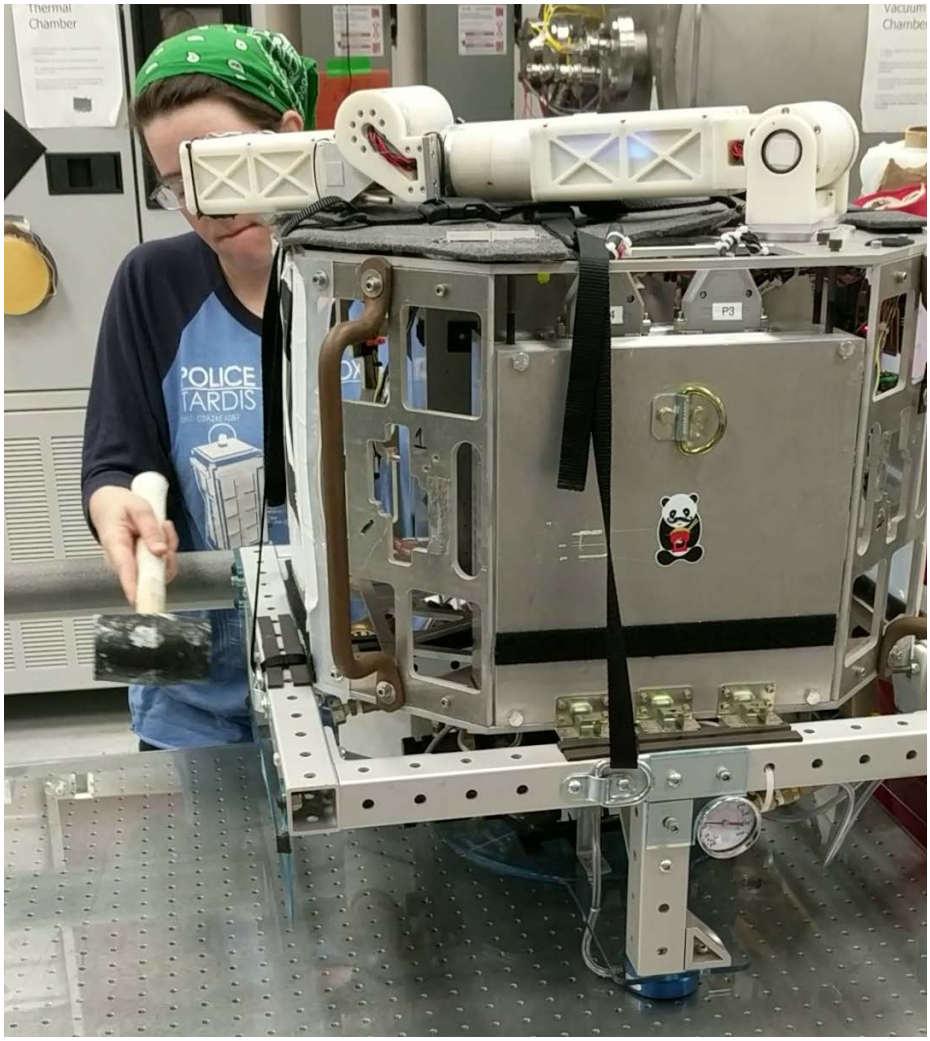

Figure 4.11: Air Bearing Table Time Synchronization

Each run consisted of a predetermined set of motions with various speeds. This was done by moving the manipulator along a series of predetermined trajectory; each motion being on the order of 10-15 seconds. Inertial measurement units (IMUs) are located at the tip of the manipulator, the base of the manipulator and inside the free-flier are used to record the dynamics

of the free-flying system. Additionally, incremental encoders in each joint were used to record the manipulator's kinematic motion.

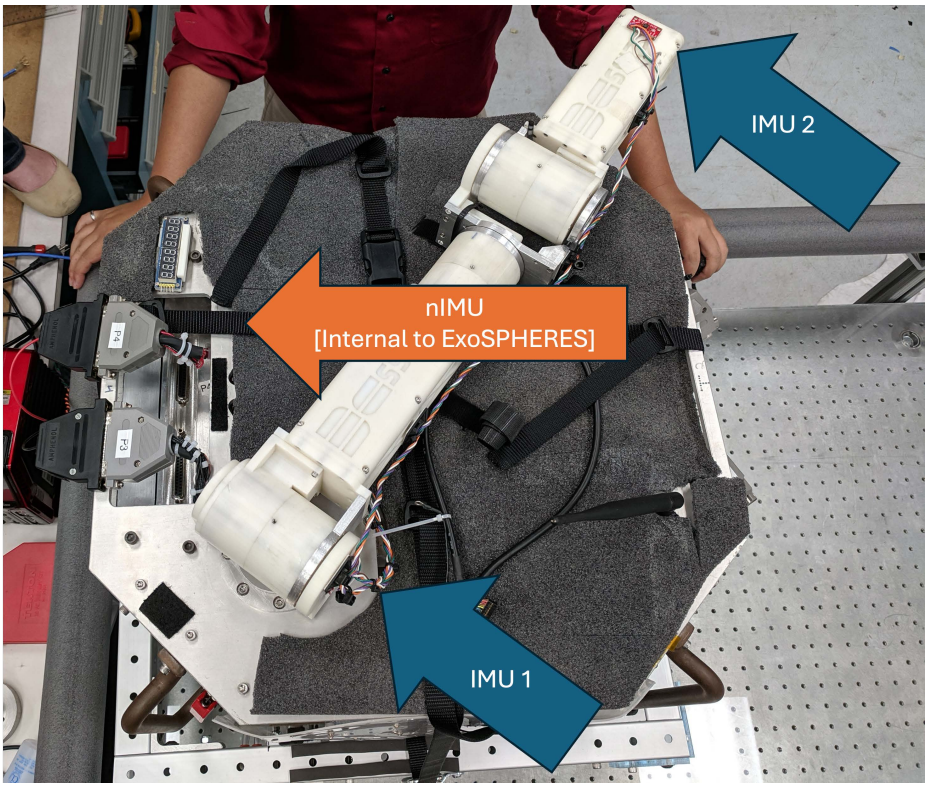

Figure 4.12: ABV IMU Locations

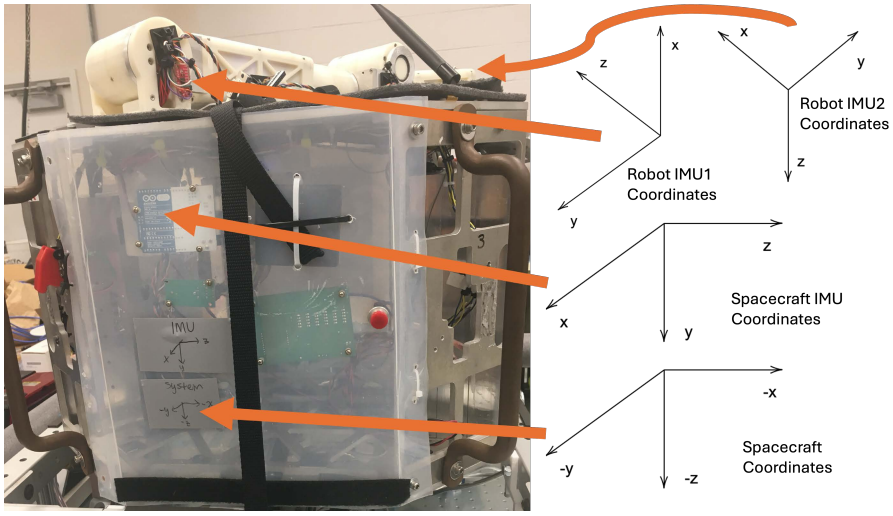

Figure 4.13: ABV Coordinate System

For the purposes of this thesis, the further details of the rest of the Command and Data

Handling (C&DH) system and Power Management (EPS) system are unimportant and further details can be found in the these further publications [94] [95] [96] [97] [98].

4.3.3 Air Bearing Table Experiment: Results

The results from the air bearing table experiment were originally designed for the determination of the spacecraft's inertial parameters. The results of the spacecraft's inertial parameters using the Bifilar pendulum method, and the nonlinear MatLab function associated [93], are shown in Table 4.3.

Parameter	**ABV Values**	**Arm Values**
Mass	43.818 Kg	3.399 kg
I_{xx} $(g * mm^2)$	0.9447	0.008303
I_{xy} $(g * mm^2)$	-0.75	0.0
I_{xz} $(g * mm^2)$	-0.12	0.0
I_{yx} $(g * mm^2)$	0.9972	0.0
I_{yy} $(g * mm^2)$	1.254	0.1647
I_{yz} $(g * mm^2)$	0.048	0.0
I_{zx} $(g * mm^2)$	-0.024	0.0
I_{zy} $(g * mm^2)$	-0.072	0.0
I_{zz} $(g * mm^2)$	2.436	0.199845

Table 4.3: ABV Inertial Parameters at CoM

As a way to check that we are getting results that are consistent with theoretical motions of the spacecraft and manipulator arm, a simulation of the expected motion of the spacecraft was performed. The simulation for this particular case used Papadopoulos' method for the spacecraft's motion [55]. The results of the simulation are shown in Figure 4.14 shown with recorded sensor data from the base IMU in the spacecraft.

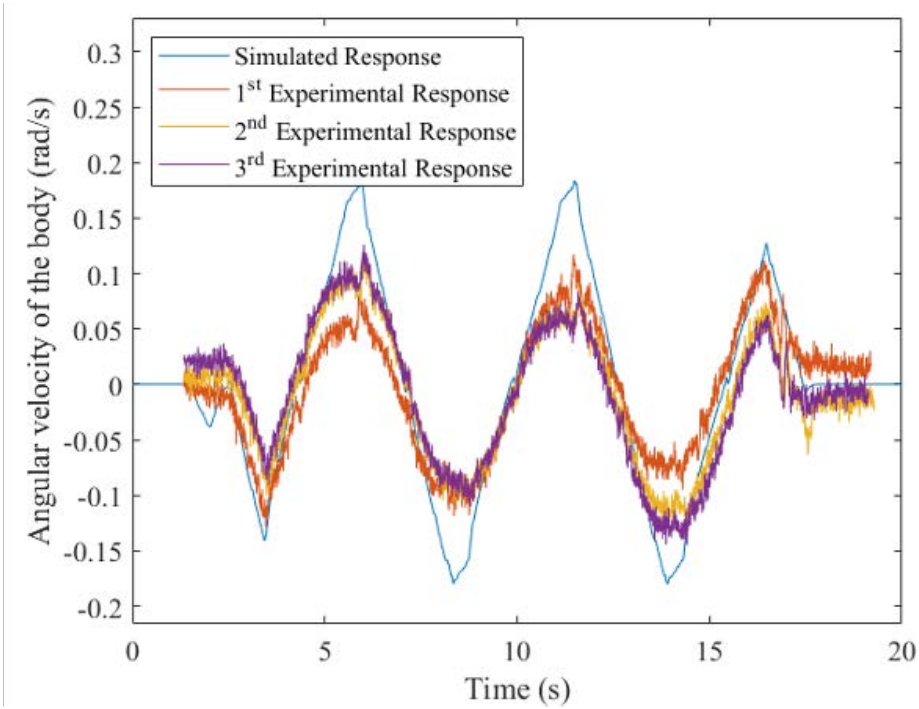

Figure 4.14: ABV Simulation with Recorded Data

We can see that we are getting good tracking of the spacecraft's motion with the simulation. As such this is a good indication that reality is matching the theoretical motion of the spacecraft. It is important to point out that there is a known source of drag in the system that is not accounted for in the simulation. This drag is due to the air bearing table and the air bearing pucks. This drag is not a constant force and is dependent on the speed of the manipulator causing higher drag forces on one of the pucks than the other two in the system. It could be remedied with a redesign to add a larger puck for the one that is dragging. This drag is not accounted for in the simulation and is the understood reason for the discrepancy between the simulation and the recorded data based upon video footage.

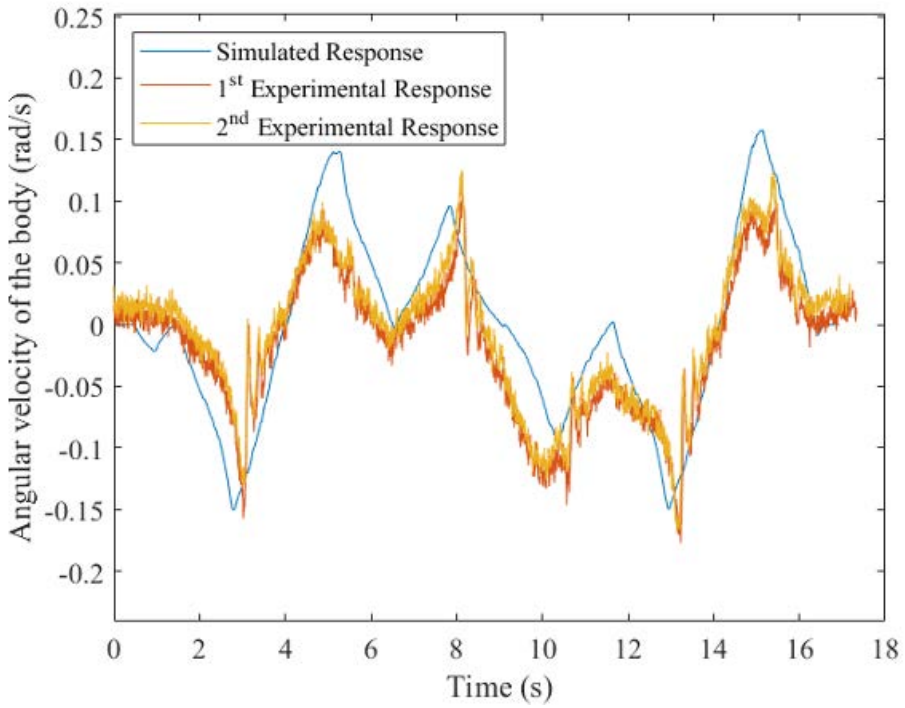

Figure 4.15: ABV Simulation with Recorded Data

It can be seen again that the simulation and experimental spacecraft's motion track well. Again, it is seen that there is a discrepancy between the simulation and the recorded data. In addition to the known drag on the system, the ABS plastic main drive plate on the output of the Harmonic Drive gearbox for joint 2 had started to fracture and was causing a jump in the motion of the arm as its center of mass shifted. This was also not accounted for in the simulation and appears in the data as a sharp jump in the motion of the spacecraft. Unfortunately, this was not caught until after the data was collected and the drive plate fully fractured preventing further testing of the system without a full tear down of the manipulator arm that would have taken weeks to repair even after managing to get the parts needed to repair the system.

4.3.4 Air Bearing Table Experiment: Lessons Learned

This simulation environment was unable to garner the wanted results due to the failure of the manipulator arm, and the puck drag on the table. However, the results that were obtained were consistent with the theoretical motion of the spacecraft and manipulator. The discrepancy between the simulation and the recorded data can be attributed to the drag on the system and the slow failure of the manipulator arm. The drag on the system is a known issue and therefore can be characterized and accounted for in future experiments. The issues encountered here can be summed up as a series of lessons learned for future experiments. The lessons learned are as follows:

- Time synchronization between systems is critical for post-processing of data.
- Characterization of external forces on the system is critical for accurate results.
- Having an external visual positioning system would be beneficial for tracking the system's motion, especially initial conditions for the system.
- The manipulator arm needs to be redesigned to be more robust for future experiments.
- Torque sensors on the manipulator arm would be beneficial to enable more observable states for the system in future experiments.

These particular set of experiments, although conducted after the parabolic flights of the next section, were the original simulation environment to prove out feasibility for the parabolic flights. The award for the parabolic flights was on a reduced timeline as the experiment was

scheduled for the final parabolic flight for the test aircraft before all parabolic operations were moved over to ZeroG corp. The results of the parabolic flights are discussed in the next section.

4.4 Parabolic Flights

The parabolic flight experiment was conducted on the NASA McDonnell Douglas C-9B Skytrain II aircraft, called Weightless Wonder VI [99]. The Weightless Wonder VI was a cargo aircraft that has been modified to support flying in a parabolic trajectory with scientific payloads. The experiments that follow were conducted as part of the NASA Reduced Gravity Student Flight Opportunities Program Announcement for Flight Opportunities 6 (AFO-6).

Figure 4.16: NASA C-9B Skytrain II Aircraft, Weightless Wonder VI [99]

4.4.1 Parabolic Flight Experiment: Configuration

The ExoSPHERES vehicle was attached to the aircraft using a custom mounting plate and table that was attached to the floor of the aircraft. The DYMAFLEX manipulator arm was attached to the ExoSPHERES vehicle using the same custom mounting plate that was used for the air bearing table experiment. The combined spacecraft and manipulator system on the aircraft is shown in Figure 4.17.

The following figures 4.18 and 4.19 show the ExoSPHERES vehicle and DYMAFLEX manipulator arm as CAD renders.

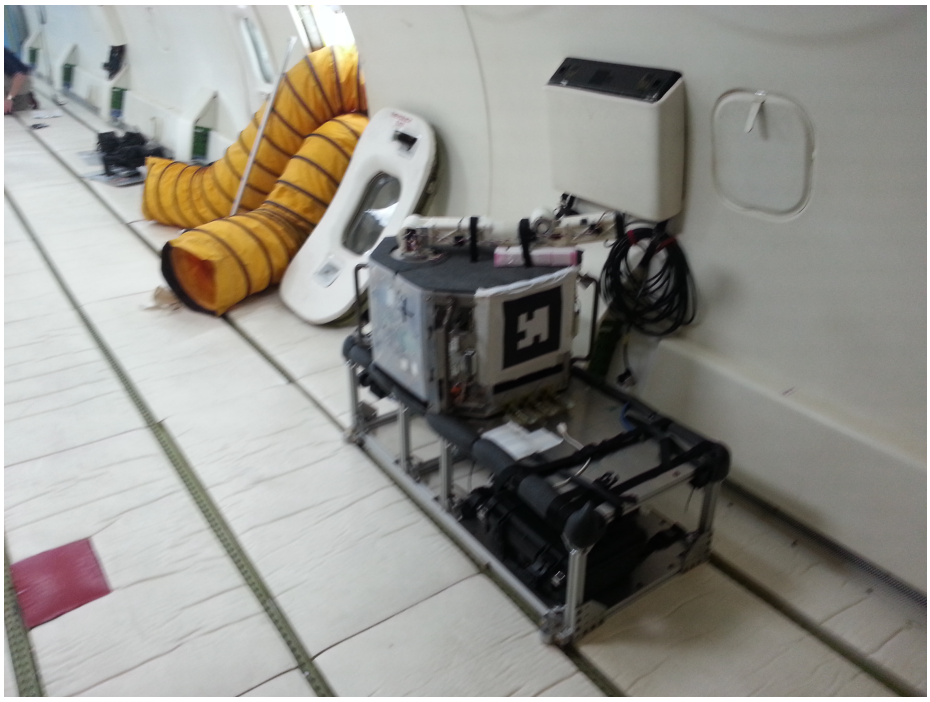

Figure 4.17: ExoSPHERES and DYMAFLEX on loaded on Parabolic Flight

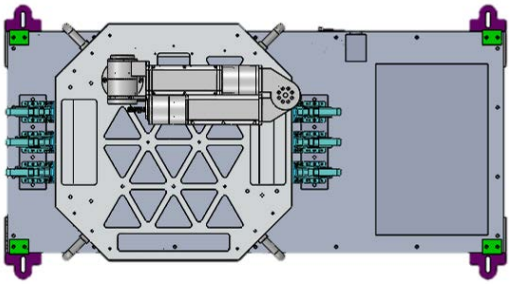

Figure 4.18: Top down parabolic flight equipment CAD render

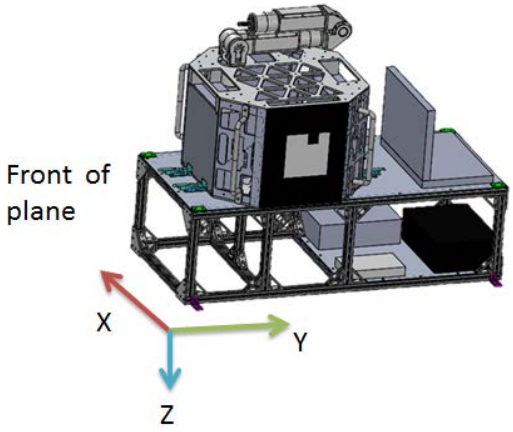

Figure 4.19: Parabolic flight equipment assembly with plane reference frame

The ExoSPHERES vehicle was attached to the aircraft using a custom mounting plate and table that was attached to the floor of the aircraft. The DYMAFLEX manipulator arm was attached to the ExoSPHERES vehicle using the same custom mounting plate that was used for

the air bearing table experiment. The combined spacecraft and manipulator system on the aircraft is shown in Figure 4.17 and the location of the ExoSPHERES vehicle and DYMAFLEX manipulator arm on the aircraft is shown in Figure 4.20.

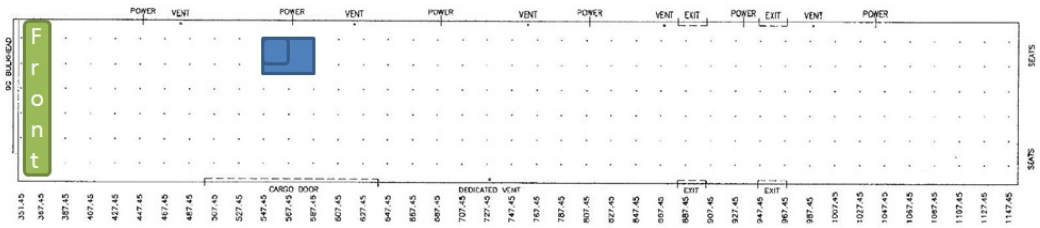

Figure 4.20: Parabolic flight equipment location on aircraft

In flight, the vehicle was unlatched from the table. Foam was placed over the exposed latches (not shown). One person will release the Free-Flier once microgravity has been achieved and bring the vehicle to the floor at the end of each parabola. A tether (not shown) from the table to the free-flier was attached at first but was removed after it was determined that the spacecraft was not a danger during the parabolas and remained off after the initial couple of test on day 1. An operator was located at the edge of the table at the laptop to command the manipulator. A third operator, shown in purple in figure 4.22, recorded video and photographs and act as an additional operator in the case of motion sickness of one of the other operators.

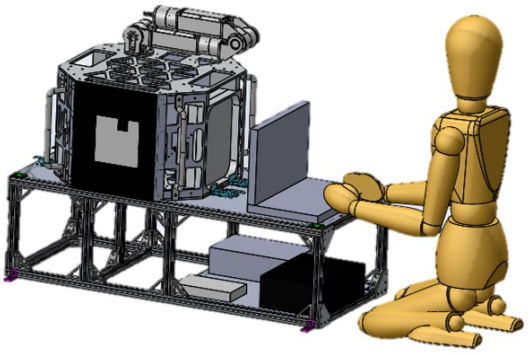

Figure 4.21: Parabolic flight equipment table layout with operator

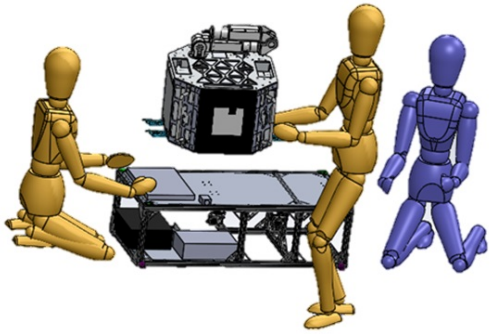

Figure 4.22: Parabolic flight operator approximate locations

4.4.2 Parabolic Flight Experiment: Procedure

The procedure for this parabolic flight experiment can be broken down into three main parts: the pre-flight, the in-flight, and the post-flight procedures. The pre-flight procedure consisted of both the setup of the test bed on the aircraft to mount the table structure to the aircraft frame, and the daily setup of the spacecraft and data acquisition systems. First the table structure was mounted to the aircraft frame followed by the ExoSPHERES vehicle being attached to the table structure via the load rated clasps. The vehicle was checked out, initialized and then the DYMAFLEX manipulator arm was then strapped down to the ExoSPHERES vehicle for takeoff. Finally, all the loose equipment was stowed, and the aircraft was prepared for takeoff.

The in-flight procedure consisted of the execution of the predetermined set of motions with various speeds. These procedures were adjusted from the first day to the second day based upon the results of the first day's testing. The first day's testing showed that the data was best excited by the fast manipulator motions. Therefore, the second day's testing was adjusted to have more fast motions and fewer slow motions. This can be seen in Table 4.4.

The post-flight procedure consisted of the tear down of the test bed and the data analysis of the data collected during the flight. A fully fleshed out procedure for these procedures can be found in Appendix A.

Figure 4.23: ExoSPHERES and DYMAFLEX released in parabolic flight

4.4.2.1 Testing Schedule

The testing schedule for the parabolic flight experiment is shown in Table 4.4. There were 40 parabolas flown in each campaign with one flight campaign per day.

Trajectory	Speed	Joint Motion	Runs: Day 1	Runs: Day 2
1	Slow	Pitch	5	0
2	Slow	Yaw	4	0
3	Medium	Pitch	2	0
4	Medium	Yaw	2	0
5	Fast	Pitch	3	10
6	Fast	Yaw	3	8
7	Slow	Pitch followed by Yaw motion	2	0
8	Medium	Pitch followed by Yaw motion	3	0
9	Fast	Pitch followed by Yaw motion	1	7
10	Slow	Both Joints at the same time	2	0
11	Medium	Both Joints at the same time	4	0
12	Fast	Both Joints at the same time	1	8

Table 4.4: Parabolic Flight Experiment Schedule

Each speed category corresponds to a manipulator tip velocity of 5 cm/s, 10 cm/s, and 25 cm/s for slow, medium, and fast respectively.

Figure 4.24: Flight 2, Parabola 3: Free-flier at release of fast pitch maneuver (upper), at the halfway point at 130 degrees from starting position (middle), and at the end of the maneuver (lower). The base has significantly rotated about a coupled axis during the single maneuver, three identical motions of the manipulator were performed during this parabola.

4.4.3 Parabolic Flight Experiment: Results

The first parabola for each of the flight days consisted of a sensor only run for calibration and checkout purposes of the sensor suite and to allow for any troubleshooting of the system. Figure 4.25 shows the ExoSPHERES vehicle strapped down to the aircraft floor for this checkout parabola.

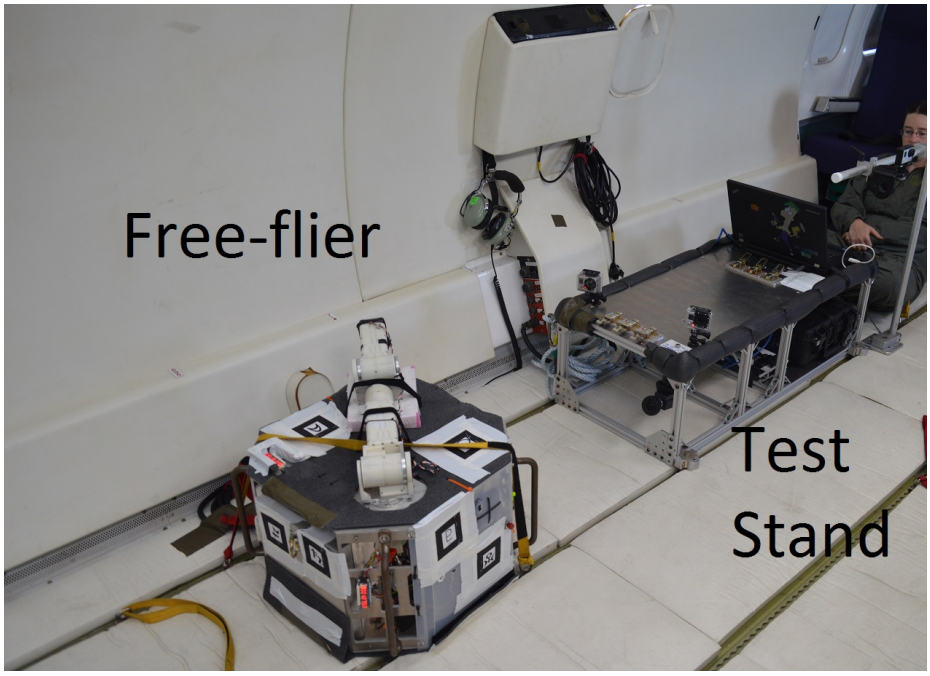

Figure 4.25: ExoSPHERES Strapped Down for Checkout Parabola

The data from this first parabola provided clean data and alignment between the different sensor suites. Figure 4.26 shows the data collected from the manipulator arm during the first parabola of the first flight day.

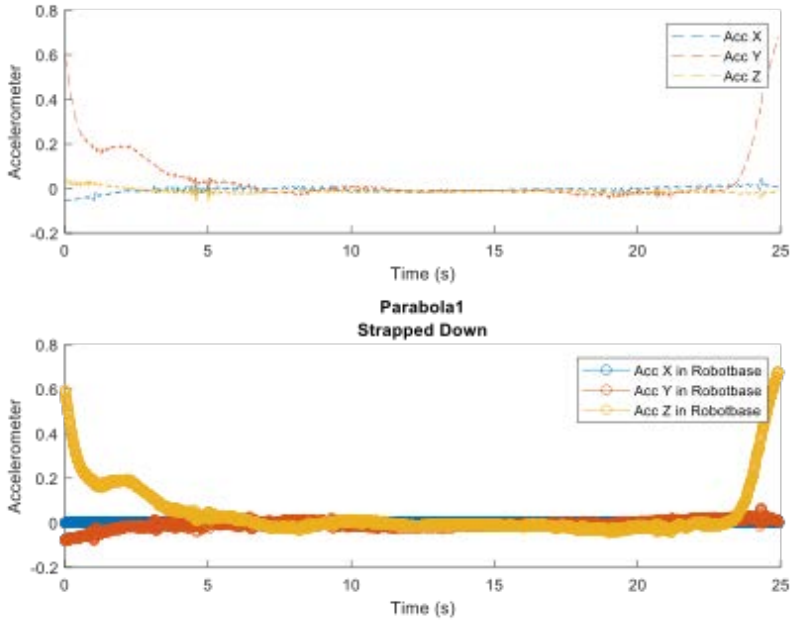

Figure 4.26: Parabolic Flight Data from First Parabola in the Robot Base Frame

It can be seen here that the spacecraft IMU registers the parabola as a transition from 1G to 0G and back to 1G. The second graph in figure 4.26 shows the data from the spacecraft body IMU transformed into the robot base frame. With the appropriate force transformations we can add the two IMUs on the robot arm to the graph to show correlation of the data between the two sets of sensors. This can be seen in Figure 4.27. The large spike in the data at around 5 seconds is the robot arm being bumped by the operator while moving the spacecraft to the floor for the first parabola.

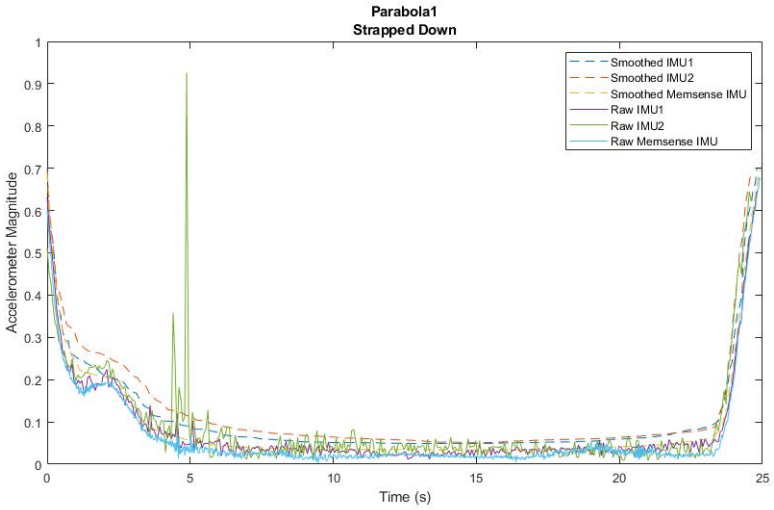

Figure 4.27: Parabolic Flight Data from First Parabola IMU Acceleration Magnitude Data

An example of the data collected from a “Fast Pitch” maneuver is shown in Figure 4.28. The data from the spacecraft IMU shows the transition from 1G to 0G and back to 1G. The second graph in Figure 4.28 shows the data from the spacecraft body IMU transformed into the robot base frame.

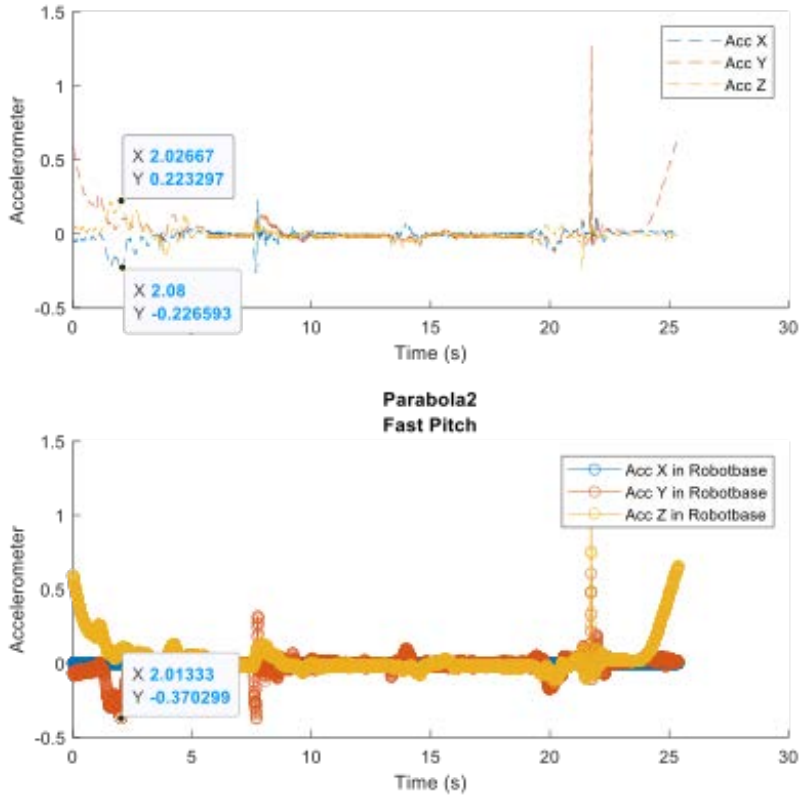

Figure 4.28: Parabolic Flight Data from Fast Pitch Maneuver in the Robot Base Frame: Day 2

As part of the process of moving the spacecraft into position for each parabola, the spacecraft was picked up from the floor of the aircraft and moved into the center of the aircraft. The data from this movement is shown in Figure 4.28 as the initial accelerations in the first five seconds. There is an initial jolt in the data when the arm starts the maneuver and again when it comes back to the home location. Right after the next pitch motion for the ends at approximately 20 seconds right after which there is a large acceleration in the data. This is the spacecraft being picked up and moved to the floor of the aircraft before the end of the parabola. A point of comparison for the pure X, Y, Z accelerations can be seen in Figure 4.29 as acceleration magnitudes for the three IMUs.

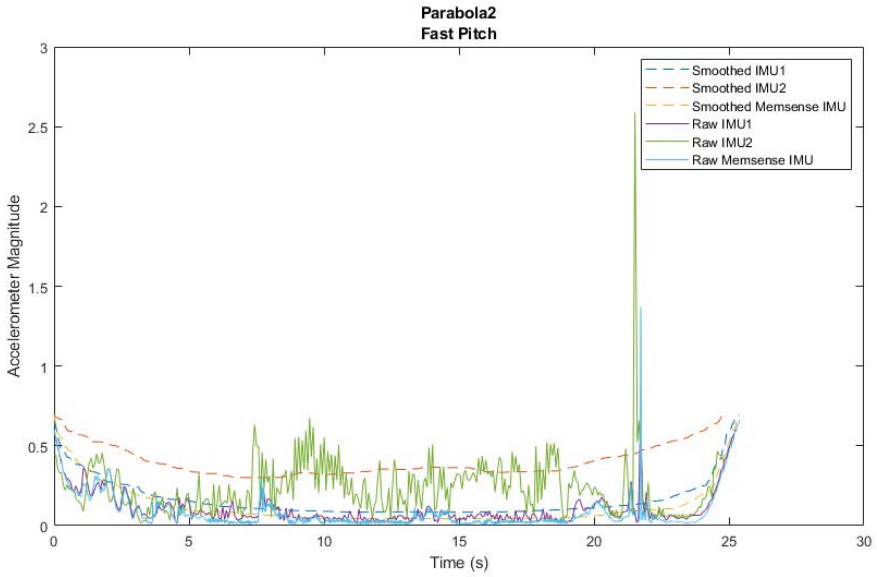

Figure 4.29: Acceleration Magnitude Data from Fast Pitch Maneuver in the Robot Base Frame: Day 2 Parabola 2

Looking at two further examples of the "Fast Pitch" maneuver data, we can compare to figure 4.29 to see the differences in the data. The first example is shown in Figure 4.30 and the second example is shown in Figure 4.31. It can be seen from these graphs that the data does not have a uniform distribution of noise between robot motions.

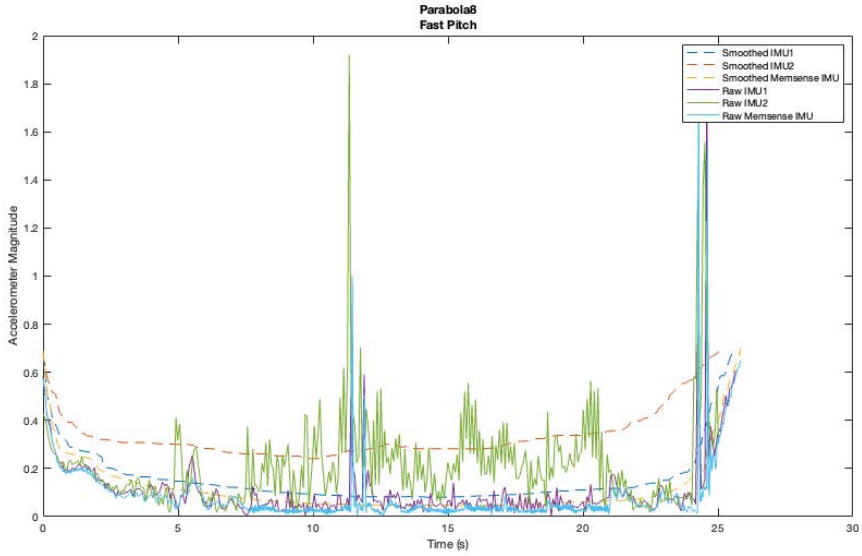

Figure 4.30: Parabolic Flight Data from Fast Pitch Maneuver in the Robot Base Frame: Day 2 Parabola 8

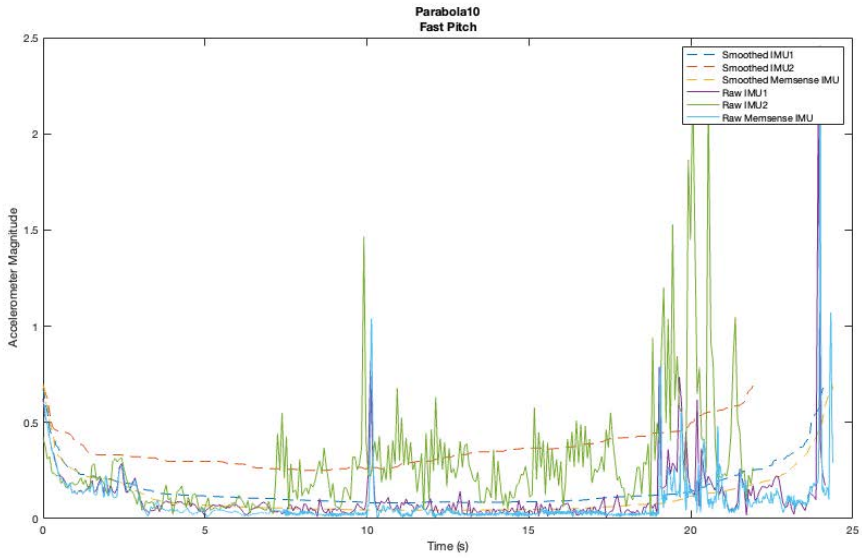

Figure 4.31: Parabolic Flight Data from Fast Pitch Maneuver in the Robot Base Frame: Day 2 Parabola 10

Additionally, the large spikes seen in the data are caused by external forces acting on the system. These forces have many causes, such as the operator catching the system to prevent it from flying into another team's experiment workspace, the system bumping into the interior of

the aircraft moving around the spacecraft, and the system being picked up and moved to the floor of the aircraft before the termination of the parabola. These forces are not accounted for in the data and cannot be isolated from the data of interest.

Finally, the position and velocity data for Joint 2 of the manipulator arm is shown in Figures 4.32 and 4.33 respectively.

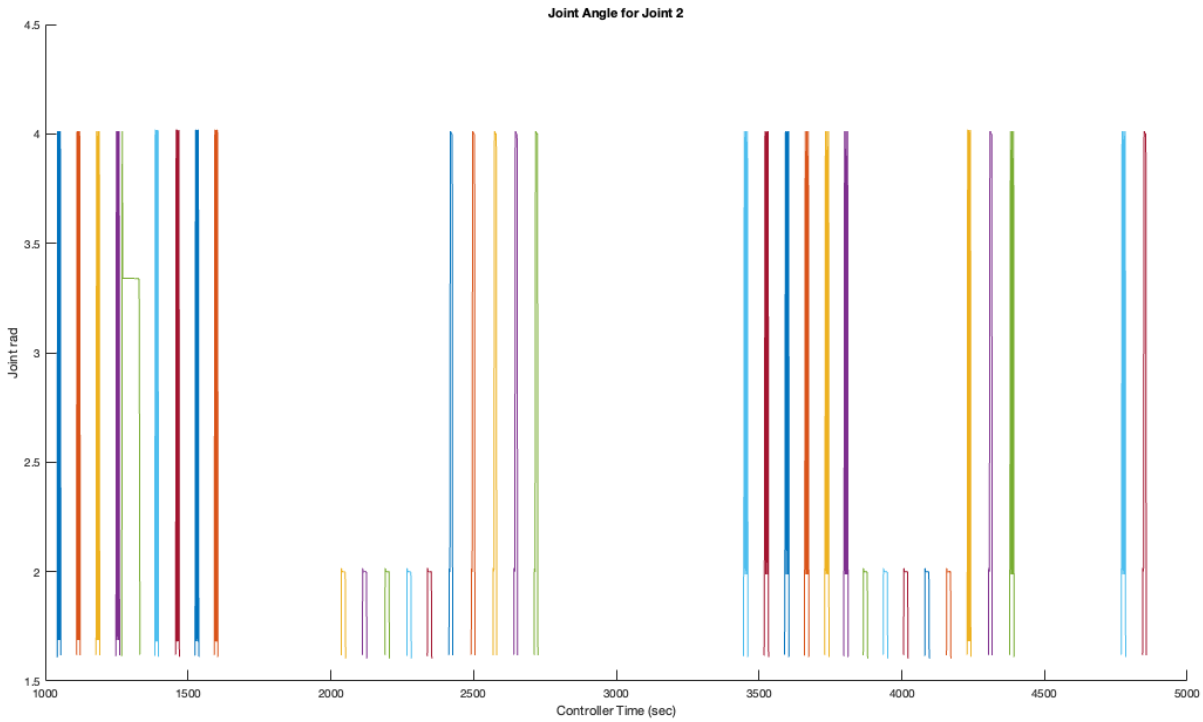

Figure 4.32: Joint 2 Position Data: Day 2

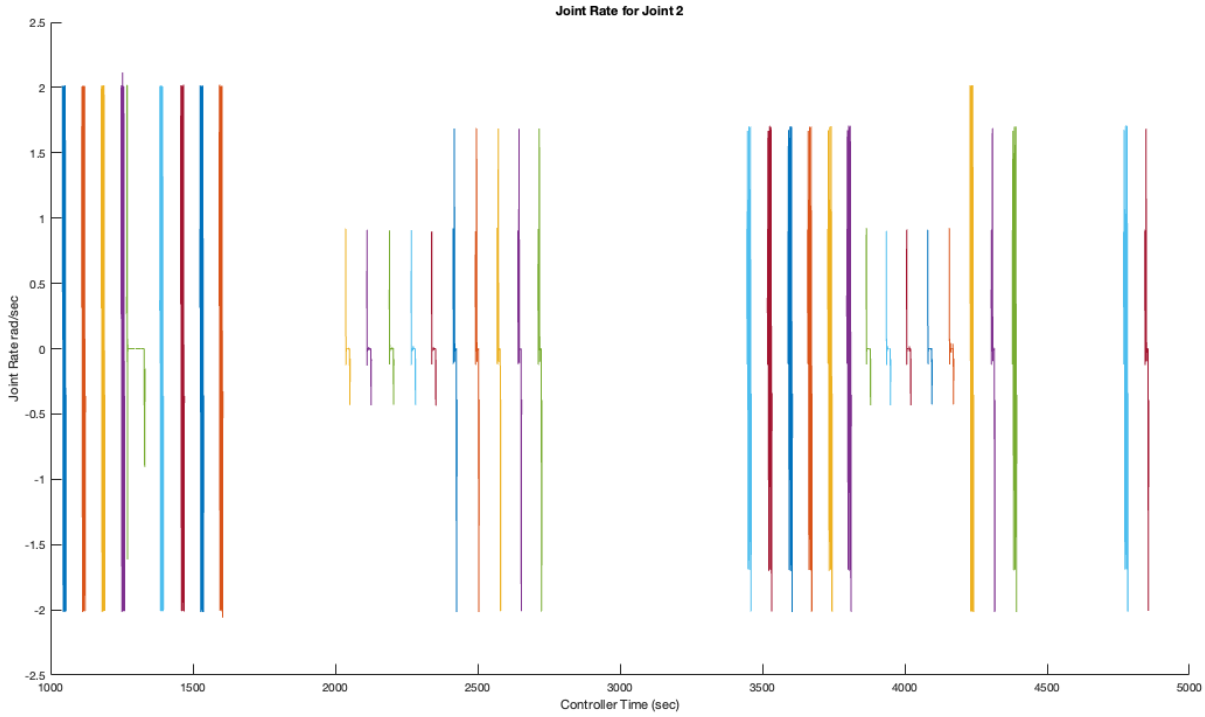

Figure 4.33: Joint 2 Velocity Data: Day 2

Despite the fact that the data for the manipulator is very clean there was an issue with the data logging system where timestamps were not recorded for synchronization between the data sets. The lack of synchronization between the inertial measurement system and the encoder data resulted in the data to be less useful than it could have been. As such the manipulator arm was not able to be synchronized with the spacecraft data and therefore the data was not able to be used for the intended purpose of the experiment.

4.4.4 Parabolic Flight Experiment: Lessons Learned

There were several lessons learned from the parabolic flight experiment. Some are the same as the air bearing table experiment and some are unique to the parabolic flight experiment. The lessons learned are as follows:

- Time synchronization between systems is critical for post-processing of data.
- Characterization of external forces on the system is critical for accurate results.
- Having an external visual positioning system would be beneficial for tracking the system's motion, especially initial conditions for the system.
  - The camera system that captured fiducial data for the experiment was too noisy to be of value for the experiment.
  - The camera system was mounted to the aircraft and therefore moved with the aircraft during the parabolas. Without an inertially fixed camera system or inertial measurement system, the camera system was not useful for tracking the system's motion.
  - Potential of a second reference free-floating object to be used as a reference for a camera system to track the system's relative motion.
- The manipulator arm needs to be redesigned to be more robust for future experiments. The third joint of the manipulator arm overheated and melted the ABS plastic motor housing. This required that the manipulator arm have all joints distal to the second joint locked out for the full experiment.
- Torque sensors on the manipulator arm would be beneficial to enable more observable states for the system in future experiments.

The biggest lesson learned for this experiment is to have a better launch mechanism for each test. Although such a mechanism was considered, it was determined to not be manufacturable and able to pass through the rigorous NASA imposed validation and verification for flight before

the scheduled flight. Therefore, the system was hand launched for each test and the system was not able to be launched in the same way each time. This caused the system to have different initial conditions for each test. Accounting this variance without external measurements of the system caused the data to be less useful than it could have been.

4.5 Suborbital Flights

The suborbital flight experiment was conducted on the NASA RockSat-X program. The RockSat-X program is a program that allows university students to fly experiments on a suborbital rocket. The experiments that follow were conducted as part of the NASA and state sponsored Space Grant Consortium's RockSat program. Experiments were flown on the Terrier-Improved Malemute rocket and launched out of the Wallops Flight Facility Range. The experiments were conducted as part of the NASA RockSat-X flight program. The payload for the 2018 flight campaign failed to start upon launch and the experiment was not conducted. After a regrouping and troubleshooting, the updated payload for the 2019 flight campaign was successfully launched, and the experiment was conducted and completed successfully.

For the 2019 program year, a half-height payload slot with two manipulator arms was used. The manipulator arms were developed by the University of Maryland Space Systems Laboratory and were used as the robotic manipulator arms of a free-flying spacecraft. The manipulator arms were attached to the payload using a custom mounting plate that interfaced with the RockSat-X rocket. An image of the payload ready for installation into the spacecraft is shown in Figure 4.34.

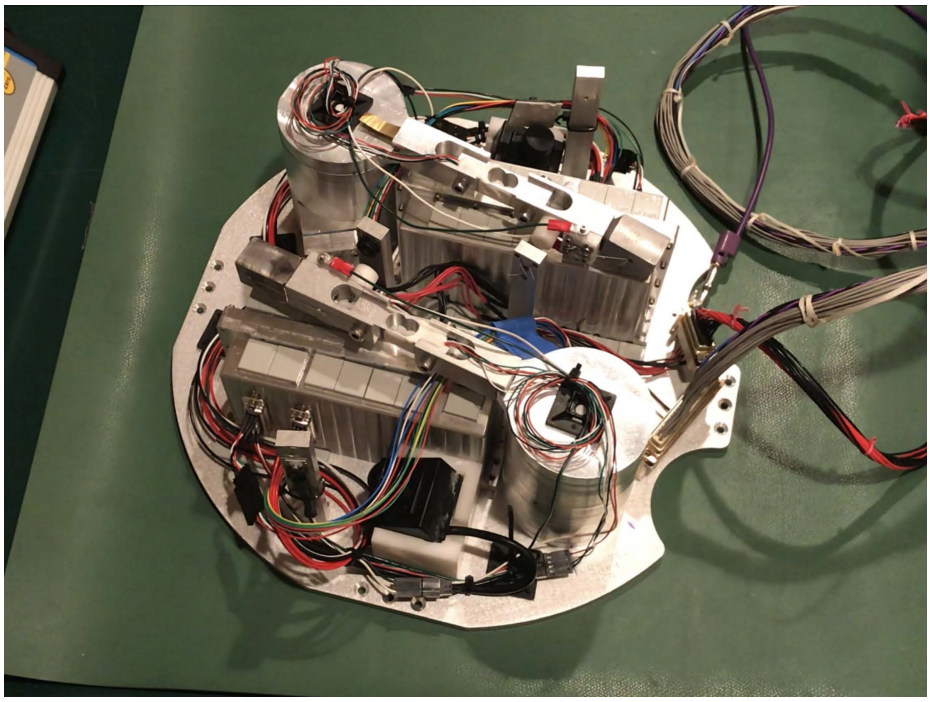

Figure 4.34: Payload for RockSat-X

4.5.1 Suborbital Flight Experiment: Configuration

Each of the two arms were identical independent systems set to run the same experiments. Each manipulator is a one degree of freedom arm manufactured out of 6061-T6 aluminum. The arm is a direct derivative of the DYMAFLEX arm used in the air bearing table and parabolic flight experiments, with the caveat that the system was waterproofed with seals for the inevitable water landing and recovery of the payload (Fig. 4.35).

Figure 4.35: Payload Recovery

The layout of the manipulator arms on the payload is shown in Figures 4.36 and 4.37.

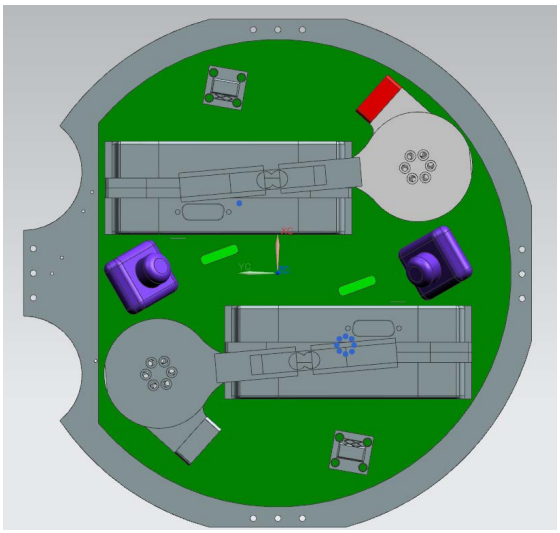

Figure 4.36: RockSat-X Payload Top View

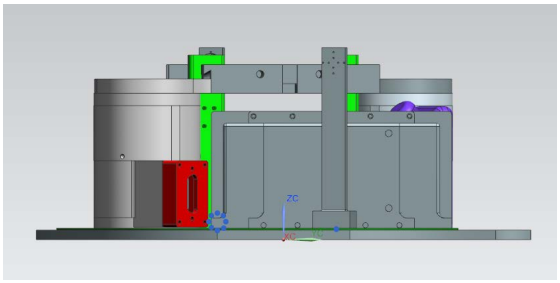

Figure 4.37: RockSat-X Payload Right Side View

Figure 4.38 is an image of the integrated payload with some major components labeled.

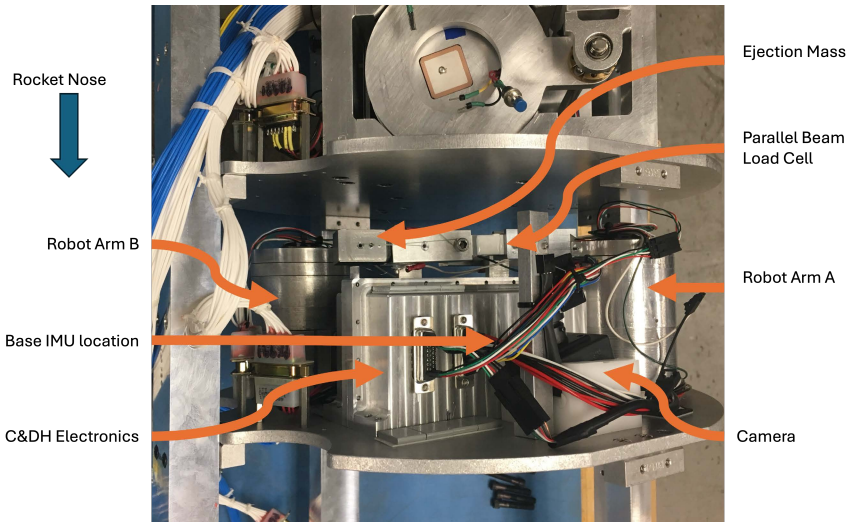

Figure 4.38: Payload for RockSat-X 2019 with Components Labeled

Drawing on the RockSat-X payloads' direct heritage from DYMAFLEX the robot arms encoders, motor, and gearbox are the same. This gives the encoders a 125,000 Counts Per Revolution (CPR) resolution or 500,000 Pulses Per Revolution (PPR) resolution. Using the logged data the encoders are used to measure the position of the manipulator arm and are used to calculate the velocity and acceleration of the manipulator arm. The manipulator is confined to $30\,\mathrm{deg}$ of motion between hard stops to prevent damage to the payload during the flight. This is a total of 10,417 encoder counts of motion between the hard stops.

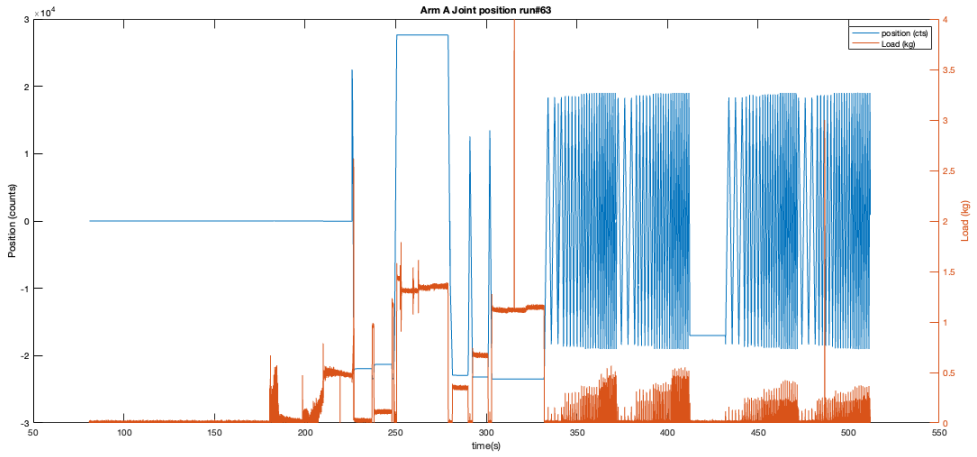

Figure 4.39: Graph showing encoder counts and load cell readings from the payload during the full suborbital flight

The ejectable mass is ejected after the first two sweeps of the manipulator arm. The manipulator arm then performs the same two sweeps after the ejection. The components of the mass ejection end effector system are shown in Figure 4.40-4.43.

Figure 4.40: Ejection mass end effector CAD model

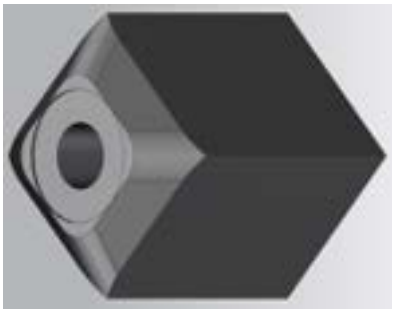

Figure 4.41: Ejection mass CAD model

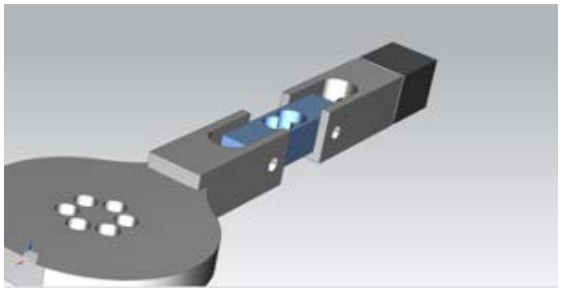

Figure 4.42: Assembled manipulator with ejection mass CAD model

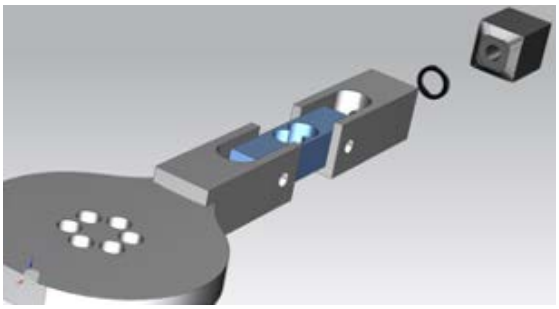

Figure 4.43: Manipulator with ejected mass CAD model

The manipulator arm is a 1 degree of freedom system with a series of reference frames that are used to describe the motion of the system. The reference frames are shown in Figure 4.44 and Figure 4.45.

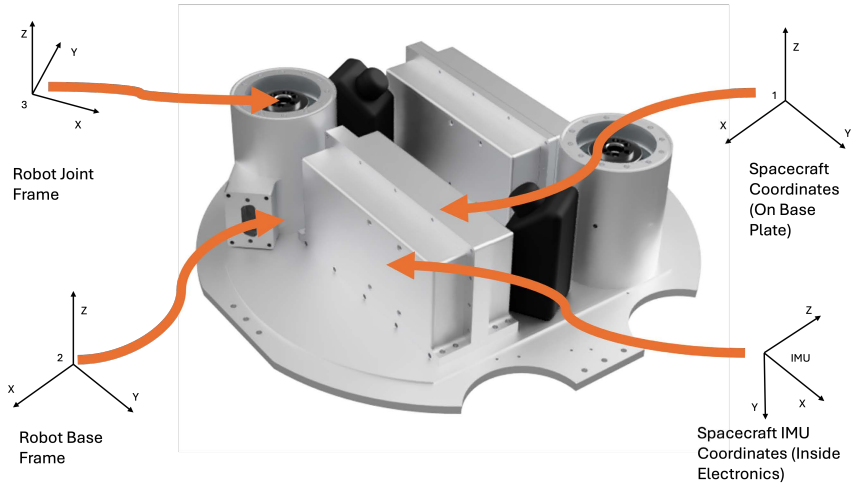

Figure 4.44: Manipulator Arm Reference Frames

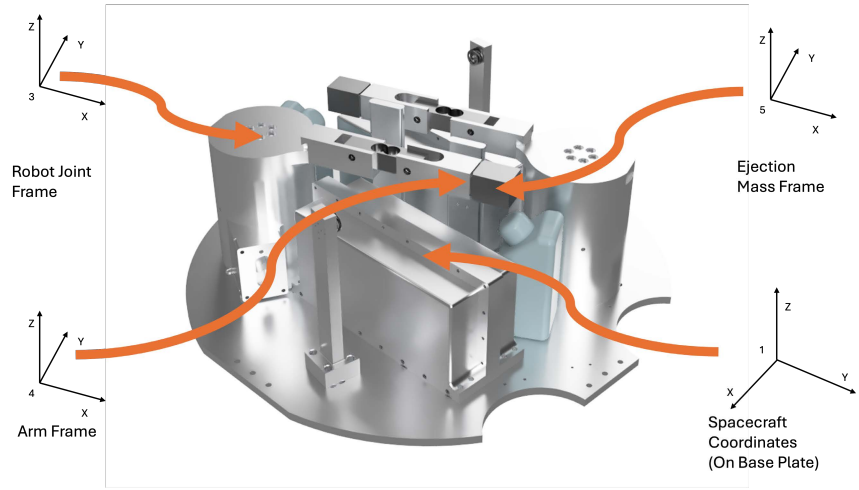

Figure 4.45: Manipulator Arm Reference Frames

Using these frames we can define a set of Denavit-Hartenberg (DH) parameters for the manipulator arm and spacecraft where the spacecraft frames are static. The DH parameters for the system are shown in Table 4.5.

Link (i)	α_{i-1} (°)	a_{i-1} (mm)	d_i (mm)	θ_i (°)
0	0	0	0	0
1	0	0	0	-55.4
2	0	116.1	0	0
3	0	0	101	θ_3
4	0	155.7	0	0
5	0	16.4	0	0

Table 4.5: Modified DH Parameters (Khalil Kleinfinger) for the RockSat-X Manipulator Arm

4.5.2 Suborbital Flight Experiment: Procedure

The payload is powered off during ascent and is turned on right before payload faring separation. The payload then starts the logging system and then the experiment is started. The payload performs two sweeps of the manipulator arm at varying speeds as well pushing against each the hard stop and soft stop to collect force data for the load cell. After the second sweep the ejectable mass at the end of the manipulator is released and the Arm runs the same two sweeps and hard stop and soft stop pushes without the ejected mass.

The data is then stored on the payload and the payload are powered off. Post payload recovery the data was downloaded for post-processing. Figure 4.46 shows an example of the data, cropped to the area of interest, but otherwise unfiltered acceleration data from the payload during the suborbital flight. As expected there is a lack of acceleration in the IMU frame Y-axis. The underlying cause is the payload is mounted to the rocket in such a way that the Y-axis of the IMU is aligned with the rocket's Z-axis.

An important part of this process is that if we are trying to perform inertial parameter identification it is needed to have a known value to compare to the experimentally generated values. Using the CAD model of the system we can get expected values for the inertial parameters of the system. The expected values for the system are shown in Table 4.6.

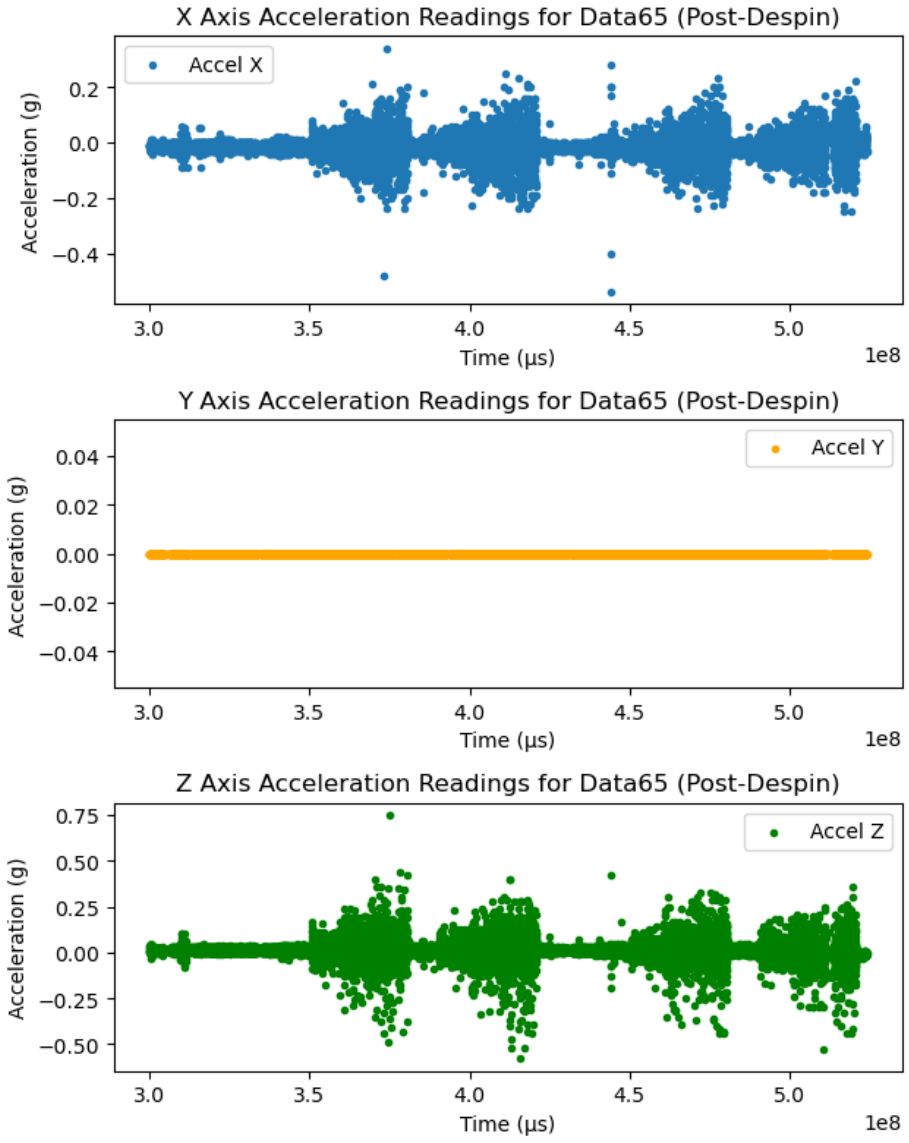

Figure 4.46: Graph showing acceleration data from the payload at the robot base during the sub-orbital flight

Parameter	"Mass" Values	Arm Values	Plate Values
Mass	66.27 g	233.13 g	10115.47 g
Length	19.05 mm	190.16 mm	331.22 mm
Width	28.58 mm	71.50 mm	331.22 mm
Height	19.05 mm	29.54 mm	116.90 mm
I_{xx} $(g * mm^2)$	5978.90	52080.30	$6.33e^{7}$
I_{xy} $(g * mm^2)$	$2.90e^{-8}$	7130.97	$7.56e^{6}$
I_{xz} $(g * mm^2)$	0.00	-38230.98	80846.12
I_{yx} $(g * mm^2)$	$2.90e^{-8}$	7130.97	$7.56e^{6}$
I_{yy} $(g * mm^2)$	4389.61	$6.99e^{5}$	$6.48e^{7}$
I_{yz} $(g * mm^2)$	0.00	1744.05	$-2.52e^{5}$
I_{zx} $(g * mm^2)$	0.00	-38230.98	80846.12
I_{zy} $(g * mm^2)$	0.00	1744.05	$-2.52e^{5}$
I_{zz} $(g * mm^2)$	5978.90	$7.33e^{5}$	$1.09e^{8}$
CoM X	0.00 mm	39.75 mm	-0.07 mm
CoM Y	-13.91 mm	1.41 mm	-7.17 mm
CoM Z	0.00 mm	5.00 mm	24.39 mm

Table 4.6: RockSat-X Payload Inertial Values From CAD Model

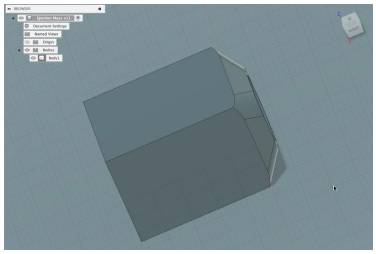

Figure 4.47: Ejectable Steel Mass CAD Model

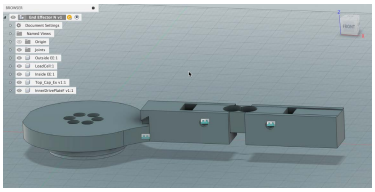

Figure 4.48: Manipulator Arm CAD Model

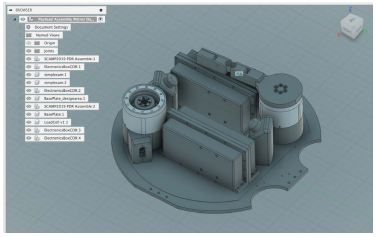

Figure 4.49: Payload Plate CAD Model

4.5.3 Suborbital Flight Experiment: Results

As seen in figure 4.39 robot A was successfully able to complete data collection for the experiment even in the absence of robot B starting. Figure 4.50 shows a zoomed in view of the first two sweeps of the manipulator arm.

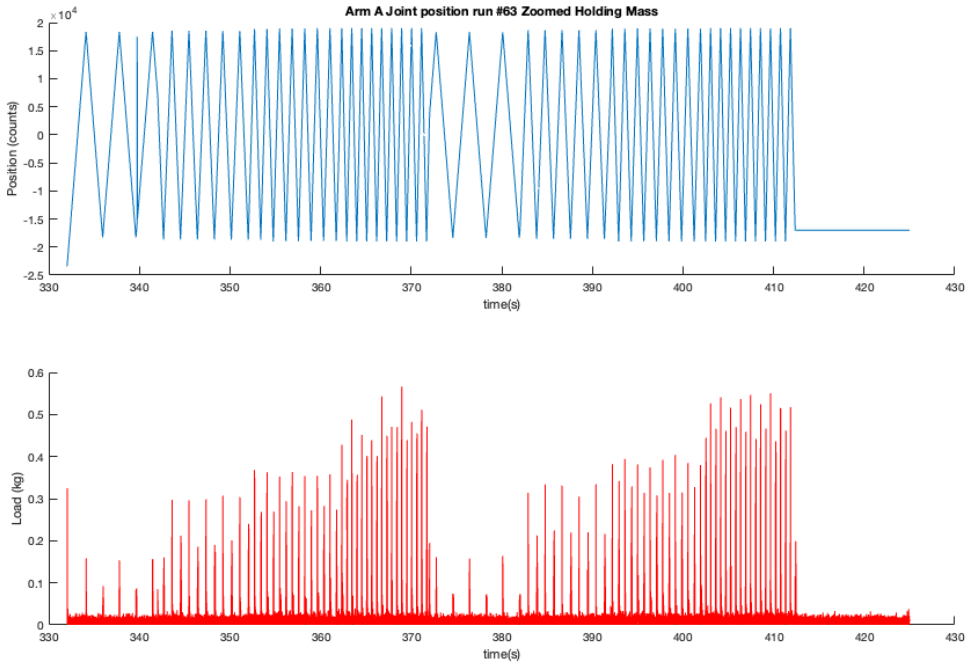

Figure 4.50: Graph showing encoder counts and load cell readings from the robot during the first two sweeps of the manipulator arm with the payload still attached

It can be seen that there is excellent correlation between the encoder counts and the load cell readings. There were two data points for the load cell that were recorded as a max reading for the load cell in the middle of a much lower reading and the two data points were filtered from the dataset. A filtered version of just the fours sets of sweeps can be seen in figure 4.51.

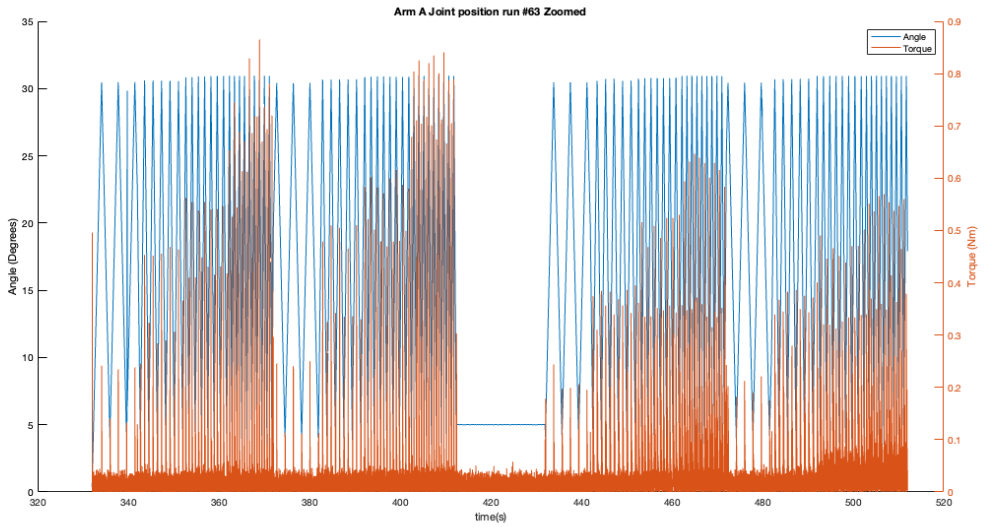

Figure 4.51: Graph showing encoder counts and noise filtered load cell readings from the payload during all sweeps of the manipulator arm

Next we need to bound the data by removing sections of the data that are tainted from external forces. The initial portion of the experiment was testing of the load cell with both a soft and hard end stop and since it did not pertain to the data for this thesis was removed from processing. It can be seen in both the video of the robot motion from the flight and the rate gyro data, figure 4.52, that the fourth sweep is tainted by drag from reentry. As such, the data from the fourth sweep was partially removed from the dataset for the tainted section that was recorded by the IMU rate gyro. The remaining data from the sweeps was then used to calculate the observable inertial parameters of the payload.

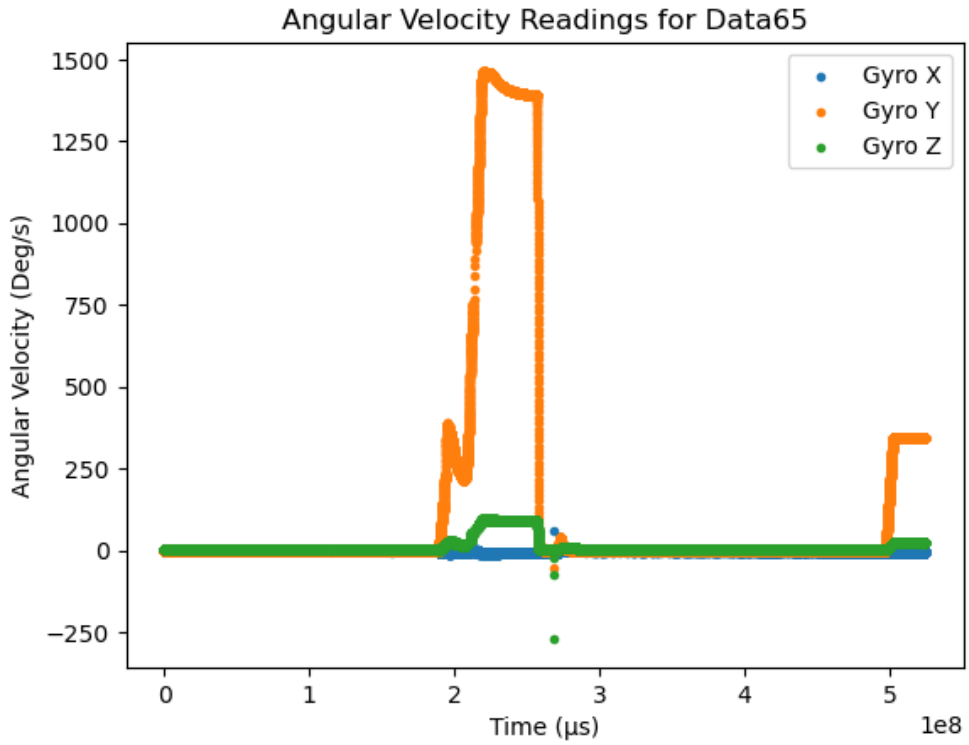

Figure 4.52: Rate gyro data from the payload during the full suborbital flight

Although we have data we also need to look at the theoretical underpinning of the system. From the set of DH parameters in table 4.5 we can find the base inertial parameters of the system. For the frames chosen for the RockSat system have some additional un-actuated frames to make the frame locations more descriptive. Frame 1 is the spacecraft frame and Frame 5 is the payload frame, with Frame 0 being the whole Rocksat payload faring. As such ${}^{3}\omega_3 = \begin{bmatrix} 0 & 0 & \dot{\theta}_3 \end{bmatrix}$ is the only non-zero angular velocity. Additionally, MY_3, MY_4, MY_5 are constant since the motion is planar. The additional energetic functions $XX_3, YY_3, ZZ_3, MX_3, MZ_3, XX_4, YY_4, ZZ_4, MX_4, MZ_4, XX_5, YY_5, ZZ_5, MX_5, MZ_5$ are all Null. The friction model is also unobservable without having accurate torque readings from the motor. Readings from a load cell distal to the actuator is used to calculate applied and reactive forces from the payload. The base inertial parameters of the system, with regrouping, are:

$$\boldsymbol{\beta} = \begin{bmatrix} ZZ_{3R} & ZZ_{4R} & ZZ_{5R} \end{bmatrix}^\top \tag{4.6}$$

with:

$$ZZ_{3R} = ZZ_3 + I_{a_3} + (m_5 + m_4)L_3^2$$

$$ZZ_{4R} = ZZ_4 + m_5 L_4^2 \qquad \Theta = \begin{bmatrix} 0 & 0 & \theta_3 & 0 & 0 \end{bmatrix}^\top$$

$$ZZ_{5R} = ZZ_5 \qquad \dot{\Theta} = \begin{bmatrix} 0 & 0 & \dot{\theta}_3 & 0 & 0 \end{bmatrix}^\top$$

$$IDM_{ZZ_3} = \begin{bmatrix} \ddot{\theta}_3 & 0 \end{bmatrix}^\top \qquad \ddot{\Theta} = \begin{bmatrix} 0 & 0 & \ddot{\theta}_3 & 0 & 0 \end{bmatrix}^\top$$

$$IDM_{ZZ_4} = \begin{bmatrix} \ddot{\theta}_3 + 0 & 0 \end{bmatrix}^\top$$

where the subscript 'R' means regrouped terms.

Using the equation for the IDIM method we can calculate the base inertial parameters of the system using equation 2.133. For the one degree of freedom for the system, equation 2.134 simplifies to $\boldsymbol{Y} = \boldsymbol{Y}_1$ and $\boldsymbol{W} = \boldsymbol{W}_1$. The torques and accelerations from the payload are shown in Figures 4.53, 4.54, 4.55, and 4.56.

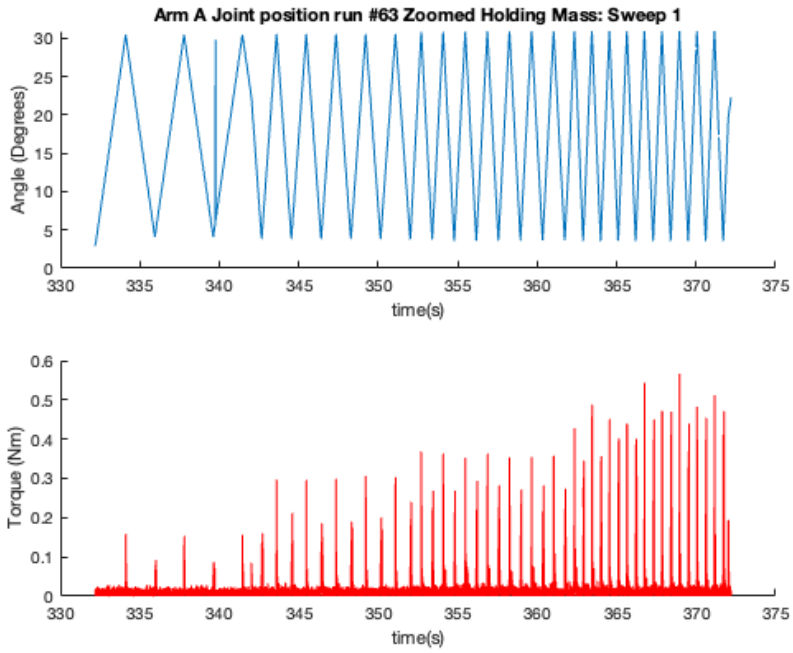

Figure 4.53: Rocksat Manipulator Torque and Acceleration: Sweep 1

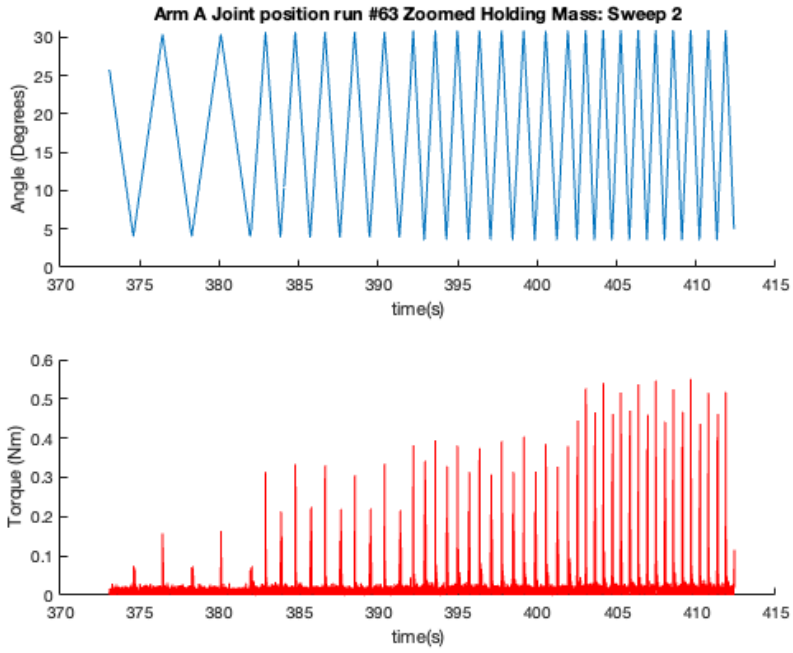

Figure 4.54: Rocksat Manipulator Torque and Acceleration: Sweep 2

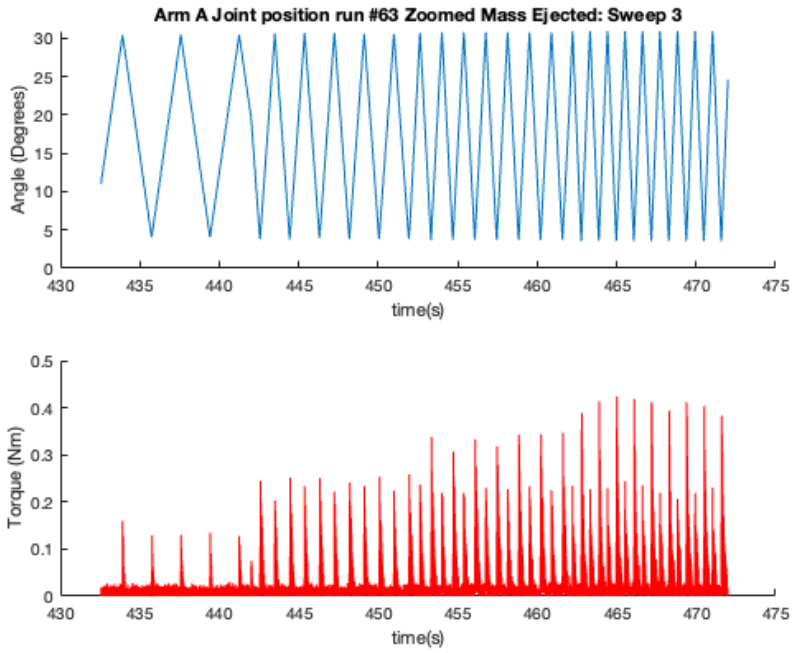

Figure 4.55: Rocksat Manipulator Torque and Acceleration: Sweep 3

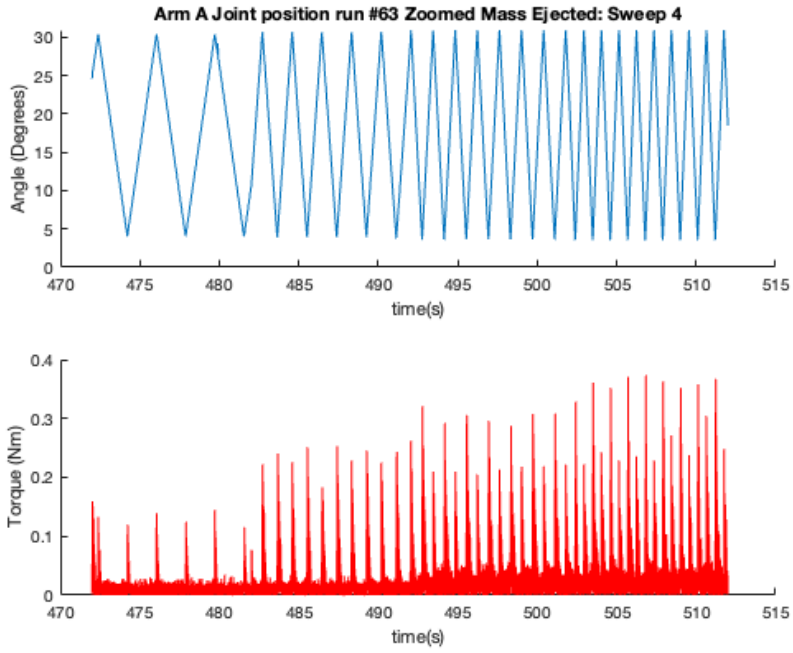

Figure 4.56: Rocksat Manipulator Torque and Acceleration: Sweep 4

The base inertial parameters of the system are then calculated using the data from the

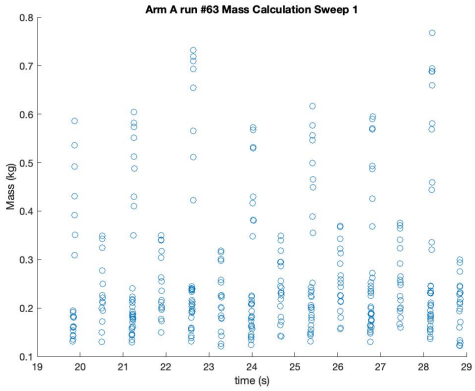

Figure 4.57: Sweep 1 Identified Mass

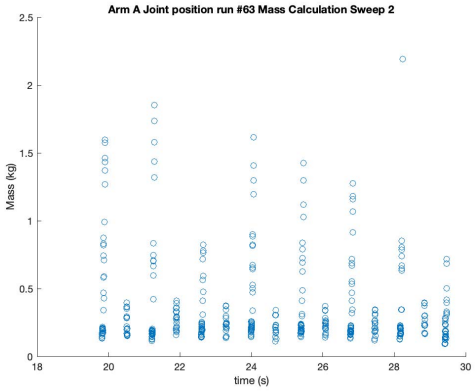

Figure 4.58: Sweep 2 Identified Mass

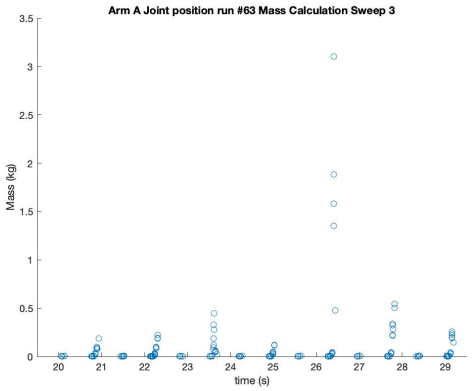

Figure 4.59: Sweep 3 Identified Mass

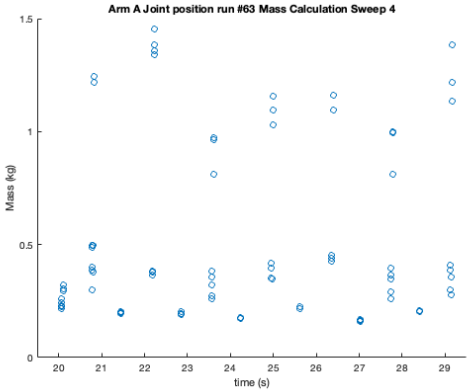

Figure 4.60: Sweep 4 Identified Mass

payload and the IDIM method. The ZZ_{3R}, ZZ_{4R}, and ZZ_{5R} were not fully identified due to a data rank deficiency in the system. Using the torques and accelerations from the payload the estimated masses are shown in figures 4.57, 4.58, 4.59, and 4.60.

Parameter	**Expected Value**	**Identified Value**	**Difference**	**Error**
m_4 (The Arm)	233.1 g	244.5 g	11.4 g	4.89%
$m_4 + m_5$	299.4 g	296 g	3.4 g	1.14%
m_5 (Tip Mass)	66.3 g	51.5 g	14.8 g	22.3%

Table 4.7: RockSat-X Payload Identified Parameter Values

What we see here is successful identification of the masses of the manipulator arm and the tip mass. The identified values are within 5% of the expected values except for the tip mass. The tip mass had an error of 22.3%. This is likely due to the tip mass, as built, not matching the CAD

model, as they were built by hand and not to the same tolerances as the rest of the system that was CNC machined.

4.5.4 Suborbital Flight Experiment: Lessons Learned

With the successful completion of the RockSat-X experiment, there were several lessons learned from the experiment:

- Torque sensors on the manipulator joint would be beneficial to enable more observable states for the system in future experiments and remove data rank deficiency
- Working with NASA and the Wallops Flight Facility to get specifications and details of the full payload stack and fairing components to improve identification of the system
- Time synchronization between data collection systems is critical for accuracy in post-processing of data
- High accuracy motor current sensors to allow for the calculation of input torques to the system, especially in microgravity environments were motor currents are small

Overall the RockSat-X experiment was a success and the data collected was used to identify the observable inertial parameters of the system.

Chapter 5: Conclusions

5.1 Contributions

The work presented in this thesis has shown that the proposed Extended Inverse Direct Dynamic Model (ExIDDM) is a viable extension of method for determining the observable inertial properties of a spacecraft, attached manipulator, and payload in a microgravity environment. Experimental validation using three separate test beds was attempted and achieved, and further refinements would improve the validation. The overall results of the experiments show that the ExIDDM method is capable of identifying the observable inertial parameters of the servicer and the grappled payload with a sufficient degree of accuracy for the excited modes.

The Extended Inverse Direct Dynamic Model (ExIDDM) is an extension of the ground-fixed Inverse Direct Dynamic Model (IDDM) to a system of a free-flying spacecraft with an attached manipulator and payload. ExIDDM follows the same rules and uses the same linearization methods as IDDM when solving for the inertial properties of the system using an Inverse Dynamic Identification Method (IDIM) to solve for the inertial properties of the system.

5.2 Experimental Results & Testing Lessons Learned

The experimental results from the air bearing table, parabolic flight, and suborbital flight experiments show some limitations of the linearized version of this method. Experiments on the air bearing table showed confirmation that predicted system dynamics matched the observed system dynamics. The parabolic flight experiments showed that the model is limited based upon how tightly the sensor noise and sensor synchronization can be controlled. Finally, the suborbital flight experiments showed that the method is capable of identifying the observable inertial properties of the servicer and the grappled payload for the excited modes.

Throughout the extensive experimentation and testing regime for this thesis, many lessons were learned that can be applied to future experiments:

- Data collection time synchronization needs to be very accurate with synchronization pulses to each of the data collection systems
- Trajectories for testing need to be well-defined to excite modes of interest, with consistent start and stop points
- External sources for tracking initial conditions of the spacecraft would provide a significant source of improvement to the initial conditions calculated from internal sensors
- Plastics, although light, can be a source of noise in the system dynamics as they are flexible and will deform over time and under load. As such they are not a good choice for the construction the major components of the manipulator joint drivetrain
- The use of a high-quality IMU is essential for the identification of the inertial properties of

the system

- High-accuracy current measurements for the motors are essential to identification of some inertial properties of the system, especially in microgravity where the currents are very low
- Torque sensors at each manipulator joint would vastly improve the quality of the data collected

Although there are individual lessons learned from each experiment, these are the major lessons learned that apply to all the experiments performed.

5.3 Proposed Further Research

With the results of the experiments in this thesis, there are many areas of further research that can be proposed. A primary area of further research is the development of a non-linear version of the ExIDDM. This would allow for the identification of the inertial properties of the system in a non-linear environment. Additionally, the integration of observers for the non-linear ExIDDM would allow for learning over time for a controller. Furthermore, a redesign of the manipulator joint drivetrain to remove the plastic components and replace them with a more rigid material coupled with the addition of torque sensors at each manipulator joint would allow for vastly improved data to be collected from further experiments. Finally, the development of a general simulation and calculation tool for the ExIDDM would simplify the data processing and identification for the observable inertial properties of the system.

Appendix A: Parabolic Flight Experiment Detailed Procedures

Here we are listing the detailed flight procedures for the parabolic flight experiment. These procedures are used to ensure that the experiment is conducted in a safe and controlled manner. The procedures are used to fulfill the NASA Flight Opportunities Program requirements and copied from the documents submitted.

A.1 Pre-Experiment Procedures

1. Test equipment power-up: All video cameras and experiment computers will be turned on.

   Contingency: The experiment can still be conducted if all cameras fail to operate. If either the test computer or Free-Flier computer fails to operate, available troubleshooting measures will be taken by the UMD personnel.

2. Test equipment preparation: Radio communication between the Test Stand and the free-flying vehicle will be established. A simple motion will be performed with the robotic arm to confirm operation.

   Contingency: Many of the planned experiments can still be conducted with two or more motor failures in the robotic arm. The order of the experiments can be easily changed based on functionality of the arm. Radio communication is required to conduct the experiment. A back-up radio system is located in Test Stand and can be applied without any tools.

3. Free-Flier deployment: Once all systems have been checked out the Free-Flier will be unlatched from the Test Stand and placed on the aircraft floor by two people. This must be done in 1G or less, as the Free-Flier weighs about 60 lbs.

A.2 Experiment Procedures

All experimental procedures are identical for every test. They follow three stages and will be repeated for each parabola.

1. Free-Flier release: The Free-Flier will be moved to, at minimum, 18 inches from any wall or object by the participants from UMD, stabilized, and released. This is performed by a single person.

2. Free-Flier motion: The free flier will perform a predetermined maneuver by moving the robotic arm onboard the Free-Flier.

3. Free-Flier capture: The participants from UMD will grab the Free-Flier and move it to the floor of the aircraft in preparation for the hyper gravity session. This is performed by a single person.

   Contingency: If at any time there is a failure or problem during an experiment the Free-Flier will be secured to the Test Stand while reasonable troubleshooting procedures are taken.

A.3 Post Experiment Procedures

1. Free-Flier securing: After the experiment has been completed, the Free-Flier will be loaded back onto the Test Stand. All four latches will be re-applied. Preferably, this would be done during a parabola to ease the loading process, but this can be completed during level flight as well.

   Contingency: Only one latch is required to retain the Free-Flier in all survivable scenarios. If a latch fails to close, reasonable troubleshooting procedures will be taken after all others have been secured.

2. Test equipment shutdown: Once all components are physically secured, the Free-Flier and test computer will be shut down.

   Contingency: If the vehicle fails to shut down, the emergency stop will be activated to manually power off its systems.

   Contingency: If at any time a structural failure occurs in the Free-Flier or its robotic arm, or any emergency occurs on the aircraft, the Free-Flier will be powered down and secured to the 80/20 Test Stand and all experimental operations will cease.

A.3.1 Post Flight

The only groundwork necessary will be charging of experiment's batteries. This will be done under constant supervision by a technician from the University of Maryland. This will occur between flights and will require that the free-flying vehicle be removed from the aircraft. Additionally, camera equipment attached to the 80/20 Test Stand must be removed for charging

and data retrieval during this time.

Appendix B: Definitions

It is important for the understanding of the document to have some terms used throughout the document to be defined as they are used in the context of robotics for the improved understanding of the reader.

Term	Definition
Centrifugal Matrix	See Coriolis Matrix
Column Space, Matrix	The set of all possible outputs of the linear transformation $A\vec{x}$
Coriolis Matrix	For robot dynamics represented in state space, the matrix $C(\Theta, \dot{\Theta})$ is a $n \times 1$ vector of centrifugal and coriolis terms. It is a collection of all the terms that have a dependence on joint velocity, $\dot{\Theta}$. [14]
Determinant	Visually this is the measure of the change in n-dimensional volume (e.g. area for 2 dimensional) of the unit basis vectors during a linear transformation. Negative values indicate a change in handedness for the unit basis vectors. The absolute value of the determinant is the scalar n-dimensional volume transformation of the unit basis vector space.

continued on next page

continued from previous page

Term	Definition
Free-Floating	A body or collection of rigidly attached bodies that are floating with tracked inertially fixed coordinates, which therefore ignores any translation of the system
Free-Flying	A body or collection of rigidly attached bodies that are floating with tracked externally referenced coordinates, which therefore allows for tracking of the translation of the system
Hermetian Matrix	A matrix that is equal to its own conjugate transpose. $A = A^{\intercal}$ [100]
Holonomic Constraint	A Holonomic Constraint is a mathematical representation of the reduced degrees of freedom for a system through a mathematical formulation. [101]
Jacobian	The Jacobian of a manipulator is a mapping between the velocities in the joint space of the manipulator to velocities in Cartesian space. i.e. $\dot{x} = J(\Theta)\dot{\Theta}$ Singularities in the manipulator can cause the Jacobian to become no longer invertible [14] Simply put a Jacobian represents the linear sensitivity of the end effector velocity $\dot{x}$ to the joint velocity $\dot{\Theta}$. The Jacobian matrix is a function of the joint variables Θ [102]

continued on next page

continued from previous page

Term	Definition
Jacobian Null Space	The Jacobian Null space is defined as $\dot{x} = J(\Theta)\dot{\Theta} = 0, \forall \dot{\Theta} \in Null(J)$. This is the set of all joint velocities that generate zero velocity in the workspace. This is a powerful tool for the analysis of redundant manipulators and allows for optimization of trajectories to allow motion of the arm while still maintaining the workspace goal of the end effector. [14], [102]
Inverse Matrix	A^{-1}. Square matrix with $A^{-1}A = \mathbb{I}$ and $AA^{-1} = \mathbb{I}$. No inverse if $\det A = 0$ and rank$(A) < n$ and $Ax = 0$ for a nonzero vector x. The inverses if AB and $A^\intercal$ are $B^{-1}A^{-1}$ and $(A^{-1})^\intercal$ [100]
Kernel, Matrix	See Null-Space Matrix.
Kronecker Product	See Tensor Product
Moment of Inertia	The moment of inertia is a measure of how much torque is needed for a fixed angular acceleration. E.g. The higher the moment of inertia, the more torque is needed to achieve the same angular acceleration.

continued on next page

continued from previous page

Term	Definition
Non-Holonomic	A non-holonomic system is a system where you can move from one set of coordinates to another and then back to the original coordinates and the state of the system will depend on the path taken. For example, a bicycle can have a set of coordinates x, y that represent the location of the system in a plane. θ represents the rotation of the bicycle about the saddle of the bike. ϕ_1, ϕ_2 will be used to represent the angle around the axis of the wheels of the valve stem of the tires. This gives the configuration space $\vec{u} \rightarrow [x, y, \theta, \phi_1, \phi_2]$. By inspection of the mechanics of the system we can see that it is extremely unlikely that ϕ_1 and ϕ_2 will have the same value they initially did unless you take exactly the same path to return as you did to leave the initial position $[x, y, \theta]$. [14]

continued on next page

continued from previous page

Term	Definition
Null-Space, Matrix	The space of all vectors that becomes null or zero after a linear transformation $A\vec{x}$
Pivot, Matrix	d. The diagonal entry (*first nonzero*) when a row is used in elimination. [100]
Positive Definite, Matrix	A Symmetric matrix with positive eigenvalues and positive pivots. By definition: $x^\intercal Ax > 0$ unless $x = 0$ [100]
Pseudoinverse	A^+ or $A^\intercal$ (Moore-Penrose inverse) The n by m matrix that "*inverts*" A from column space back to row space, with $N\left(A^+\right) = N\left(A^\intercal\right)$ A^+A and AA^+ are the projection matrices onto the row space and column space respectively. Rank $\left(A^+\right)$ = Rank $\left(A\right)$ [100]
Rank, Matrix	Number of dimensions in the output of a linear transformation. This is also the number of columns in the column space of the matrix.
Regressor Matrix	A matrix that is used to represent the dynamics of a system. The regressor matrix is used to represent the dynamics of a system in a linear form. This is useful for the identification of the dynamics of a system. The matrix has the dimension of n-by-p, where n is the number of samples observed, and p is the number of variables measured in all samples. [103]

continued on next page

continued from previous page

Term	Definition
Semi-Definite, Matrix	A. A Positive Semi-definite matrix is a symmetric matrix with $x^\intercal Ax \geq 0$ for all vectors x. A positive Semi-definite matrix will have all eigenvalues $\lambda \geq 0$ with no negative pivots. [100]
Singular Value Decomposition	$A = U\Sigma V^\intercal$ where U and V are orthogonal matrices and Σ is a diagonal matrix with the singular values of A on the diagonal. [100]
Skew-Symmetric Matrix	By definition a matrix A that has the following property $A^\intercal = -A$ Where the individual entries $a_{ji} = -a_{ij}$ [100]
Skew-Symmetric Vector	$x^\intercal = -x$ [100]
Symmetric Matrix	A matrix A such that $A^\intercal = A$ [100]
Tensor	A tensor is a mathematical object that is a generalization of a vector. A vector is a tensor of rank 1. A matrix is a tensor of rank 2. A scalar is a tensor of rank 0. [100]
Task Space	The collection of vectors that define the kinematics of the robotic manipulator The space of all possible outputs of a linear transformation $A\vec{x}$

continued on next page

continued from previous page

Term	Definition
Tensor	"A tensor is a new mathematical object. Unlike a vector it does not have a clear geometric representation. However, mathematically it satisfies the same definition of a vector" "That is [that] it is a member of a vector space because it obeys addition, subtraction and scalar multiplication. In fact, it satisfies the same eight properties that vectors do." [101]
Tensor Product	Also called an outer product. It is essentially $v \bigotimes w = vw^\intercal$ It is a linear transform from $\mathbb{R}^v \bigotimes \mathbb{R}^w = \mathbb{R}^{v \times w}$ See reference for a full explanation [104]

Bibliography

[1] D. J. Kessler and B. G. Cour-Palais, "Collision frequency of artificial satellites: The creation of a debris belt," *Journal of Geophysical Research*, vol. 83, no. A6, p. 2637, 1978. DOI: 10.1029/ja083ia06p02637.

[2] B. R. Sullivan, "Technical and economic feasibility of telerobotic on -orbit satellite servicing," Copyright - Database copyright ProQuest LLC; ProQuest does not claim copyright in the individual underlying works; Last updated - 2021-05-24, Ph.D. dissertation, University of Maryland, College Park, 2005, p. 308, ISBN: 978-0-542-18070-5. [Online]. Available: https://www.proquest.com/dissertations-theses/technical-economic-feasibility-telerobotic-on/docview/304991965/se-2?accountid=14696.

[3] A. Ellery, J. Kreisel, and B. Sommer, "The case for robotic on-orbit servicing of spacecraft: Spacecraft reliability is a myth," *Acta Astronautica*, vol. 63, no. 5-6, pp. 632–648, Sep. 2008. DOI: 10.1016/j.actaastro.2008.01.042.

[4] J.-C. Liou, "An active debris removal parametric study for leo environment remediation," *Advances in Space Research*, vol. 47, no. 11, pp. 1865–1876, Jun. 2011, ISSN: 0273-1177. DOI: 10.1016/j.asr.2011.02.003.

[5] M. Shan, J. Guo, and E. Gill, "Review and comparison of active space debris capturing and removal methods," *Progress in Aerospace Sciences*, vol. 80, pp. 18–32, Jan. 2016. DOI: 10.1016/j.paerosci.2015.11.001.

[6] B.-Z. Zhou, X.-F. Liu, and G.-P. Cai, "Motion-planning and pose-tracking based rendezvous and docking with a tumbling target," *Advances in Space Research*, vol. 65, no. 4, pp. 1139–1157, Feb. 2020. DOI: 10.1016/j.asr.2019.11.013.

[7] T. Oki, S. Abiko, H. Nakanishi, and K. Yoshida, "Time-optimal detumbling maneuver along an arbitrary arm motion during the capture of a target satellite," in *2011 IEEE/RSJ International Conference on Intelligent Robots and Systems*, Sep. 2011, pp. 625–630. DOI: 10.1109/IROS.2011.6095159.

[8] N. Uyama and T. Narumi, "Hybrid impedance/position control of a free-flying space robot for detumbling a noncooperative satellite," *IFAC-PapersOnLine*, vol. 49, no. 17, pp. 230–235, 2016. DOI: 10.1016/j.ifacol.2016.09.040.

[9] K. Sun, Z. Wang, Y. Zhang, and H. Liu, "Triaxial contact detumbling of large-scale space debris," in *2018 IEEE 3rd Advanced Information Technology, Electronic and Automation Control Conference (IAEAC)*, IEEE, Oct. 2018. DOI: 10.1109/iaeac.2018.8577610.

[10] W. Cheng, L. Tianxi, and Z. Yang, "Grasping strategy in space robot capturing floating target," *Chinese Journal of Aeronautics*, vol. 23, no. 5, pp. 591–598, Oct. 2010. DOI: 10.1016/s1000-9361(09)60259-4.

[11] P. Gasbarri and A. Pisculli, "Dynamic/control interactions between flexible orbiting space-robot during grasping, docking and post-docking manoeuvres," *Acta Astronautica*, vol. 110, pp. 225–238, May 2015. DOI: 10.1016/j.actaastro.2015.01.024.

[12] J. Luo, L. Zong, M. Wang, and J. Yuan, "Optimal capture occasion determination and trajectory generation for space robots grasping tumbling objects," *Acta Astronautica*, vol. 136, pp. 380–386, Jul. 2017. DOI: 10.1016/j.actaastro.2017.03.026.

[13] C. Wei, J. Luo, H. Dai, Z. Bian, and J. Yuan, "Learning-based adaptive prescribed performance control of postcapture space robot-target combination without inertia identifications," *Acta Astronautica*, vol. 146, pp. 228–242, May 2018. DOI: 10.1016/j.actaastro.2018.03.007.

[14] J. J. Craig, *Introduction to robotics: mechanics and control, 3/E*. Pearson Education, 2009.

[15] J. Denavit and R. S. Hartenberg, "A kinematic notation for lower-pair mechanisms based on matrices," *Journal of Applied Mechanics*, vol. 22, no. 2, pp. 215–221, May 1955. DOI: 10.1115/1.4011045.

[16] P. I. Corke, "A simple and systematic approach to assigning denavit–hartenberg parameters," *IEEE Transactions on Robotics*, vol. 23, no. 3, pp. 590–594, May 2007. DOI: 10.1109/tro.2007.896765.

[17] P. I. Corke, *Robotics, Vision & Control*, Second. Springer, 2017, ISBN: 978-3-319-54413-7. [Online]. Available: https://www.ebook.de/de/product/28453919/peter_corke_robotics_vision_and_control.html.

[18] H. Mayeda, K. Yoshida, and K. Osuka, "Base parameters of manipulator dynamic models," in *Proceedings. 1988 IEEE International Conference on Robotics and Automation*, IEEE Comput. Soc. Press, 1988. DOI: 10.1109/robot.1988.12258.

[19] E. Stoneking, "Newton-euler dynamic equations of motion for a multi-body spacecraft," in *AIAA Guidance, Navigation and Control Conference and Exhibit*, 2007, p. 6441. DOI: 10.2514/6.2007-6441.

[20] J. K. Davidson and K. H. Hunt, *Robots and Screw Theory: Applications of Kinematics and Statics to Robotics*. Oxford University PressOxford, Mar. 2004, ISBN: 9781383028966. DOI: 10.1093/oso/9780198562450.001.0001.

[21] Z. Chen and J. C. Hung, "Application of quaternion in robot control," *IFAC Proceedings Volumes*, vol. 20, no. 5, pp. 259–263, Jul. 1987, ISSN: 1474-6670. DOI: 10.1016/s1474-6670(17)55326-4.

[22] A. Valverde and P. Tsiotras, "Spacecraft robot kinematics using dual quaternions," *Robotics*, vol. 7, no. 4, p. 64, Oct. 2018, ISSN: 2218-6581. DOI: 10.3390/robotics7040064.

[23] D. L. Pieper, "The kinematics of manipulators under computer control," English, Copyright - Database copyright ProQuest LLC; ProQuest does not claim copyright in the individual underlying works; Last updated - 2023-02-23, Ph.D. dissertation, Stanford University, 1969, p. 169. [Online]. Available: https://www.proquest.com/dissertations-theses/kinematics-manipulators-under-computer-control/docview/302481631/se-2.

[24] C. Lewandowski, D. Akin, B. Dillow, *et al.*, "Development of a deep-sea robotic manipulator for autonomous sampling and retrieval," in *2008 IEEE/OES Autonomous Underwater Vehicles*, IEEE, Oct. 2008. DOI: 10.1109/auv.2008.5290533.

[25] (. National Research Council, *Future Needs in Deep Submergence Science, Occupied and Unoccupied Vehicles in Basic Ocean Research*. National Academy Press, 2004, p. 135, ISBN: 9780309529174.

[26] D. L. Akin, M. L. Minsky, E. D. Thiel, and C. R. Kurtzman, "Space applications of automation, robotics and machine intelligence systems (ARAMIS), phase 2. volume 1: Telepresence technology base development," Massachusetts Inst. of Tech, Tech. Rep., Oct. 1983. [Online]. Available: https://ntrs.nasa.gov/citations/19840002515.

[27] K. Yamada, K. Tsuchiya, Y. Ohkami, and T. Klda, "Modeling and control of space manipulators," *The Journal of Space Technology and Science*, vol. 1, no. 2, pp. 14–22, 1985. DOI: 10.11230/jsts.1.2_14.

[28] P. Putz, "Space robotics in europe: A survey," *Robotics and Autonomous Systems*, vol. 23, no. 1-2, pp. 3–16, Mar. 1998. DOI: 10.1016/s0921-8890(97)00053-5.

[29] E. E. Vance, "Adaptive control of free-floating and free-flying robotic manipulators," Copyright - Database copyright ProQuest LLC; ProQuest does not claim copyright in the individual underlying works; Last updated - 2016-05-12, Ph.D. dissertation, University of Maryland, 1998, p. 384, ISBN: 9780599208537. [Online]. Available: https://search.proquest.com/docview/304419416?accountid=14696.

[30] A. Flores-Abad, O. Ma, K. Pham, and S. Ulrich, "A review of space robotics technologies for on-orbit servicing," *Progress in Aerospace Sciences*, vol. 68, pp. 1–26, 2014, ISSN: 0376-0421. DOI: https://doi.org/10.1016/j.paerosci.2014.03.002. [Online]. Available: http://www.sciencedirect.com/science/article/pii/S0376042114000347.

[31] E. Papadopoulos, F. Aghili, O. Ma, and R. Lampariello, "Robotic manipulation and capture in space: A survey," *Frontiers in Robotics and AI*, vol. 8, Jul. 2021. DOI: 10.3389/frobt.2021.686723.

[32] J. Shoemaker and M. Wright, "Orbital express space operations architecture program," in *SPIE Proceedings*, J. Peter Tchoryk and M. Wright, Eds., SPIE, Aug. 2004. DOI: 10.1117/12.544067.

[33] A. Ogilvie, J. Allport, M. Hannah, and J. Lymer, "Autonomous robotic operations for on-orbit satellite servicing," in *SPIE Proceedings*, R. T. Howard and P. Motaghedi, Eds., SPIE, Apr. 2008. DOI: 10.1117/12.784081.

[34] A. Ogilvie, J. Allport, M. Hannah, and J. Lymer, "Autonomous satellite servicing using the orbital express demonstration manipulator system," in *Proc. of the 9th International Symposium on Artificial Intelligence, Robotics and Automation in Space (i-SAIRAS'08)*, 2008, pp. 25–29.

[35] M. Oda, "Coordinated control of spacecraft attitude and its manipulator," in *Proceedings of IEEE International Conference on Robotics and Automation*, IEEE, 1996. DOI: 10.1109/robot.1996.503861.

[36] M. Oda, K. Kibe, and F. Yamagata, "ETS-VII, space robot in-orbit experiment satellite," in *Proceedings of IEEE International Conference on Robotics and Automation*, IEEE, 1996. DOI: 10.1109/robot.1996.503862.

[37] M. Oda, "Experiences and lessons learned from the ETS-VII robot satellite," in *Proceedings 2000 ICRA. Millennium Conference. IEEE International Conference on Robotics and Automation. Symposia Proceedings (Cat. No.00CH37065)*, IEEE, 2000. DOI: 10.1109/robot.2000.844165.

[38] N. Inaba and M. Oda, "Autonomous satellite capture by a space robot: World first on-orbit experiment on a japanese robot satellite ETS-VII," in *Proceedings 2000 ICRA. Millennium Conference. IEEE International Conference on Robotics and Automation. Symposia Proceedings (Cat. No.00CH37065)*, IEEE, 2000. DOI: 10.1109/robot.2000.844757.

[39] P. Motaghedi and S. Stamm, "6 DOF testing of the orbital express capture system (invited paper)," in *SPIE Proceedings*, P. Motaghedi, Ed., SPIE, May 2005. DOI: 10.1117/12.606222.

[40] P. Motaghedi, "On-orbit performance of the orbital express capture system," in *SPIE Proceedings*, R. T. Howard and P. Motaghedi, Eds., SPIE, Apr. 2008. DOI: 10.1117/12.780132.

[41] D. King, "Space servicing: Past, present and future," in *Proceedings of the 6th International Symposium on Artificial Intelligence and Robotics & Automation in Space: i-SAIRAS*, 2001, pp. 18–22.

[42] R. B. Friend, "Orbital express program summary and mission overview," in *SPIE Proceedings*, R. T. Howard and P. Motaghedi, Eds., SPIE, Apr. 2008. DOI: 10.1117/12.783792.

[43] T. Debus and S. Dougherty, "Overview and performance of the front-end robotics enabling near-term demonstration (FREND) robotic arm," in *AIAA Infotech@Aerospace Conference*, American Institute of Aeronautics and Astronautics, Apr. 2009. DOI: 10.2514/6.2009-1870.

[44] K. Yoshida, N. Sashida, R. Kurazume, and Y. Umetani, "Modeling of collision dynamics for space free-floating links with extended generalized inertia tensor," in *Proceedings 1992 IEEE International Conference on Robotics and Automation*, IEEE Comput. Soc. Press, 1992. DOI: 10.1109/robot.1992.220182.

[45] K. Yoshida, "Experimental study on the dynamics and control of a space robot with experimental free-floating robot satellite," *Advanced Robotics*, vol. 9, no. 6, pp. 583–602, Jan. 1994. DOI: 10.1163/156855395x00319.

[46] C. R. Carignan and D. L. Akin, "The reaction stabilization of on-orbit robots," *IEEE Control Systems Magazine*, vol. 20, no. 6, pp. 19–33, Dec. 2000, ISSN: 1941-000X. DOI: 10.1109/37.887446.

[47] D. E. Hastings, B. L. Putbrese, and P. A. L. Tour, "When will on-orbit servicing be part of the space enterprise?" *Acta Astronautica*, vol. 127, pp. 655–666, Oct. 2016. DOI: 10.1016/j.actaastro.2016.07.007.

[48] C. G. Henshaw, S. Glassner, B. Naasz, and B. Roberts, "Grappling spacecraft," *Annual Review of Control, Robotics, and Autonomous Systems*, vol. 5, no. 1, pp. 137–159, May 2022. DOI: 10.1146/annurev-control-042920-011106.

[49] Z. Vafa and S. Dubowsky, "On the dynamics of manipulators in space using the virtual manipulator approach," in *IEEE International Conference on Robotics and Automation*, Institute of Electrical and Electronics Engineers, 1987. DOI: 10.1109/robot.1987.1088032.

[50] R. W. Longman, R. E. Lindbergt, and M. F. Zedd, "Satellite-mounted robot manipulators — new kinematics and reaction moment compensation," *The International Journal of Robotics Research*, vol. 6, no. 3, pp. 87–103, Sep. 1987. DOI: 10.1177/027836498700600306.

[51] S. Dubowsky, E. E. Vance, and M. A. Torres, "The control of space manipulators subject to spacecraft attitude control saturation limits," in *Proc. of the NASA Conference on Space Telerobotics*, Massachusetts Inst. of Tech.; Dept. of Mechanical Engineering.; Cambridge, MA, United States, vol. 4, NASA, Jan. 1989, pp. 409–418. [Online]. Available: https://ntrs.nasa.gov/api/citations/19900020555/downloads/19900020555.pdf.

[52] Z. Vafa and S. Dubowsky, "The kinematics and dynamics of space manipulators: The virtual manipulator approach," *The International Journal of Robotics Research*, vol. 9, no. 4, pp. 3–21, Aug. 1990, ISSN: 0278-3649. DOI: 10.1177/027836499000900401.

[53] Z. Vafa, "The kinematics, dynamics and control of space manipulators : The virtual manipulator concept," Ph.D. dissertation, Massachusetts Institute of Technology, 1987.

[54] E. G. Papadopoulos, "Path planning for space manipulators exhibiting nonholonomic behavior," in *Proceedings of the IEEE/RSJ International Conference on Intelligent Robots and Systems*, IEEE, 1992. DOI: 10.1109/iros.1992.587419.

[55] E. G. Papadopoulos, "On the dynamics and control of space manipulators," Ph.D. dissertation, Massachusetts Institute of Technology, 1990. [Online]. Available: http://hdl.handle.net/1721.1/13705.

[56] E. Papadopoulos and S. Dubowsky, "Coordinated manipulator/spacecraft motion control for space robotic systems," in *Proceedings. 1991 IEEE International Conference on Robotics and Automation*, IEEE Comput. Soc. Press, 1991. DOI: 10.1109/robot.1991.131864.

[57] K. Strickland, "An experimental evaluation of space manipulator dynamics," M.S. thesis, University of Maryland (College Park, Md.), Oct. 2012. [Online]. Available: http://hdl.handle.net/1903/13034.

[58] P. C. Hughes, *Spacecraft attitude dynamics*. Courier Corporation, 2012.

[59] Y. Umetani and K. Yoshida, "Resolved motion rate control of space manipulators with generalized jacobian matrix," *IEEE Transactions on Robotics and Automation*, vol. 5, no. 3, pp. 303–314, Jun. 1989, ISSN: 2374-958X. DOI: 10.1109/70.34766.

[60] P. C. Hughes, "Dynamics of a chain of flexible bodies," *J. of the Astronautical Science*, vol. 27, no. 4, pp. 359–380, 1979. [Online]. Available: https://cir.nii.ac.jp/crid/1573950401226058112.

[61] Y. Umetani and K. Yoshida, "Experimental study on two-dimensional free-flying robot satellite model," in *Proceedings of the NASA Conference on Space Telerobotics*, H. S. G. Rodreguez, Ed., ser. 89-7, NASA, vol. IV, JPL Publication, 1989, pp. 229–240. [Online]. Available: https://ntrs.nasa.gov/search.jsp?R=19900020558.

[62] K. Yoshida and Y. Umetani, "Control of space free-flying robot," in *29th IEEE Conference on Decision and Control*, IEEE, 1990. DOI: 10.1109/cdc.1990.203553.

[63] J.-J. E. Slotine and S. S. Sastry, "Tracking control of non-linear systems using sliding surfaces, with application to robot manipulators," *International Journal of Control*, vol. 38, no. 2, pp. 465–492, Aug. 1983. DOI: 10.1080/00207178308933088.

[64] J.-J. E. Slotine, J. K. Hedrick, and E. A. Misawa, "On sliding observers for nonlinear systems," in *1986 American Control Conference*, IEEE, Jun. 1986. DOI: 10.23919/acc.1986.4789217.

[65] J.-J. E. Slotine, J. K. Hedrick, and E. A. Misawa, "On sliding observers for nonlinear systems," *Journal of Dynamic Systems, Measurement, and Control*, vol. 109, no. 3, pp. 245–252, Sep. 1987. DOI: 10.1115/1.3143852.

[66] J.-J. E. Slotine and L. Weiping, "Adaptive manipulator control: A case study," *IEEE Transactions on Automatic Control*, vol. 33, no. 11, pp. 995–1003, 1988. DOI: 10.1109/9.14411.

[67] J.-J. E. Slotine and W. Li, *Applied nonlinear control*. Prentice Hall, 1991, p. 459, ISBN: 0130408905.

[68] H. Asada and J.-J. E. Slotine, *Robot analysis and control*, First. J. Wiley, 1986, p. 266, ISBN: 0471830291.

[69] M. W. Spong, R. Ortega, and R. Kelly, "Comments on "adaptive manipulator control: A case study" by j. slotine and w. li," *IEEE Transactions on Automatic Control*, vol. 35, pp. 761–762, 6 Jun. 1, 1990, ISSN: 2334-3303. DOI: 10.1109/9.53565.

[70] P. Culbertson, J.-J. Slotine, and M. Schwager, "Decentralized adaptive control for collaborative manipulation of rigid bodies," *IEEE Transactions on Robotics*, vol. 37, no. 6, pp. 1906–1920, Dec. 2021. DOI: 10.1109/tro.2021.3072021.

[71] B. T. Lopez and J.-J. E. Slotine, "Universal adaptive control of nonlinear systems," *IEEE Control Systems Letters*, vol. 6, pp. 1826–1830, 2022. DOI: 10.1109/lcsys.2021.3133359.

[72] S. Arimoto, "Learning control theory for robotic motion," *International Journal of Adaptive Control and Signal Processing*, vol. 4, no. 6, pp. 543–564, Nov. 1990. DOI: 10.1002/acs.4480040610.

[73] K. Nanos and E. G. Papadopoulos, "On the dynamics and control of flexible joint space manipulators," *Control Engineering Practice*, vol. 45, pp. 230–243, Dec. 2015. DOI: 10.1016/j.conengprac.2015.06.009.

[74] X.-y. Yu and L. Chen, "Modeling and observer-based augmented adaptive control of flexible-joint free-floating space manipulators," *Acta Astronautica*, vol. 108, pp. 146–155, Mar. 2015. DOI: 10.1016/j.actaastro.2014.12.002.

[75] G. Heinzinger, D. Fenwick, B. Paden, and F. Miyazaki, "Robust learning control," in *Proceedings of the 28th IEEE Conference on Decision and Control*, IEEE, Dec. 13, 1989. DOI: 10.1109/cdc.1989.70152.

[76] P. Bondi, G. Casalino, and L. Gambardella, "On the iterative learning control theory for robotic manipulators," *IEEE Journal on Robotics and Automation*, vol. 4, no. 1, pp. 14–22, 1988, ISSN: 0882-4967. DOI: 10.1109/56.767.

[77] J.-J. E. Slotine and W. Li, "On the adaptive control of robot manipulators," *The International Journal of Robotics Research*, vol. 6, no. 3, pp. 49–59, Sep. 1987, ISSN: 1741-3176. DOI: 10.1177/027836498700600303.

[78] B. Siciliano, L. Sciavicco, L. Villani, and G. Oriolo, *Robotics*. Springer London, 2009. DOI: 10.1007/978-1-84628-642-1.

[79] C. Wei, J. Luo, C. Xu, and J. Yuan, "Low-complexity stabilization control of combined spacecraft with an unknown captured object," in *2017 36th Chinese Control Conference (CCC)*, IEEE, Jul. 2017. DOI: 10.23919/chicc.2017.8027489.

[80] Q. Leboutet, J. Roux, A. Janot, J. R. Guadarrama-Olvera, and G. Cheng, "Inertial parameter identification in robotics: A survey," *Applied Sciences*, vol. 11, no. 9, p. 4303, May 2021. DOI: 10.3390/app11094303.

[81] W. Khalil, E. Dombre, and M. L. Nagurka, "Modeling, identification and control of robots," *Applied Mechanics Reviews*, vol. 56, no. 3, B37–B38, May 2003. DOI: 10.1115/1.1566397.

[82] W. Khalil and E. Dombre, *Modeling, Identification and Control of Robots.* (Kogan Page Science Paper Edition), New ed., Kogan Page Science paper edition, digitaler Nachdr. London [u.a.]: Butterworth-Heinemann, 2004, 480 pp., Includes bibliographical references (p. [447]-473) and index, ISBN: 9781903996669. [Online]. Available: https://search-ebscohost-com.proxy-um.researchport.umd.edu/login.aspx?direct=true&db=nlebk&AN=249358&site=ehost-live.

[83] W. Khalil, M. Gautier, and P. Lemoine, "Identification of the payload inertial parameters of industrial manipulators," in *Proceedings 2007 IEEE International Conference on Robotics and Automation*, IEEE, Apr. 2007. DOI: 10.1109/robot.2007.364241.

[84] M. Gautier, "Numerical calculation of the base inertial parameters of robots," *Journal of Robotic Systems*, vol. 8, no. 4, pp. 485–506, Aug. 1991, ISSN: 1097-4563. DOI: 10.1002/rob.4620080405.

[85] M. Gautier, S. Briot, and G. Venture, "Identification of consistent standard dynamic parameters of industrial robots," in *2013 IEEE/ASME International Conference on Advanced Intelligent Mechatronics*, IEEE, Jul. 2013. DOI: 10.1109/aim.2013.6584295.

[86] S. A. A. Moosavian and E. Papadopoulos, "On the kinematics of multiple manipulator space free-flyers and their computation," *Journal of Robotic Systems*, vol. 15, no. 4, pp. 207–216, Apr. 1998. DOI: 10.1002/(sici)1097-4563(199804)15:4<207::aid-rob3>3.0.co;2-t.

[87] S. A. A. Moosavian and E. Papadopoulos, "Explicit dynamics of space free-flyers with multiple manipulators via SPACEMAPLE," *Advanced Robotics*, vol. 18, no. 2, pp. 223–244, Jan. 2004. DOI: 10.1163/156855304322758033.

[88] S. A. A. Moosavian and E. Papadopoulos, "Free-flying robots in space: An overview of dynamics modeling, planning and control," *Robotica*, vol. 25, no. 5, pp. 537–547, Sep. 2007. DOI: 10.1017/s0263574707003438.

[89] K. Yoshida, "Space robot dynamics and control: To orbit, from orbit, and future," in *Robotics Research*, Springer London, 2000, pp. 449–456. DOI: 10.1007/978-1-4471-0765-1_54.

[90] K. Yoshida and S. Abiko, "Inertia parameter identification for a free-flying space robot," in *AIAA Guidance, Navigation, and Control Conference and Exhibit*, American Institute of Aeronautics and Astronautics, Jun. 2002. DOI: 10.2514/6.2002-4568.

[91] K. Yoshida, "ETS-VII flight experiments for space robot dynamics and control," in *Experimental Robotics VII*, Springer Berlin Heidelberg, 2002, pp. 209–218. DOI: 10.1007/3-540-45118-8_22.

[92] K. Yoshida, "Engineering test satellite VII flight experiments for space robot dynamics and control: Theories on laboratory test beds ten years ago, now in orbit," *International Journal of Robotics Research*, vol. 22, no. 5, pp. 321–335, May 2003. DOI: 10.1177/0278364903022005003.

[93] M. Jardin. "Improving mass moment of inertia measurements." (2010), [Online]. Available: https://www.mathworks.com/company/technical-articles/improving-mass-moment-of-inertia-measurements.html (visited on 04/04/2024).

[94] D. Akin, N. Limparis, and K. McBryan, "Enabling dexterous manipulation and servicing by smallsats," *26th Annual AIAA/USU Conference on Small Satellites*, 2012. eprint: https://digitalcommons.usu.edu/cgi/viewcontent.cgi?article=1053&context=smallsat. [Online]. Available: https://digitalcommons.usu.edu/smallsat/2012/all2012/47/ (visited on 10/24/2023).

[95] D. L. Akin, K. McBryan, and N. Limparis, "Dymaflex: Dynamic manipulation flight experiment," MARYLAND UNIV COLLEGE PARK, Tech. Rep., Sep. 3, 2013. [Online]. Available: https://apps.dtic.mil/sti/pdfs/ADA589986.pdf (visited on 10/24/2023).

[96] D. L. Akin, K. McBryan, N. Limparis, and N. D'Amore, "Economies of (small) scale: Exploring the potential for smallsat-based dexterous robotics," in *AIAA SPACE 2014 Conference and Exposition*, American Institute of Aeronautics and Astronautics, Aug. 2014. DOI: 10.2514/6.2014-4339.

[97] N. Limparis, K. McBryan, C. Carlsen, and D. L. Akin, "Micro-sat based dexterous robotic satellite servicing: A case for miniaturization," in *65th International Astronautical Congress*, International Astronautical Federation (IAF), Oct. 2014. [Online]. Available: https://iafastro.directory/iac/archive/browse/IAC-14/B4/6A/22780/.

[98] N. Bolatto, C. Hanner, N. M. Limparis, and D. L. Akin, "Small dexterous space manipulators: Technology development and mission applications," in *ASCEND 2022*, American Institute of Aeronautics and Astronautics, Oct. 2022. DOI: 10.2514/6.2022-4364.

[99] NASA. "Nasa airborne science program: Aircraft list c-9b," NASA. (Apr. 1, 2024), [Online]. Available: https://airbornescience.nasa.gov/aircraft/C-9B (visited on 02/23/2023).

[100] G. Strang, *Introduction to Linear Algebra*. Wellesley Cambridge Pr, 2003, p. 568, ISBN: 9780961408893.

[101] N. J. Kasdin, *Engineering dynamics, a comprehensive introduction*. Princeton University Press, 2010, ISBN: 9780691135373.

[102] K. M. Lynch and F. C. Park, *Modern Robotics Mechanics, Planning and Control, Mechanics, Planning and Control*. Cambridge University Press, 2017, p. 544, ISBN: 9781107156302.

[103] R. A. Johnson and D. W. Wichern, *Applied Multivariate Statistical Analysis (6th Edition)*. Prentice Hall, 2007, p. 800, ISBN: 9780131877153.

[104] T.-D. Bradley. "The tensor product demystified." English, math3ma. (Nov. 2018), [Online]. Available: https://www.math3ma.com/blog/the-tensor-product-demystified.